HYDROCLIMATIC VARIATION OVER SOUTHERN AFRICA AT INTRA-ANNUAL AND INTER-ANNUAL TIME SCALES WITH SPECIAL REFERENCE TO THE ROLE OF THE OCEANS

Report to the

Water Research Commission

by

M Rouault, CJR Reason, N Vigaud,
A Mavume & N Fauchereau
Department of Oceanography, University of Cape Town

WRC Report No 1476/1/08
ISBN 978-1-77005-654-1

APRIL 2008

DISCLAIMER

This report has been reviewed by the Water Research Commission (WRC) and approved for publication. Approval does not signify that the contents necessarily reflect the views and policies of the WRC, nor does mention of trade names or commercial products constitute endorsement or recommendation for use.

Executive summary

Over the last century, South Africa has suffered from dramatic interannual changes in rainfall, characterized by severe droughts and wet spells. Such variability of rainfall affects water resources, the agricultural industry and thus the Gross National Product. It has a particularly detrimental effect on rural subsistence farmers, the health of people in rural areas and the sustainable management of the natural environment. There is a need to enable resource managers (water and agriculture) to optimally exploit best current climatological knowledge in dealing with hydroclimatic variability, thereby enhancing their decision-making ability for the short, medium and long term

Over the last 15 years much knowledge has been gained on how the oceans can modify the global climate and affect the rainfall of southern Africa, from the decadal to interannual scales. Previous research has shown that many droughts occur in southern Africa during the mature phase of El Niño, when the central and eastern Pacific and the Indian Ocean are warmer. Conversely, during La Niña conditions, wet spells are more likely to happen. The equatorial and tropical oceans have a profound effect on the world's weather patterns due to high sea surface temperatures, elevated heat contents of the first hundred metres below the surface and associated high rainfall rates. Southern African interannual climate variability is also affected, but in a manner that offers some predictability depending on how well ocean-atmosphere processes are understood.

Although the El Niño Southern Oscillation (ENSO) phenomenon is the dominant regulator of Southern Africa summer rainfall, the Indian and Atlantic Oceans also have a role to play. In fact it seems that the warming of the Indian Ocean since the 1950's has made ocean variability more important for southern Africa and this has increased the spatial extent and intensity of drought in Southern Africa since the mid-seventies. On top of it are long-term trends; for instance, the ocean's temperature has risen globally during the last 50 years due to the anthropogenic increase in CO_2. Given the high correlation between ocean surface temperature and southern African rainfall, this increase must be taken seriously.

This project set out to enhance the understanding of hydroclimatic variability in southern Africa with special reference to the role of the oceans and thereby address some of the needs of resource managers in this connection.

Specific objectives were to:

- Assess the suitability of indices used to represent hydroclimatic variation over southern Africa from a joint ocean/atmosphere system and water-resource management perspective.

- Select, assess and apply the most promising of advanced remote sensing and modelling products which would assist in achieving the objectives of this project.

- Test hypotheses concerning the importance of the heat content of upper ocean layers and evaporation from the oceans in influencing the weather and climate of countries in southern Africa.

- Familiarise water resource managers with advances in, capabilities of and potential benefits of using improved prediction tools.

As a first step in pursuing these objectives, the benefits of the standardised precipitation index (SPI) for characterising and monitoring droughts were examined. The SPI allows the intensity and spatial extent of droughts to be monitored at different time scales (3, 6, 12 and 24 months). It is linked to the probability of occurrence of dry or wet events and can be used for operational drought monitoring at any location, where the rainfall time series extends over at least 30 years. In this study, the SPI was employed to do a retrospective analysis of the spatial extent and intensity of droughts in South Africa from 1921 to 2000, using data from the 93 Rainfall Districts of the South African Weather Service. According to this index, the 8 most severe droughts at the 6-month time scale for the summer rainfall region of South Africa happened in 1926, 1933, 1945, 1949, 1952, 1970, 1983 and 1992. There is also considerable decadal variability and it was only for the average number of dry districts per year that a cyclic variation (18 to 20 year period) could be found. The average number of wet districts seems to have increased in the 1960's. Drought lasting for 3 years has not been uncommon for each of the 8 South African rainfall regions defined by the South African Weather Service. The SPI was also used in a retrospective analysis of the spatial extent of droughts in Southern Africa (south of 10°S) from 1901 to 1999. In terms of spatial extent, the 8 most severe droughts at the 6-month scale (October-April) for the summer rainfall region of Southern Africa ended in 1916, 1924, 1933, 1949, 1970, 1983, 1992 and 1995. At the 2-year scale, they ended in 1906, 1933, 1983, 1984, 1992, 1993, 1995 and 1996. Areas affected by those droughts ranged from 3.4 to 2 million km^2. Eight of those 12 years are El Niño years. Preliminary data indicate that 2001/2002, 2002/2003 (El Niño year) and 2003/2004 experienced severe droughts at a number of scales and that 2005/2006, a La Niña year, was the wettest year since the mid 70's. This confirms the increase in the spatial extent of drought in Southern Africa since the 1970's due to the stronger relationship between ENSO and southern African rainfall. It is clear that combining retrospective analysis with real time monitoring could be extremely beneficial in the development of drought response strategies and awareness plans. Indeed, following these results, the South African Weather Service is now using the SPI for monitoring drought in South Africa.

With regard to the role of the ocean in regulating southern African climate, better understanding of the mechanisms leading to warm and cold sea surface temperatures and variations of the heat content of the upper ocean is of prime importance. These mechanisms have been investigated in ocean areas that correlate to Southern African rainfall.

A study of the behaviour of tropical cyclones over the Mozambique Channel using remote sensing was carried out, with specific focus on the interaction with the water masses in the channel of two cyclones that moved into the region from the east (Hudah, Eline) and one that was generated over the channel itself (Japhet). Movement over warm ocean eddies in the Mozambique Channel was concomitant with increases in wind speeds of all cyclones from 30 m s^{-1} to 50 m s^{-1}. There was an association between the increase in tropical cyclone intensity and the anomalously high heat content of warm eddies traversed under the track of each cyclone. Cooling of surface waters in the wake of cyclones was manifested by temperature decreases of between 2 and 7ºC indicating mixing to depths of 80 m or more. At that depth, the temperature difference in an eddy and outside is about 5ºC, potentially making these eddies an extra source of energy for cyclones.

Evaporation at the surface of the ocean leads to cooling at the surface and turbulent flux of moisture from the ocean to the atmosphere (also called turbulent latent heat flux). Estimates of turbulent latent heat fluxes were obtained in various studies. In one such study, in the Agulhas Current Retroflection region south of Africa, it was

found that by not accounting for sharp gradients of SST and wind speed, the commonly used NCEP reanalysis data underestimates the monthly mean of latent and sensible fluxes over Agulhas eddies by a factor of three. Due to the high heat content of eddies, the impact of eddy-associated SST gradients on the overlying atmosphere is durable and can last for a few months. The implication of this finding is that models that rely on NCEP data to simulate atmospheric behaviour may overlook a potentially important source of climate variability such as the Agulhas current region.

Another mechanism leading to cooling or warming of the ocean is advection by currents. Use of satellite remote sensing has enabled this project to discover a never-before documented current, now named the South Indian Ocean Countercurrent (SICC). The structure of the subtropical SICC was revealed by altimeter-derived, absolute geostrophic surface velocities. It is a narrow, eastward-flowing current between 22° and 26°S. Multi-year averaging identifies it as a well-defined current between Madagascar and 80°E, continuing with lower intensity between 90° and 100°E. Volume transports down to 800 dbar are of the order of 10^7 m^3s^{-1}. Evidence has been found of a narrow branch of the South Equatorial Current (SEC) approaching Madagascar near 18°S and feeding the East Madagascar Current (EMC), which appears to continue westward around the southern tip of Madagascar. It then partially retroflects and nourishes the SICC.

The deepening or shoaling of the thermocline is also a key process controlling the sea surface temperature of the ocean, and propagation of Kelvin and Rossby waves is known to control the development of warm and cold anomalies in the upper ocean, especially at the equator. These effects have been investigated in a study of the variability of the tropical southeast Atlantic, a sector to date neglected by the international research community. This study has covered the origin, development and demise of extreme warm episodes in the South-east Atlantic Ocean (known as Benguela Niños) as well as minor warm events and cold episodes. To this end, different sets of observations have been combined with outputs from a numerical simulation of the tropical Atlantic. It has been shown that both warm and cold surface events develop regularly in the same specific region along the coast of Angola and Namibia. Some cold events compete in magnitude with major warm episodes. Local sea-air heat flux exchanges do not seem to pre-condition the sea surface in the Angola-Benguela region prior to the arrival of an event. Most warm and cold episodes are large-scale events despite their limited surface signature. They appear to be generated by wind anomalies in the western and central equatorial Atlantic in the same way as Benguela Niños. Seasonal fluctuations of the depth and shape of the tropical thermocline seem partly to control the way subsurface anomalies eventually impact the surface. During the austral summer, surface anomalies create an identifiable pool centered near 15ºS, whereas in winter they show an elongated pattern along the coast stretching towards the equator. Local upwelling or downwelling-favourable wind regimes, as well as local net heat fluxes, may modulate the surface expression of events. In the late austral summer of 2001, warmer than average sea surface temperatures that persisted for about three months were observed by the Tropical Rainfall Mission Microwave Imager in the Angola Benguela Current system. These coastal anomalies extended offshore by 1 to 4 degrees longitude and were not due to local ocean-atmosphere interaction or relaxation of the upwelling favourable southerly winds. Instead, they were remotely forced by ocean-atmosphere interaction in the tropical Atlantic. Satellite remote sensing and a linear ocean model suggest that relaxation of trade winds along the equator triggered Kelvin waves that crossed the basin within a month in early 2001. Westerly wind anomalies were also observed in December 2000 and January 2001 over most of the Tropical Atlantic contributing to a warm preconditioning due to an enhancement of

the oceanic annual cycle. This led to abnormal sea level heights near equatorial Africa that propagated southwards along the coast towards the Angola-Benguela Frontal zone. This process increased the seasonal penetration of warm and salty water of tropical origin into the Angola-Benguela upwelling system. Evidence has been found of a connection between such warm events and northern summer rainfall over coastal West Africa. The strongest relationships exist between April-May sea surface temperature (SST) in the Angola-Benguela Frontal Zone area, May-June latent heat fluxes in this area, and July-August rainfall over the region 5^{o}W-5^{o}E, 5-10^{o}N. Anomalously wet summers in this region are also characterised by a weaker African Easterly Jet, a stronger Tropical Easterly Jet and, in many cases, reduced rainfall further north over the southern Sahel.

This project has also made significant advances in the study of winter rainfall variability, establishing the existence of a relationship between the Antarctic Oscillation (AAO) and winter rainfall over southwestern South Africa. It was found that 9 (8) of the 11 (11) wettest (driest) winters (June-August) over the 1948-2004 period are associated with negative (positive) AAO phase, i.e. negative (positive) pressure anomalies over Antarctica and positive (negative) anomalies over the midlatitudes of the Southern Hemisphere. The statistical relationship between the AAO and winter rainfall is stronger at one and two month lead than at zero lead time, suggesting that knowledge of the AAO phase in early winter may give some indication of late winter/early spring rainfall anomalies over southwestern South Africa. The mechanisms by which the AAO appears to influence winter rainfall over southwestern South Africa involve shifts in the subtropical jet, changes to the surface latent heat flux upstream over the South Atlantic and modulations of mid-level uplift, low-level convergence and relative vorticity over the region. To further understand the behaviour of the AAO, the 50-year long Marion Island dataset has been examined. In recent decades, instrumental data recorded at the South African Weather Service station on Marion Island (46^{o}54' S and 37^{o}51' E) in the Southern Ocean shows that the local climate of this island has undergone significant changes since the 1960's, mostly in the austral summer. These include a decrease in rainfall, increase in non-rainy days, changes in wind speed and direction, increase in maximum and minimum local air temperature and increase in near-shore sea surface temperature. This study analysed surface temperature, pressure, sea surface temperature and rainfall recorded daily at Marion Island together with NCEP re-analysis data to explore the mechanisms potentially associated with these changes. It is suggested that the changes to the local climate of Marion Island are linked to the well documented shift in phase of the semi-annual oscillation and the AAO in the Southern Hemisphere after about 1980.

Moisture input from the South Atlantic and Indian Oceans over southern Africa has been examined through zonal water vapour transport. Along the west coast, variations in intensity and latitudinal position of the South Atlantic anticyclone and modulations of the westerly flow that penetrates from the tropical Atlantic, contribute the most in January-February to variability in moisture advection from the South/tropical Atlantic, thus affecting rainfall at subtropical/tropical latitudes respectively. Events related to low phases of the Southern Oscillation are marked by an eastward shift of the ascending branch of the Walker circulation over Indian Ocean regions, suppressing convection over the subcontinent and reducing rainfall. Regarding anomalously wet events, the southern extension of the African Easterly Jet could act to transfer more moisture from the tropics southwards. Along the east coast, modulations of moisture advection in the tropics affect rainfall east of the Great Rift escarpment in November-December. Changes in the midlatitude westerly circulation support/reduce the meridional transfer of energy within the Subtropical and Intertropical Convergence Zone through sustained/weakened convection,

leading to wet/dry conditions over central and southeastern regions of South Africa. Secondly, the Indian anticyclone ridging more/less over the subcontinent is found to inhibit/favour convection over southeast South Africa where below/above-normal rainfall is expected in October-November. A decrease/increase in moisture advection inland results in reduced/enhanced rainfall over northern Mozambique/southern Tanzania while an opposite situation prevails over north Angola. Finally, alterations of the meridional circulation in September-October bring changes in the equatorial easterly flux from the Indian Ocean, the northern trades latitudes and the midlatitude westerly circulation. Reduced/enhanced moisture availability along the east coast and the central tropics together with shifts of the Walker circulation descending/ascending limb over central southern Africa, lead to dry/wet conditions over these regions. In conclusion, the study of zonal water vapour transport may help in explaining southern African rainfall variability and thus in assessing issues such as climate predictability over southern Africa.

Lastly, a web site has been established to monitor anomalies in ocean conditions conducive to droughts or floods in Southern Africa (http://realtime.sea.uct.ac.za/). The quality of near real-time data assimilated by models is the key to the success of any forecasting system. Near real-time ocean and atmospheric data can also be used to monitor ocean states and to compare present to past conditions. Daily, weekly and monthly near real-time intermediate resolution products (4 to 35 km resolution) are freely and readily available with delays of a few days to a week in many research centres in many part of the world. Such products include sea surface temperature, wind speed, sea surface height, ocean colour and geostrophic currents. Data are transferred twice a day through ftp transfer and subsequently automatically processed on a PC. They are displayed on a web site showing charts of mean and anomalous conditions.

In most respects, this project has fulfilled its objectives. The SPI is already being used by the South African Weather Service while agencies such as the Benguela Current Commission are making use of near real-time information being made available on the project web site, which will continue to operate in terms of a follow-on research contract with the Water Research Commission. The research outcomes also motivated the deployment of an ocean-atmosphere interaction measuring mooring off Angola, being financed by the international community. The discovery of a current in the Indian Ocean, an unexpected outcome of the project, made headlines internationally and locally. For the first time, as a result of this project, it has been possible to link drought in the Western Cape to the vagaries of the Antarctic Oscillation in the Southern Ocean.

The quality and quantity of the publications stemming from this research project testify to the important contribution that has been made in understanding and monitoring climate variability. Despite the great strides that have been made, there is still a long way to go in developing an understanding of all the factors that regulate inter-annual variability of southern African climate. Some of the important questions that have emerged are the following:

- Why is there no linear relationship between El Niño Southern Oscillation (ENSO) and SA rainfall variability?
- Why are some El Niño events not linked to drought?
- What is the impact of El Niño and La Niña at the catchment scale?
- What is the role of the Antarctic oscillation (AAO) on summer rainfall?
- What is the interaction of ENSO and AAO and how this affects Southern African Climate?

Many of these questions will be addressed in the follow-on project that has made continuity of the research possible.

Acknowledgements

We would like to thank Dr George Green, Dr Renias Dube and the remainder of the project steering committee (Dr W Landman, P van Niekerk, E Nel, O Wilson, J Malherbe, Prof Bruce Hewitson and Prof Hannes Rautenbach) for pertinent inputs and guidance. Scientific contributions from Dr Pierric Penven, Dr Serena Illig, Dr Yves Richard, Prof Gerold Ziedler, Dr Pierre Florenchie, Dr Pascal Roucou, Dr Abderahim Bentamy, Prof Johann Lujteharms are acknowledged. We would like to thank Rachmat Harris and Helen King for clerical support and Jeremy Main and Christo Whittle for technical support. Thanks to Hannekie Botha and Anne D'Albis on behalf of the France-South Africa cooperative project (NRF and CNRS); the South African Weather Service for providing weather data and the University of Cape Town, University of Dijon, IRD and CNRS for significant support. Thanks are due to the Water Research Commission for funding the project.

TABLE OF CONTENTS

1. Introduction

Over the last century, South Africa has suffered from dramatic interannual changes in rainfall, characterised by severe droughts and wet spells. Such variability of rainfall affects the agricultural industry, water reserves and thus the Gross National Product. It has a particularly detrimental effect on rural subsistence farmers, the health of people in rural areas and the sustainable management of the natural environment. There is a need to enable resource managers (water and agriculture) to optimally exploit best current climatological knowledge in dealing with hydroclimatic variability, thereby enhancing their decision-making ability for the short, medium and long term

Over the last 15 years much knowledge has been gained on how the oceans can modify the global climate and affect the rainfall of southern Africa, from the decadal to interannual scales. A large proportion of this knowledge was generated during several WRC projects carried over in the Department of Oceanography at UCT (Jury et al., 1998, 1996; Rouault et al., 2003, 1999; Reason et al., 2003); this led to numerous publications in scientific journals. This currently-reported WRC project is, in many respects, a continuation of those projects.

The previous projects have shown that most droughts happen in Southern Africa during the mature phase of El Niño, when the central and eastern Pacific and the Indian Ocean are warmer. Due to their high sea surface temperatures, the major heat contents of the first hundred meters below these surface and the associated high rainfall rates, the equatorial and tropical oceans have a profound effect on the world's weather patterns. Southern Africa climate interannual variability is affected as such and this offers predictability.

Conversely, wet spells are more likely to happen during La Niña conditions. The El Niño Southern Oscillation (ENSO) phenomenon is the dominant regulator of Southern Africa summer rainfall, but the Indian and Atlantic Ocean also have a role to play. In fact it seems that the warming of the Indian Ocean since the 50's has made ocean variability more important for southern Africa and this has increased the spatial extension and intensity of drought in Southern Africa since the mid seventies. On top of it are long term trends; for instance, the ocean's temperature has risen globally during the last 50 years due to the anthropogenic increase in CO_2. Given the high correlation between ocean surface temperature and southern African rainfall, this increase must be taken seriously.

At the commencement of this project, the following were among the key questions that needed to be addressed: Are the indices currently used in South Africa for drought monitoring the most efficacious? If not, what other indices may provide better insight? Can such indices be optimised for use in southern Africa? What recent developments in remote sensing are particularly useful for understanding and monitoring climate variability in southern Africa, particularly pertaining to rainfall? What effect does the heat content of the upper layers of the adjacent oceans have on the rainfall over southern Africa? What predictive ability does this variable have? What effect do changes in evaporation over the adjacent oceans have on rainfall over southern Africa? How accessible can new knowledge, information, data and/or improved modelling approaches resulting from this project be made to operational forecasters of climate variation and to water resource managers? How can end users, while appreciating limitations, derive benefits from research products delivered? This project set out to address some of these questions, intending to enhance the understanding of hydroclimatic variability in southern Africa with special reference to the role of the oceans and thereby also to address some of the needs of water resource managers in this regard.

Specific objectives were to:

- Assess the suitability of indices used to represent hydroclimatic variation over southern Africa from a joint ocean/atmosphere system and water-resource management perspective.

- Select, assess and apply the most promising of advanced remote sensing and modelling products which would assist in achieving the objectives of this project.

- Test hypotheses concerning the importance of the heat content of upper ocean layers and evaporation from the oceans in influencing the weather and climate of countries in southern Africa.

- Familiarise water resource managers with advances in, capabilities of and potential benefits of using improved prediction tools.

Following this introductory chapter, Chapter 2 examines the benefits of the standardised precipitation index (SPI) in characterising and monitoring droughts at different time scales in southern Africa. Chapter 3 deals with the role of the ocean in regulating southern African climate. New knowledge contributed in this regard includes: the discovery of a new current; the specific role of the Tropical South East Atlantic; and, the potential effect of Mozambique Channel Eddies on the intensification of tropical cyclones. Chapter 4 deals with the mechanisms whereby the oceans impact on winter rainfall, a subject that has up until recently not received much attention. Chapter 5 reports a thorough study of the moisture flux from adjacent oceans and its impact on rainfall. Chapter 6 describes a near real time ocean early warning system that uses indices based on the data that helped us unravel issues researched in the previous chapters. We conclude with a brief report on the contribution of the project to capacity building and extent of knowledge dissemination that took place.

2. Monitoring droughts at different time scales in southern Africa with the standardized precipitation index

2.1 Introduction

Drought is a regular and recurrent feature of the southern African climate. A drought is a shortage of precipitation over an extended period. Its impact on society depends on its intensity but also on its duration. A common time-scale for agricultural droughts is the season (3 to 6-month time scales) when deficiency in precipitation results in damage to the crop. Hydrological drought is associated with precipitation shortage on a longer time scale (12 months to 2 years or more) and its effect on surface or subsurface water supply. Hydrological or agricultural drought can be out of phase and their impacts on various economic sectors can be appreciably different. It takes longer for precipitation shortage to become evident in soil moisture, stream flow, groundwater and dam levels. It is therefore useful to define a drought index that will represent different time scales from 1 month to 3 years. We have applied the standardized precipitation index (SPI) to 2 different datasets, one for South Africa (1920-2000) from the South African Weather Service (SAWS) and one for Southern African (1901-2000) from the Climate Research Unit in United Kingdom (CRU). This chapter describes the SPI in detail, presents some applications and brings new results on the ENSO-southern African rainfall relationship and the recent increase in spatial extension and intensity of droughts and wet periods.

2.2 Standardized Precipitation Index

McKee et al. (1993, 1995) from the Colorado Climate Center formulated the SPI in 1993. In summary, the SPI allocates a single numeric value to the precipitation (-3 to 3), which can be compared across regions with different climates. The SPI was designed to state that it is possible to simultaneously experience wet conditions on one or more time scales, and dry conditions at other time scales. The SPI is based on the probability of precipitation for a given time period. Technically, the SPI is the number of standard deviations that the observed value would deviate from the long-term mean, for a normally distributed random variable. Since precipitation is not normally distributed, a transformation is first applied so that the transformed precipitation values follow a normal distribution. The SPI allows determining the probability occurrence of dry or wet events at different time scales (from monthly to two yearly mean rainfall). The SPI can be used on all stations having more than 30 years of rainfall (Hayes et al., 1999).

Thus an SPI of 2 or more happens about 2.3 % of the time and a normal condition (SPI between 1 and -1) happens 68.2 % of the time. This allows establishing a classification values for SPI values (Table 2).

A SPI of -2.00 and less will identify an extreme drought that happens twice per century; from -1.5 to -1.99 about 4 times per century; from -1 to -1.5 about 9 times per century. An SPI of 0 to -1 will be related to normal or slightly below normal condition happening 34 times per century. Detail of the SPI algorithm can be found in Guttman (1998 and 1999), McKee et al. (1993, 1995) and Hayes et al. (1999). The SPI has been favourably evaluated and compared with others indices (Keyantash and Dracup, 2002) and is now integrated in the set of indices used by the Drought Monitor in the USA (Svoboda et al., 2002). Because the SPI is linked to percentage of occurrence and based on rainfall only, it can be used in any country

Table 1: SPI and Corresponding cumulative probability in relation to the base period (Hayes et al., 1999)

SPI	Cumulative Probability
-3.0	0.0014
-2.5	0.0062
-2.0	0.0228
-1.5	0.0668
-1.0	0.1587
-0.5	0.3085
0.0	0.5000
+0.5	0.6915
+1.0	0.8413
+1.5	0.9332
+2.0	0.9772
+2.5	0.9938
+3.0	0.9986

Table 2: SPI classification (Hayes et al., 1999)

SPI Value	Drought Category	Occurrence
2.00 and above	Extremely wet	2.3 %
1.5 to 1.99	Very wet	4.4 %
1. to 1.49	Moderately wet	9.2 %
-0.99 to 0.99	Near normal	68.2 %
-1.00 to -1.49	Moderately dry	9.2 %
-1.50 to -1.99	Severely dry	4.4 %
-2.00 and less	Extremely dry	2.3 %

We have calculated the SPI for a precipitation total ranging between 3 months and 2 years for each of the 1921 to 2001 SAWS 93 districts rainfall data and for the CRU 0.5x0.5 degrees 1901-2000 dataset using the techniques developed by Hayes et al. (1999). The 3-month SPI can be used to characterise a seasonal drought index well suited to describe the beginning, the heart or the end of the rainy season. The total rainy season can be described using the 6-month index and 12-month and 24-month SPI can be used for long-term drought. The X-month SPI (X=3, 6, 12 or 24) is used to compare the precipitation over a specific X-month period with the precipitation totals from the same period for all the years of the dataset.

Hayes et al. (1999) used the standardized precipitation index (SPI) to monitor the 1996 drought in the United States of America. They show how the SPI can be used operationally to detect the start of a drought, its spatial extension and temporal progression Hayes et al. (1999) shows that the onset of the drought in the USA in 1996 could have been detected one month in advance of the Palmer Drought Severity Index (PSDI). Although it is quite a recent index, the SPI has been used in Turkey (Komuscu, 1999), Argentina (Seiler et al., 2002), Canada (Anctil et al., 2002), Spain (Lana et al., 2003), Korea (Min et al., 2003), Hungary (Domonkos, 2003), China (Wu et al., 2001) and Europe (Lloyd-Hughes and Saunders, 2002) for real time monitoring or retrospective analysis of droughts. The SPI is consistent with regard to the spatial distribution of rainfall that occurs with great variability in South Africa due to geographical location, orography and the influence of the oceans. Using that index to develop a climatology of the spatial extension and intensity of droughts gives also

an additional understanding of its characteristics and an indication of the probability of recurrence of drought at various levels of severity. The SPI can also be used to monitor excess moisture during a wet season that can aggravate consequences of floods. This may indicate a saturated catchment conducive to flood development if rainfall continues.

In Figure 1 we show the 3-month SPI values using the precipitation total of October, November and December 1982 while the 6-month SPI calculated for December 1982 use the precipitation total of July 1982 to December 1982.

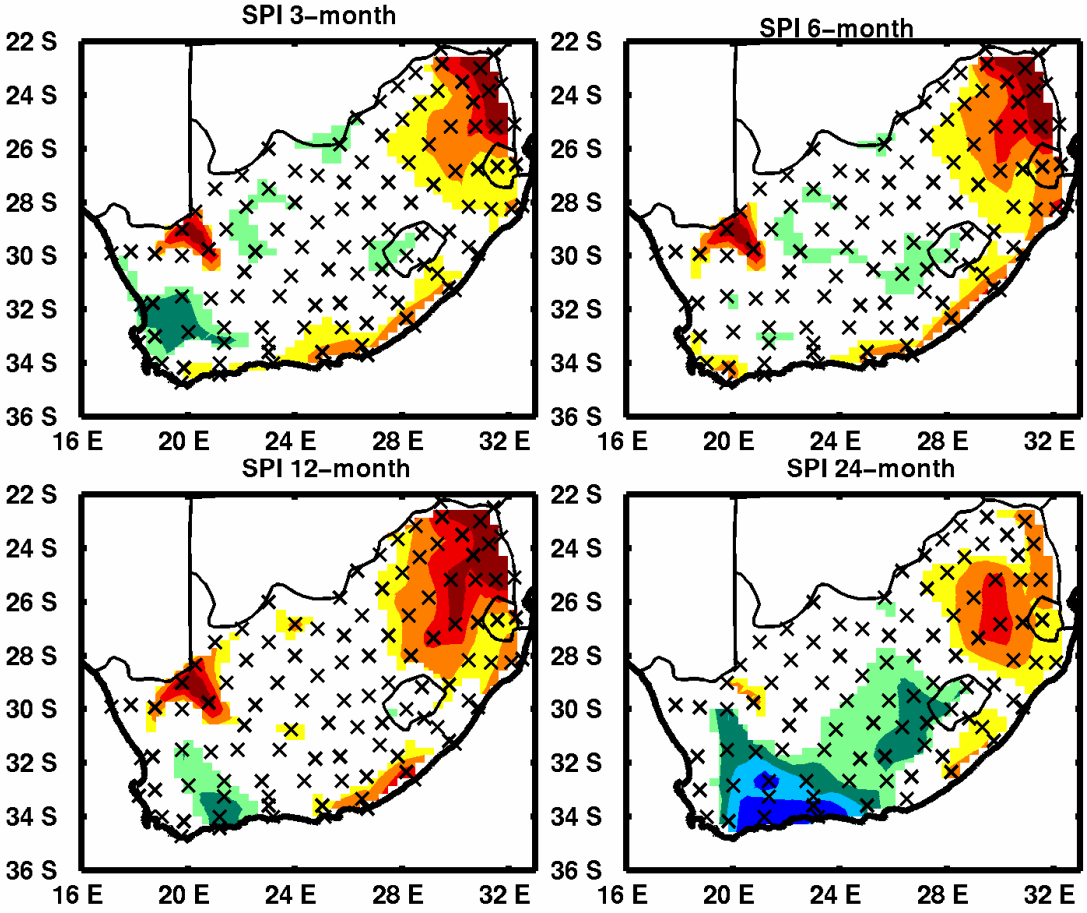

Figure 1: Spatial extent of the SPI at 3, 6, 12 and 24-month time scale at the end of December 1982. Colour code: brown (-3 to -2), red (-2 to -1.5), orange (-1.5 to -1), yellow (-1 to-0.5), dark blue (3 to 2), light blue (2 to 1.5), dark green (1.5 to 1), green (1 to 0.5).

A 3-month SPI can be used to monitor soil moisture conditions at the start of the growing season or precipitation during the different stages of plant development or reproduction. The 3-month SPI for the end of December 1982 shows a deficit in rainfall in the North-Eastern Interior. However, dry conditions in the South African summer rainfall regions began in 1982, as can be seen in the 12-month and 24-month SPI. In fact the 24-month SPI is more intense that the 3-month SPI due to dry conditions in 1982. A study of the SPI for the 1981 and 1982 shows some serious deficit at the 6-month scale for the Northeast part of South Africa and a more widespread dry condition at the 3-month scale at the end of March 1982. The evolution of the 3-month SPI for each month of the summer rainy season in 82/83 shows dry to extreme dry conditions at the end of December 82 in the Northeast and along the East coast increasing and spreading to all summer rainfall areas during

that season. Comparison with other rainy seasons shows that the start of the rainy season was one of the worst since 1922. Interestingly one can note that the coastal regions were experiencing a drought at the 3-month scale but wetter conditions at the 2-year scale. In that region in spite of a bad start of the year, water storage must have been plentiful.

The 3-month and 6-month SPI may be misleading in regions where it is normally dry during a 6-month period. For instance the 6-month SPI at the end of December 1982 resembles the 3-month SPI. During the dry season large negative or positive SPIs may be associated with precipitation totals not very different from the mean. This caution can be demonstrated with the climate of Western Cape, where very little rain falls from November to March. Because this is a period with little rain, these mean totals will be small and relatively small deviations on either side of the mean could have large negative or positive SPI. Nevertheless, it is important to have a drought index for longer time scales. A normal 3-month period could occur in the middle of a longer-term drought that would only be visible at longer time scales.

2.3 Application of the SPI to South Africa for 1920-2000

The SAWS divides the country into 93 rainfall districts. Each district combines an average of typically 5 to 15 rain-gauge stations. The 93 districts are parts of 8 climatic regions (Figure 2). Those regions were determined by the SAWS based on a cluster analysis of South African rainfall (South African Weather Bureau, 1972).

Table 3: The 8 climatic areas defined by the South African Weather Service (SAWS)

Number	Name
1	North-Western Cape
2	South-Western Cape
3	South Coast
4	Southern Interior
5	Western Interior
6	Central Interior
7	KwaZulu-Natal
8	North-Eastern Interior

Because precipitation associated with droughts in one area or one season corresponds to flood in others areas or another season, the temporal and spatial differences of rainfall in South Africa make it difficult to represent a coherent picture. Furthermore, the onset of the rainy season and the timing of maximum rainfall are different for the 8 areas making water management and mitigation of agricultural or hydrological drought difficult. A problem using normalised anomalies (difference from the mean divided by standard deviation) is that the normalised anomaly is not symmetrical (positively skewed) because flood leads to a bigger anomaly from the mean than drought. The SPI addresses those problems because it is normalised in time and in space.

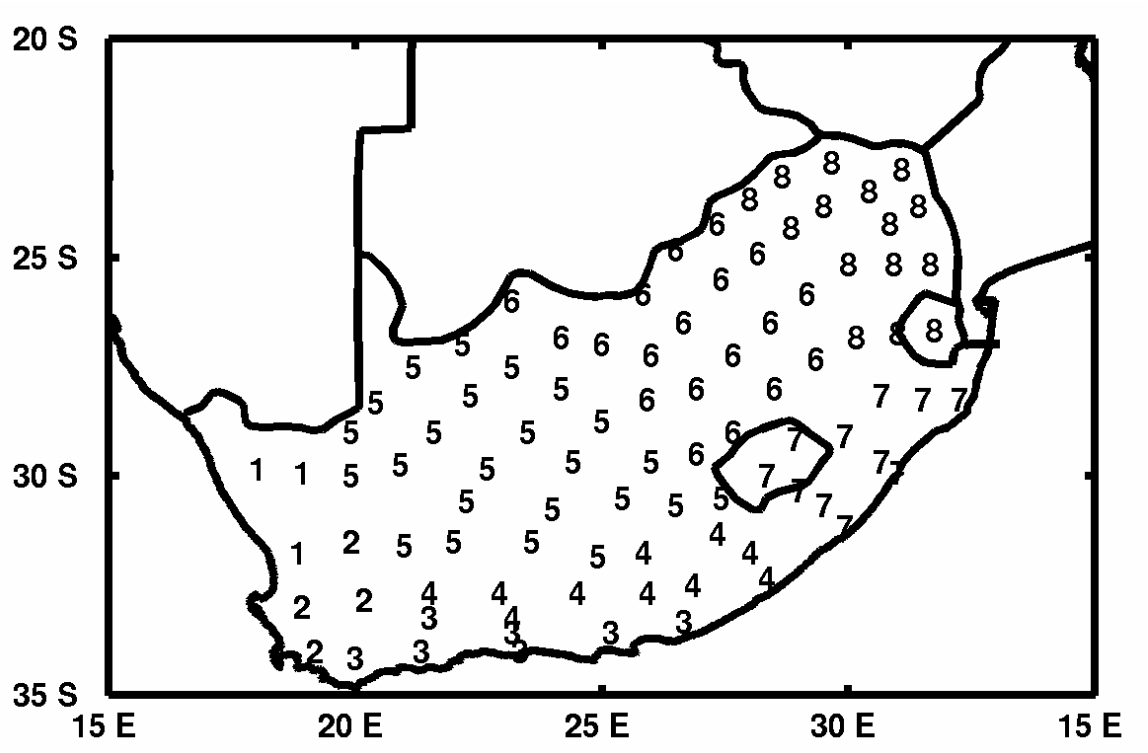

Figure 2 The 8 SAWS climatic regions

2.3.1 Spatial extension of droughts in South Africa

The SPI when applied to the 80 districts representing the summer rainfall season (areas 4 to 8) allows a particular classification of droughts at different time scale as a function of the number of districts within a certain range. Fig. 3 shows the spatial extension and intensity of 20 of the worst droughts experienced in the summer rainfall area since 1922. In 1926, 1933, 1945, 1949, 1952, 1970, 1983 and 1992 more than half of the 80 summer rainfall districts had an SPI <-1, 6 of those year are El Nino year.

The 3-month SPI can be used to look at the beginning or the end of the rainy season. For instance in 1973 (El Nino), there were 60 dry districts at the end of January at the 3 months scale but good late season rainfall (no dry district at the end of April at the 3-month scale) mitigated the drought. Likewise in 1922 (El Nino), there was no dry district at the 3-month scale at the end of January but a dry late season brought the total of dry districts at the 3-month scale to 50. The 3-month and 6-month SPI show that 1982/1983 was the worst drought since 1922 according to that index.

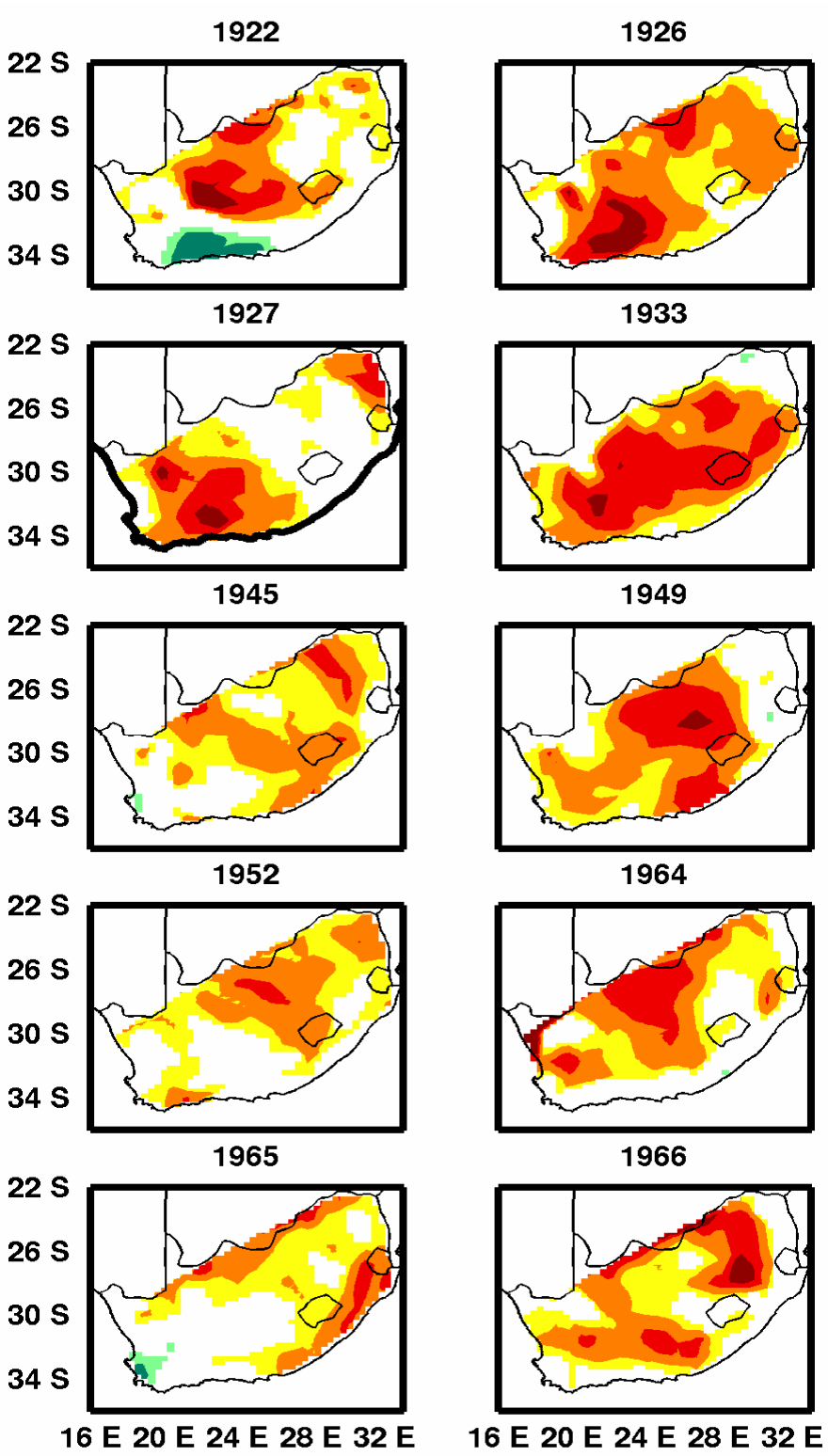

Figure 3a: Spatial extent of the 6-month SPI at the end of April for 10 of the worst dry years in South Africa since 1922. Colour code: brown (-3 to -2), red (-2 to -1.5), orange (-1.5 to -1), yellow (-1 to-0.5), dark blue (3 to 2), light blue (2 to 1.5), dark green (1.5 to 1), green (1 to 0.5).

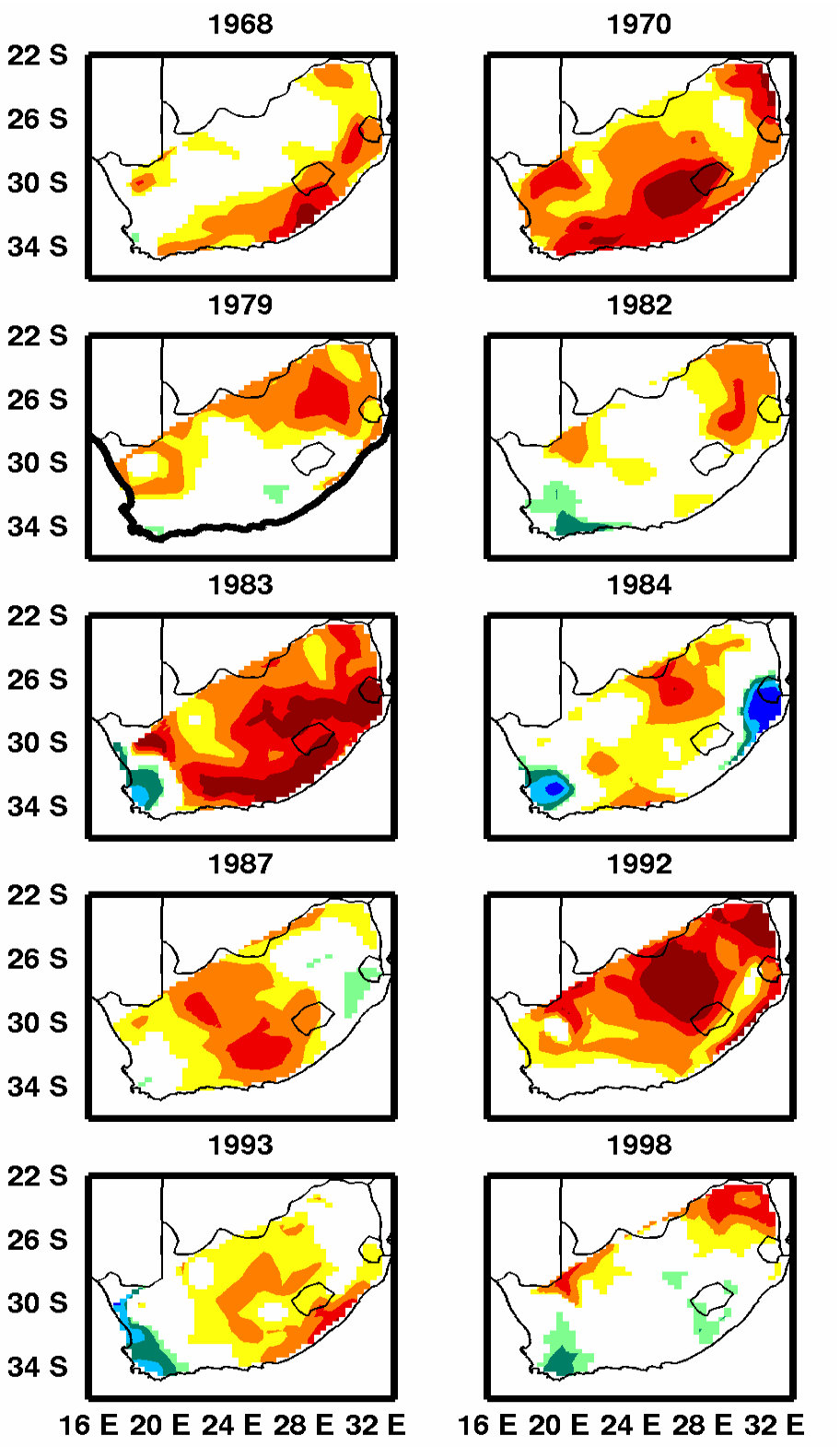

Figure 3b: Spatial extent of the 6-month SPI at the end of April for 10 of the worst dry years in South Africa since 1922. Colour code: brown (-3 to -2), red (-2 to -1.5), orange (-1.5 to -1), yellow (-1 to-0.5), dark blue (3 to 2), light blue (2 to 1.5), dark green (1.5 to 1), green (1 to 0.5).

The 3-month SPI can be used to look at the beginning or the end of the rainy season. For instance in 1973, there were 60 dry districts at the end of January at the 3 months scale but good late season rainfall (no dry district at the end of April at the 3-

month scale) mitigated the drought. Likewise in 1922, there was no dry district at the 3-month scale at the end of January but a dry late season brought the total of dry districts at the 3-month scale to 50. The 3-month and 6-month SPI show that 1982/1983 was the worst drought since 1922 according to that index.

2.3.2 Time series

The SPI can be used in a time series to compare real time SPI with the SPI of the previous 80 years. Figure 4 show the SPIs at the end of March since 1922 for the summer rainfall regions at the heart of the rainy season for area 4 (eastern Cape). The SPI is symmetrical for occurrence of wet and dry events. It represents an advantage on the normalised anomaly (anomaly from the mean divided by standard deviation) where wet anomalies have a higher absolute value. This gives us a climatology of major drought and wet spells at different time scales. For Area 4 the worst drought at the 2-year scale was in 1946 and 1947. Neither the normalised anomaly (not shown) nor a 3-month SPI at the end of March indicates the severity of the situation.

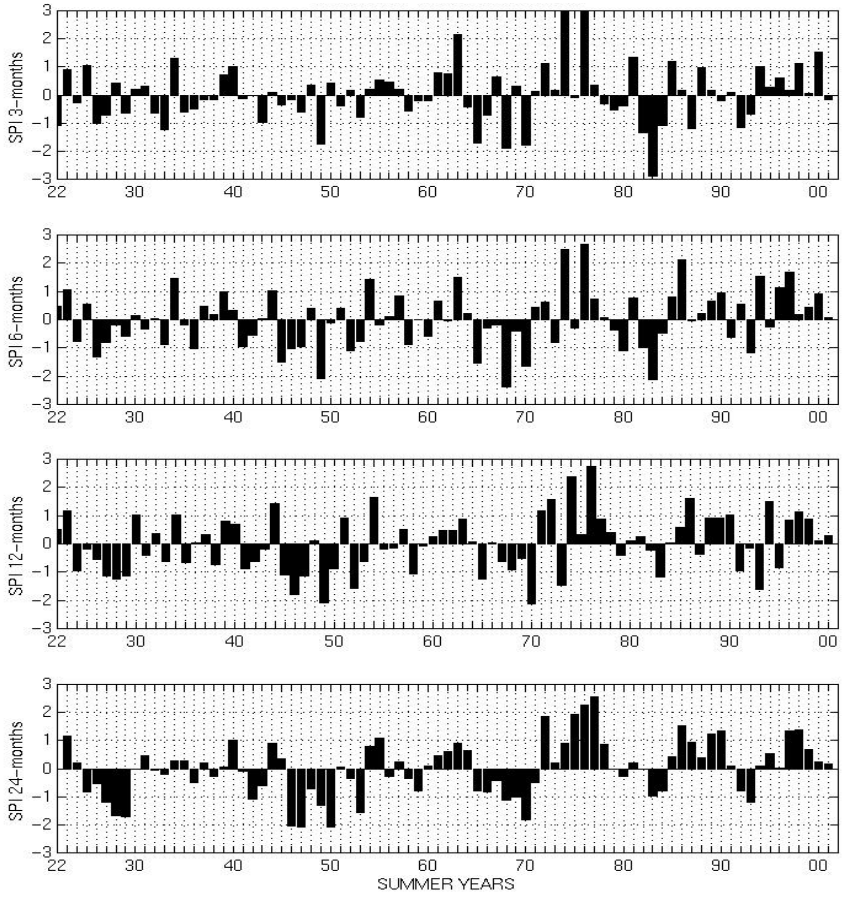

Figure 4: Standardised Precipitation Index at 3, 6, 12 and 24 months (top to bottom) at the end of March for Southern Interior from 1922 to 2001

The SPI can be also used in a time series to look at the real time evolution of the SPI. Fig. 5 shows the SPI for the South Western Cape at the end of every month from 1994 to 2001 at different time scales. This shows how the SPI can be used operationally to monitor the start and end of dry or wet period at different time scales. It can be seen that the heavy rain of the winter 2002 is reflected in a 3-month SPI > 1 from July to October 2002 but due to below-normal rainfall in 1999, 2000 and most of

2001 one-year and two-year SPIs are not as high as one would think. In fact the 2-year SPI is higher from winter 1996 to winter 1998. Looking at Fig. 5 it is not surprising why dam levels in summer 96/97 in the Western Province were higher that in 2001/2002 in spite of a 20 year maximum for winter rainfall in 2001. We also note that this decade did not have some serious droughts. For operational use, caution must be used when using the SPI in summer months when a flood can create a high SPI index. Hayes et al. (1999) have shown that for some regions a good rainfall for one month can create the impression that the drought is over but until all the SPIs are not above a certain value at all scales (typically -1) a drought will still affect a region in one way or another.

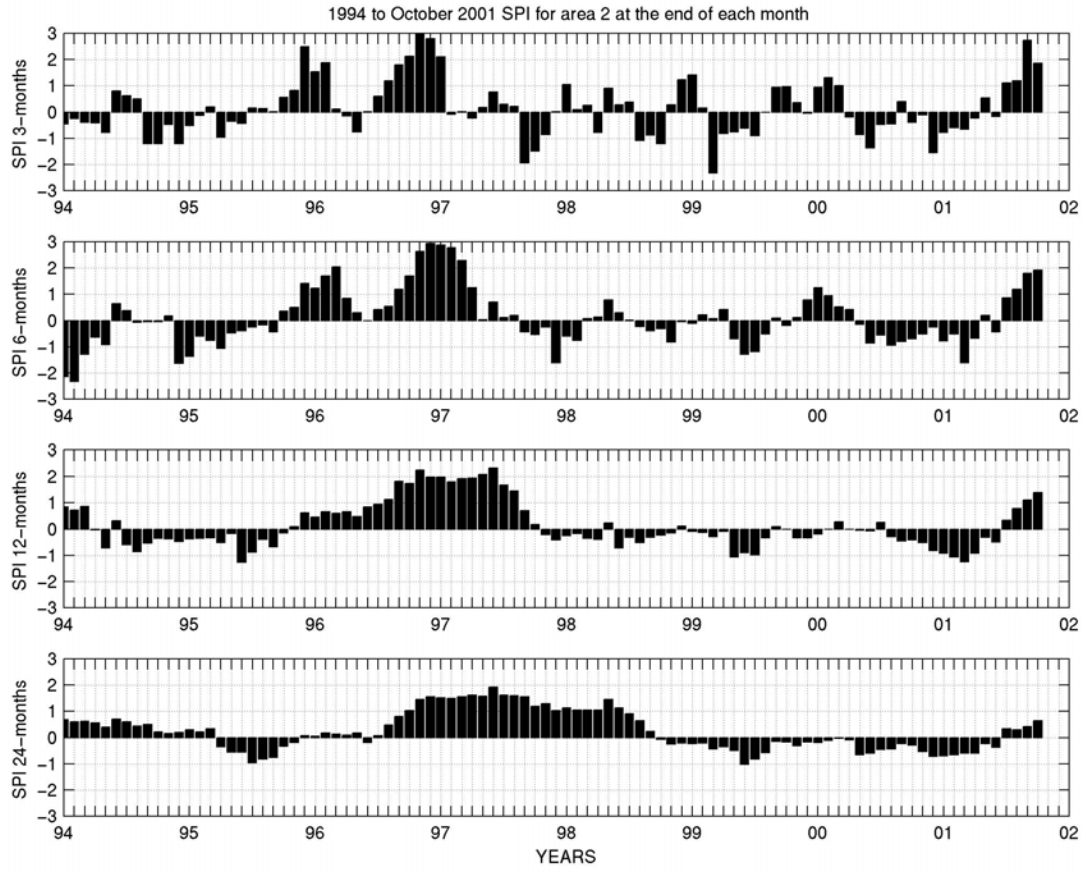

Figure 5: Standardised Precipitation Index at 3 6 12 and 24 months (top to bottom) for all months for South-Western Cape (area 2) at the end of every month from January 1994 to October 2001.

2.3.3 Decadal variability of summer rainfall

More attention should be paid to decadal variability of rainfall in order to produce accurate seasonal forecasts and for better management of water resources. We look in this section at the number of dry or wet districts since 1922 for the summer rainfall area using the 6-month SPI at the end of April. Fig. 6 shows the number of dry districts (SPI < -1) per year for the 80 summer rainfall districts (Area 4, 5, 6, 7 and 8) from 1922 to 2001 with a 9-year window running mean that indicates the average number of dry districts per year for each decade. The average number of dry districts is 13. There is considerable decadal variability in the average number of dry districts per year. The 16-20 years cycle in total rainfall anomaly documented by Tyson et al.

(1975), Louw (1982) and Reason and Rouault (2002) is visible in Fig. 6. It seems to have become longer in the 90's. The number of dry districts per year is seen to have increased by the end of the century, this result being in line with a preceding study (Richard et al., 2001). If we consider years with more than 20 dry districts as dry, then 1926, 1927, 1933, 1945, 1947, 1949 and 1952 were the dry years prior to 1962. Incidentally, 1926, 1933 and 1952 were El Niño years (Trenberth, 1997; Compagnucci et al., 2002). El Niño is usually linked to drought in South Africa (Van Heerden et al., 1988; Lindesay and Vogel, 1990). Since 1962, we had 10 dry years with an average of 44 dry districts. Seven of those years were El Niño years (1966, 1970, 1973, 1979, 1983, 1987, 1992 and 1995). This is consistent with the work of Richard et al. (2000).

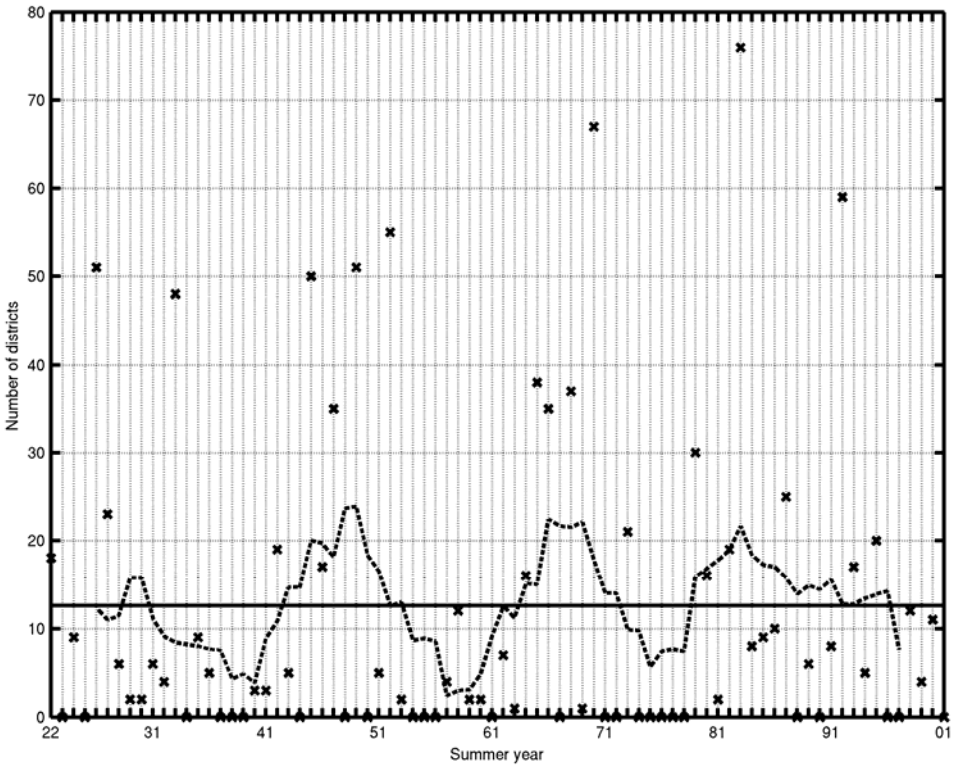

Figure 6: Number of dry districts (SPI 6-month < -1) per year for the 80 summer rainfall districts (Area 4 to 8) at the end of April with 9-year window running mean (dashed line) and 1922-2001 mean number of dry districts (solid line).

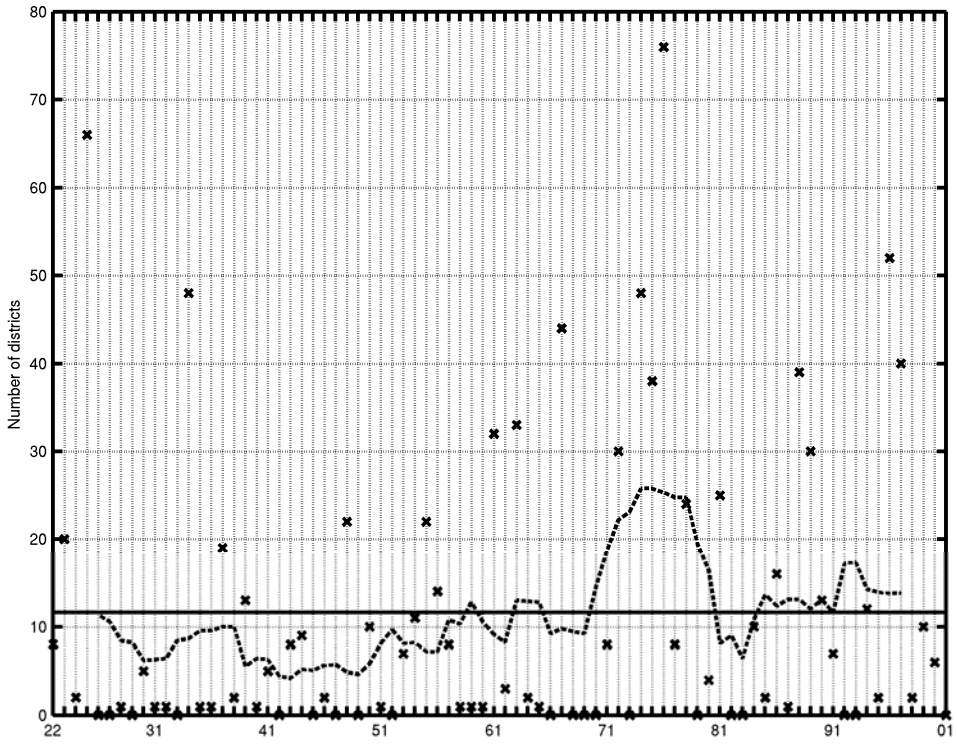

Figure 7: Number of wet districts (SPI 6-month > 1) per year for the 80 summer rainfall districts (Area 4 to 8) at the end of April with 9-year window running mean (dashed line) and 1922-2001 mean number of wet districts (solid line).

Fig. 7 plots the number of wet districts per year (SPI>1) with a 9-year window running mean. On average there are 12 wet districts per year. The 16-20 years cycle is not seen in the number of wet districts per decade. There is an increase in the number of years experiencing a large number of wet districts. This confirms the work done by Mason et al. (1999), Alexander (1995) and Dai and Trenberth (1998). Indeed before 1962, 6 years (1923, 1925, 1934, 1948, 1955 and 1961) had more than 20 wet districts (SPI>1). The years 1925 and 1955 were La Niña year (Compagnucci et al., 2002). After 1962, years with more than 20 wet districts increased twofold (1963, 1967, 1972, 1974, 1975, 1976, 1978, 1981, 1988, 1989, 1996 and 1997). The years 1974, 1975, 1976, 1989 and 1996 were La Niña years according to Trenberth (1997) and Compagnucci et al. (2002). The definition of El Niño and La Niña years is not trivial and the evolution of El Niño has varied throughout the century (Trenberth and Stepaniak, 2002). Tyson et al. (2002) show an 80-year rainfall cycle for at least the last 3500 years that is consistent with Fig. 7.

To summarize, Fig. 8 displays the total number of wet and dry districts per year for the 6-month SPI at the end of April and a 9-year window running mean. There are more dry or wet districts per decade since 1970. Dai and Trenberth (1998) have observed such an increase world-wide as well as in southern Africa. They consider this increase in the global variation of wet and dry spells to be due to global warming and the increase in El Niño events since 1970. Their hypothesis is that the increase in the combined percentage of areas experiencing dry or wet seasons is due to an enhanced hydrological cycle caused by the increase in greenhouse gases. Extreme events (floods and droughts) increase but the mean remains the same. Whether the increase shown in Fig. 7 is part of a natural cycle (Tyson et al., 2002) or due to global warming (Dai and Trenberth, 1998) must be studied more deeply.

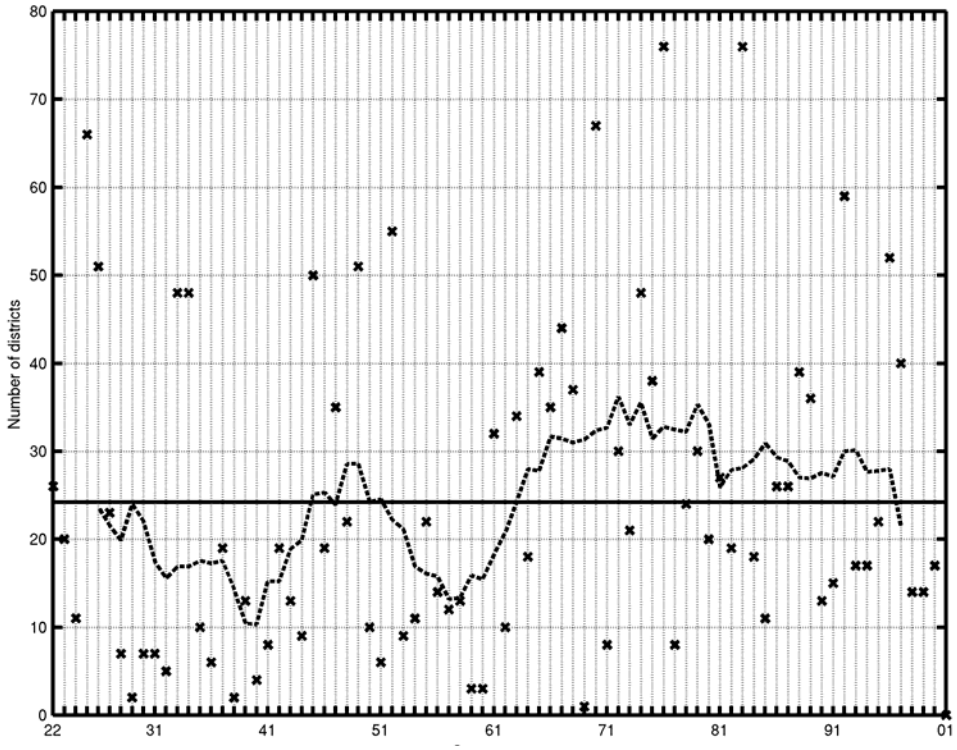

Figure 8: Total number of wet (SPI 6-month > 1) and dry districts (SPI 6-month < -1) per year for the 80 summer rainfall districts (area 4 to 8) at the end of April with 9-year window running mean (dashed line) and 1922-2001 mean number of dry and wet districts (solid line).

2.4 Application of the SPI to Southern Africa (1901-2000)

We calculated the SPI for precipitation totals ranging between 3 months and 2 years at the end of each month using the 1901-1999 CRU2 precipitation. From this we determined the area with SPI < -1 for Southern Africa, south of 10^{o} S. To avoid misleading values of SPI, we used grid cells with mean summer (October to April) rainfall > 10 mm. This leaves us with a total surface of 6.65 10^{6} km^{2}. The area taken out corresponds mostly to the Namib Desert and western coast of South Africa. Table 4 shows the areas affected by drought in square degree and the percentage of the affected areas from our domain study as well as the El Niño Southern Oscillation (ENSO) Index for the eight worst droughts at the end of April at the 6-month and 2-year scales. Incidentally, 8 of those 12 dry years identified in Table 4 were ENSO years (Trenberth, 1997; Compagnucci et al., 2002). At the 2-year scale, the most severe droughts have occurred during the last 20 years. The strong intensity and extent of observed droughts since 1970 is associated with a reinforced influence of El Nino in the context of a warmer tropical and subtropical Indian Ocean (Richard et al., 2000; Goddard and Graham, 1999). Fig. 9 and 10 shows the dry area (SPI < -1) at the 6 months and 2-year scale at the end of April for our domain study from 1901 to 1999 with a 9-year window running mean that indicates the mean yearly dry area per decade. The average dry area is about 1 10^{6} km^{2} per year at the 6-month and 2-year scale, about 17 % of our domain study. There is inter-decadal variability in the decadal mean dry area per year at the 6-month scale, a feature of Southern African rainfall variability (Reason and Rouault; 2002) that makes the detection of trends difficult. Nevertheless there is a clear increase at the 2-year scale since the mid 70's. Precipitation shortage in the austral summer season of 2002, 2003 and 2004 seems to confirm that behaviour. Southern Africa experienced drought at different time

scales in 2002, 2003 and 2004 with major societal implications. Dry conditions during the first three months of 2002 in Zimbabwe, Lesotho, South Africa, Swaziland, southern Mozambique, Zambia, and Botswana led to low crop production and were partly responsible for the threat to life of 14.4 million people. (IRI, 2002). South Africa, Zimbabwe, Mozambique, and Zambia were affected by a drought in 2002/2003 with a major impact on agriculture (IRI, 2003). In 2004, the first half of the October-March rainy season produced below-normal precipitation in South Africa, Zimbabwe, Mozambique, Lesotho and Swaziland (IRI, 2004). Precipitation deficiency at different time scales from January 1986 to April 2004 were inferred from rain gauge observational data of the Global Precipitation Climatology Center (GPCC) a monthly analysis of surface precipitation at 1^{o} latitude × 1^{o} longitude resolution. Normalised anomalies (anomalies divided by standard deviation) and SPI values were calculated at each grid point at different time scale. This allowed us to do a preliminary assessment of the 2001-2004 droughts. Because the CRU encompasses 100 years and GPCC 19 years we cannot directly compare the area affected by drought using the SPI. Moreover, there are some discrepancies between the two datasets, especially in 97/98 and 98/99.

Area in square degrees and percentage of Southern Africa south of 10 S affected by drought for the eight worst droughts at the end of April.							
6-months scale (SPI <-1)				2-years scale (SPI<-1)			
Year	Area	%	ENSO	Year	Area	%	ENSO
1916	230	38 %	Neutral	1906	180	30 %	El Nino
1924	220	36 %	El Nino	1933	245	41 %	El Nino
1933	265	44 %	El Nino	1983	243	40 %	El Nino
1949	227	38 %	Neutral	1984	177	30 %	Neutral
1970	265	44 %	El Nino	1992	244	40 %	El Nino
1983	280	47 %	El Nino	1993	250	42 %	El Nino
1992	307	51 %	El Nino	1995	278	48 %	El Nino
1995	282	47 %	El Nino	1996	201	33 %	Neutral

Table 4: Area and percentage of Southern Africa land for the worst eight droughts at the 6 months and two year scale at the end of April with status of ENSO in summer of corresponding years.

According to GPCC data, 2002 was drier than normal during the heart of the rainy season, while part of southern Africa experienced a serious drought at all time scales during the 2003 rainy season. The beginning of the rainy season was very dry in 2004. Incidentally, ENSO happened in 2002/2003. GPCC data indicates that total rainfall at the 2-year scale was well below normal from December 2002 to April 2004 (in spite of above normal rainfall in February to April 2004) although the area impacted was not as extensive as for 1992 and 1993. The dry area with 2 year SPI < -1 at the end of April 2003 and April 2004 were respectively 60 % and 50 % of the dry areas for 1992. This would still place those years above the maximum value of the nine year running window mean (dashed line in Fig 9) using the 1992 value obtained with the CRU dataset and this extends in time the trend shown in Fig 9. It is important to note that the bad start to the 2003/2004 rainy season (third lowest total dry area for October to December 2003 of the 1986-2004 GPCC dataset) that followed the bad 2002/2003 rainy season (fourth lowest total dry area for November 2003 to April 2004) led to the third worst total dry area at the 2-year scale of December 2003 since 1986 (Fig 10).

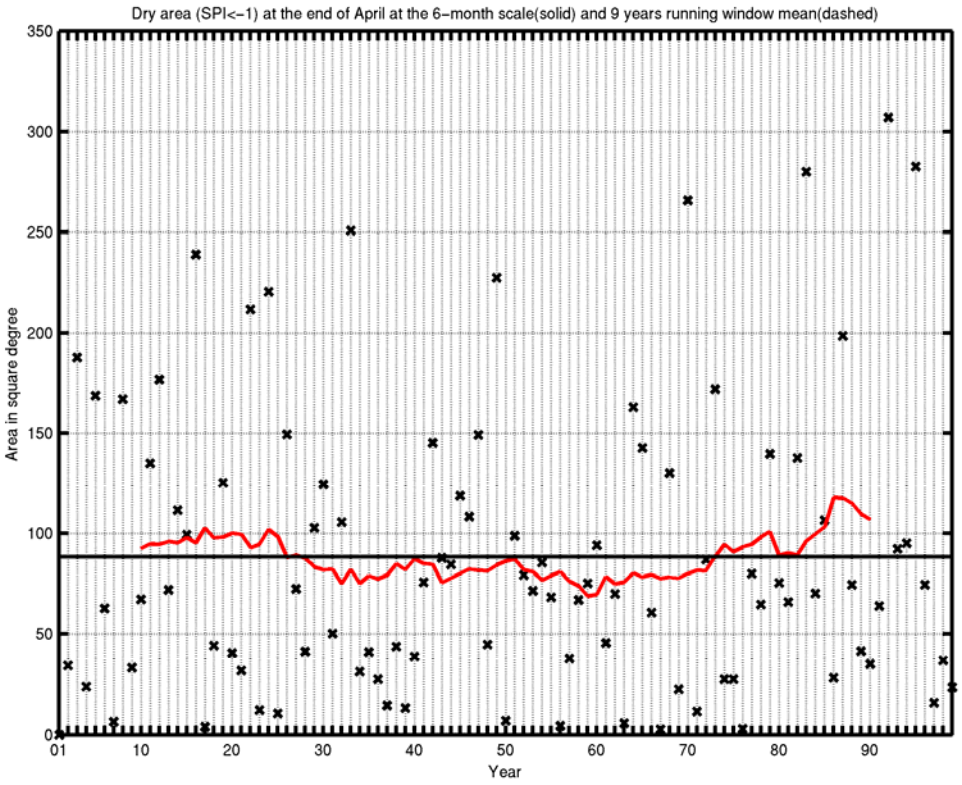

Figure 9: Area (in square degrees) affected by drought (SPI < -1) at the 6-month scale at the end of April of each year since 1901 (*) with a 9 years mean running windows (dashed line) and the overall 1901-1999 mean dry area (solid line).

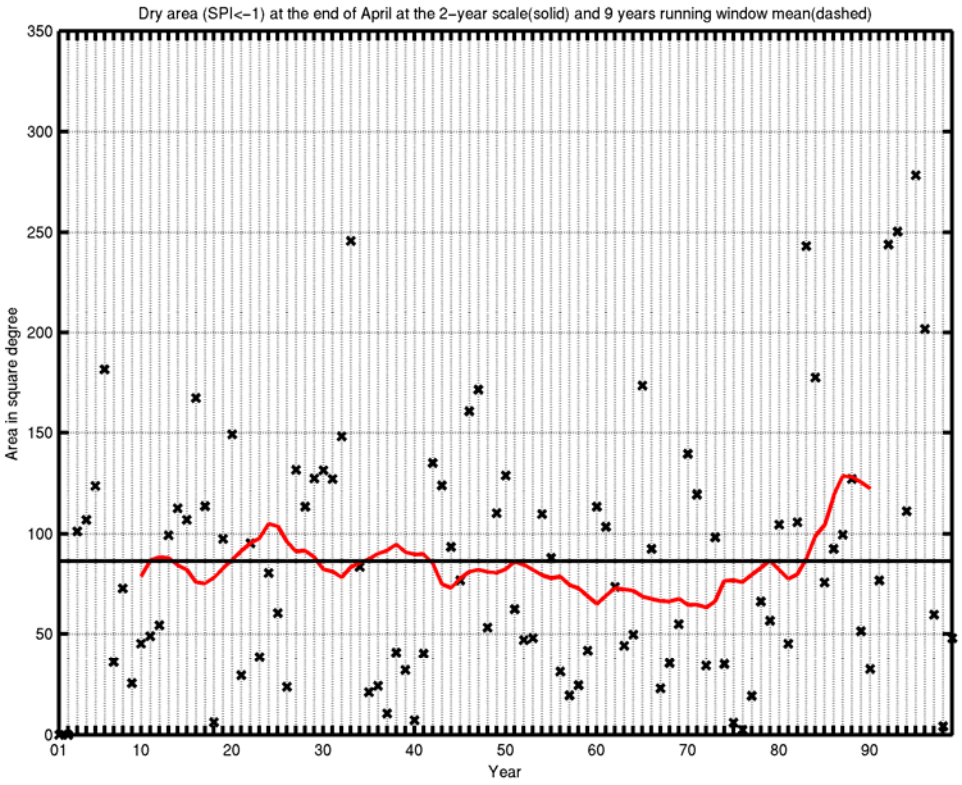

Figure 10: Area (in square degrees) affected by drought (SPI < -1) at the 2-year scale at the end of April of each year since 1903 (*) with a 9 years mean running windows (dashed line) and the overall 1903-1999 mean dry area (solid line).

3. Role of the ocean

3.1 El Niño, La Niña and Southern African Rainfall

Since the 70's the El Niño and La Niña phenomena have had an important impact on South African rainfall. Figure 1 show the correlation between sea surface temperature in the Pacific Ocean (Index Nino 3.4) and South African rainfall from 1970 to 1999, using 7500 rainfall stations from the WRC's daily raster database.

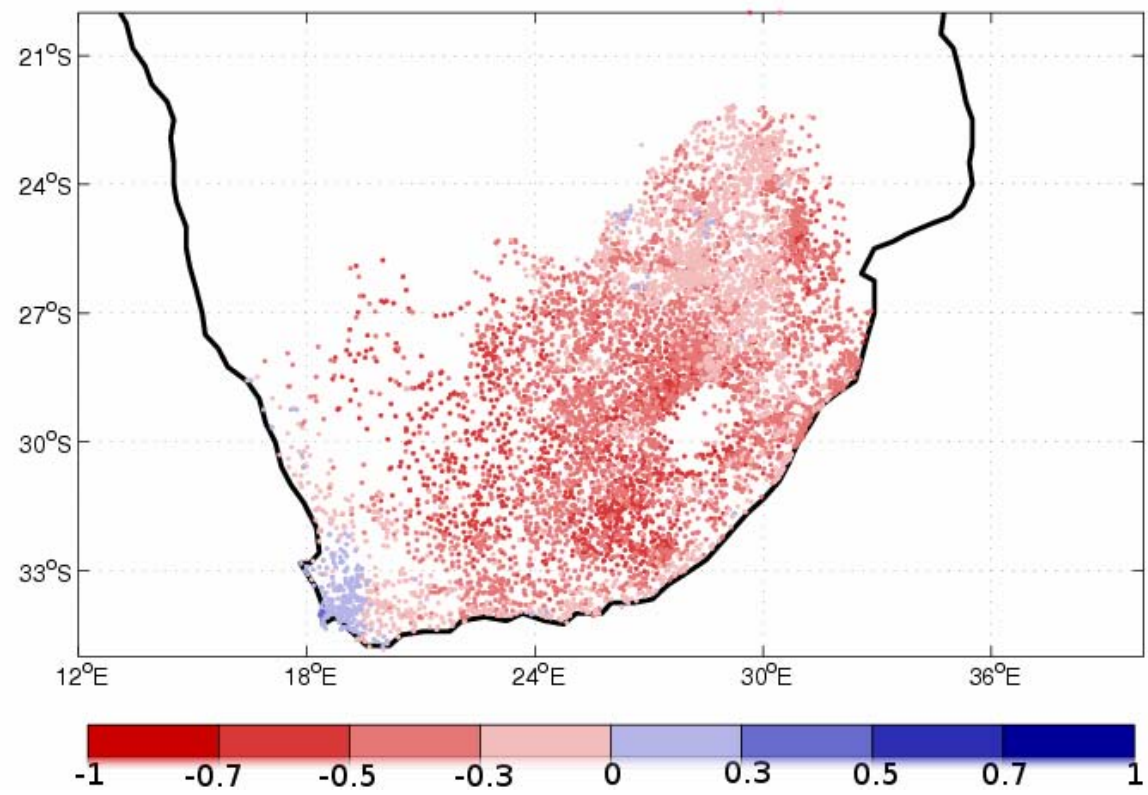

Figure 1: Synchronous correlation between Nino Index sea surface temperature and southern African rainfall for the 1970-1999 mean of November December January and February.

Figure 2 shows the correlation between sea surface temperature and South African mean summer (December-January-February) rainfall for the period 1958-2001. Figure 3 shows the correlation between South African summer rainfall and the depth of the thermocline (Z20) for the same period. The thermocline is found at a depth of between about 200 to 100 m and is a quantity that is closely linked to the heat content of the upper ocean. Our studies show that this quantity is just as relevant as SST in throwing light on the role of the oceans in influencing climate. Figure 3 proves that the whole upper ocean is involved in the forming of the SST anomalies that are linked to Southern African rainfall. While Figures 2 and 3 differ, some of the highly correlated domains are the same. The degree of correspondence gives us a better understanding of the mechanisms ruling the SST variations in keys areas, especially in relation to changes in the heat content of the ocean. Joint consideration of SSTs and ocean heat content also opens new avenues of research that this project has set out to pursue.

Two ocean areas stand out: the Pacific Ocean (especially the NINO 3.4 area) and the Indian Ocean. They are also the regions with the best correlation between the SST and the depth of the thermocline (Figure 4) and this relationship will help in using SST in key regions to forecast rainfall. It is now possible to calculate and display Z20, the upper ocean temperature or heat content and warm water volumes in real time. This gives us more elements than SST alone to study the mechanisms responsible for the SST anomalies at different time scales, from monthly to decadal. It already shows which areas act as the real triggers of the oceanic teleconnections with continents. For instance, negative SST anomalies in the Southern Oceans correspond to passive responses of the oceans to weather changes due to El Niño. South of 20S latitude decreases in wind speed due to El Niño decrease ocean mixing and exchange of energy due to the evaporation (latent heat flux is reduced when wind decrease). The area of negative anomalies in the subtropical northwest Atlantic is also a response to El Niño. So, in many respects, most of the signal see in Figures 2 and 3 is due to El Niño and its impact on the other oceans.

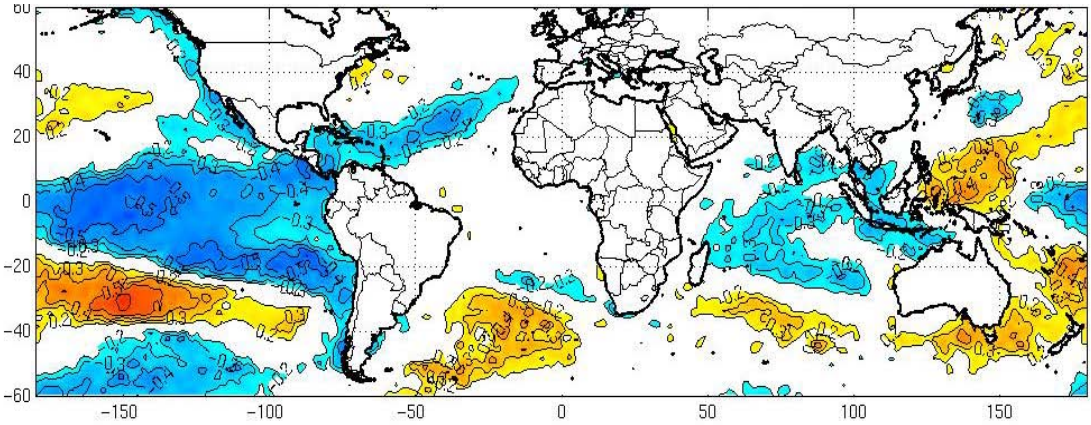

Figure 2: Synchronous correlation between sea surface temperature and southern African rainfall for the period 1958-2001 (mean of December January and February).

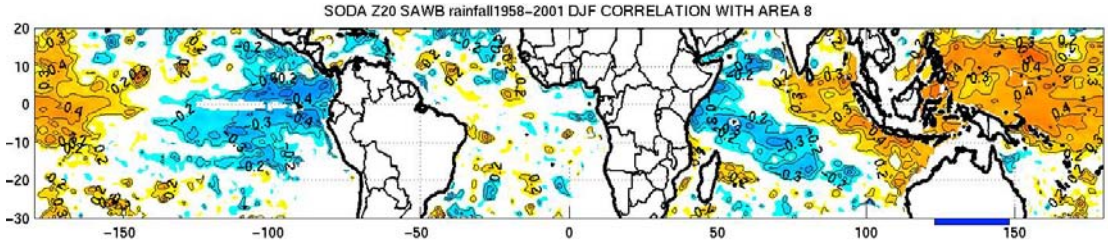

Figure 3: Correlation between the depth of the 20 C isotherms and southern African rainfall for the period 1958-2001 (mean of December January and February).

To highlight the last point, we present the mean sea surface temperature anomalies during El Niño in Figure 4 and the mean global rainfall during El Niño in Figure 5.

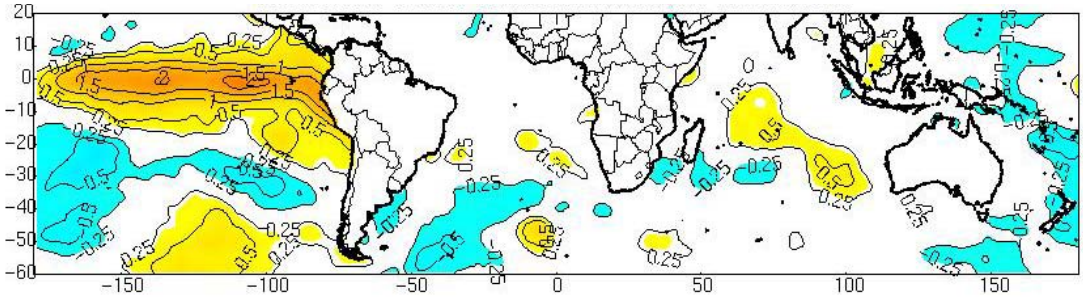

Figure 4: Sea surface temperature composite anomalies for the period 1982-2002 (mean of December January and February) during the mature phase of El Niño (82/83, 86/87 91/92 95/96 98/99).

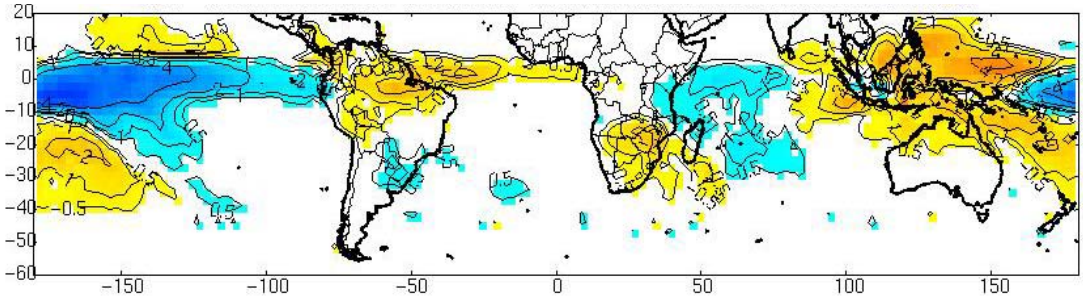

Figure 5: Precipitation composite anomalies (mm/day) for the period 1982-2002 (mean of December January and February) during the mature phase of El Niño (82/83, 86/87 91/92 95/96 98/99).

Figure 6 shows the correlation between rainfall in each of the 8 homogeneous rainfall regions and the NINO 3.4 domain index for each month of the year, the regions being North Western Cape (1), South-Western Cape (2), South Coast (3), Southern Interior (4), Western Interior (5), Central Interior (6), KwaZulu-Natal (7) and North-Eastern Interior (8). It further strengthens the relationship developed above at the regional scale. The correlation is for the 1950-2005 period. It is important to note that the correlation is even stronger from 1975 onwards, a relationship established during a previous WRC project (WRC Report Number 953/1/03; Rouault et al., 2003)

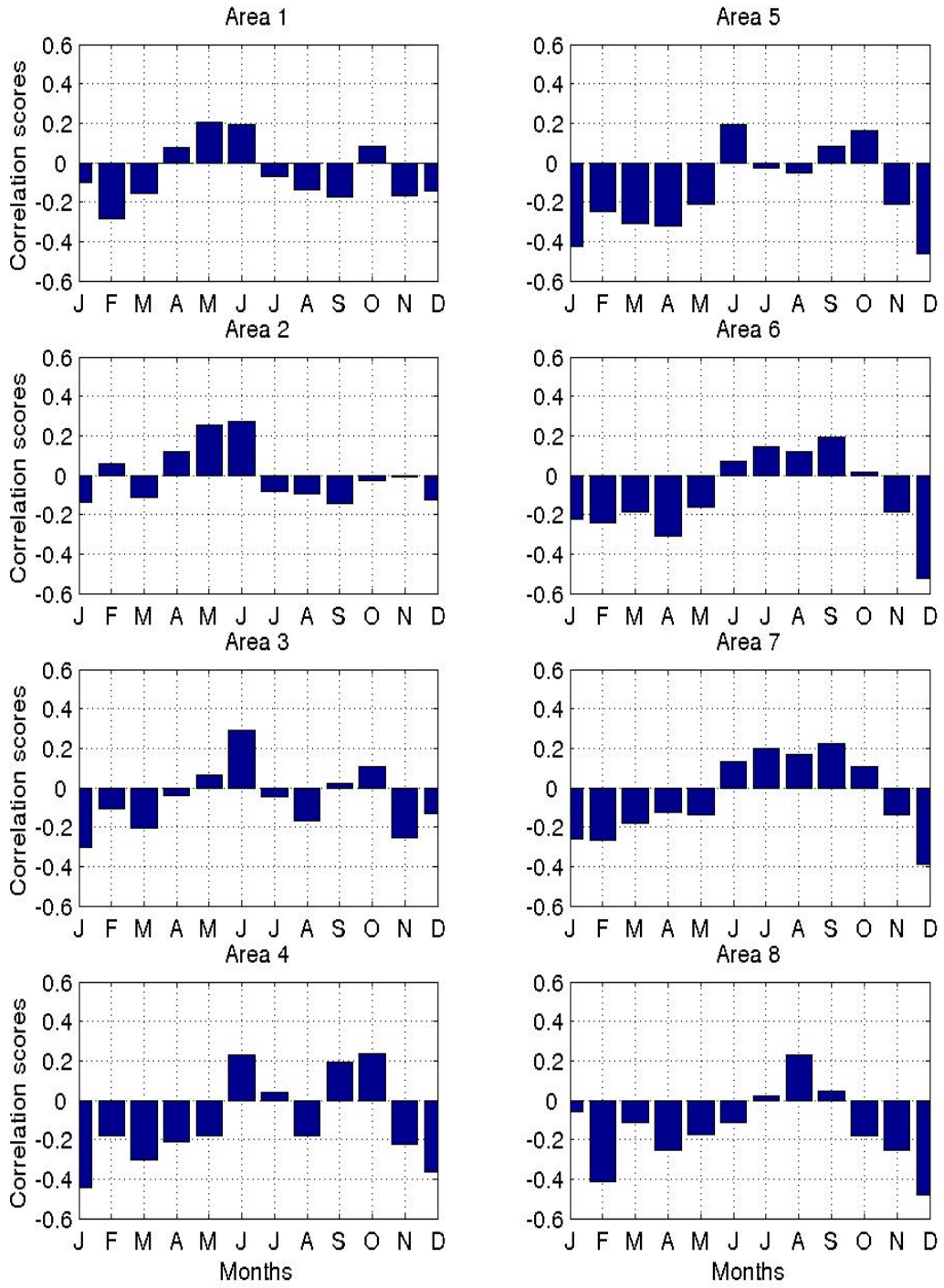

Figure 6: Synchronous correlation between the 8 rainfall areas of South Africa and NINO3.4 domain sea surface temperature index from January to December using data from 1950 to 2005. North-Western Cape (1); South-Western Cape (2), South Coast (3), Southern Interior (4), Western Interior (5), Central Interior (6), KwaZulu-Natal (7), North-Eastern Interior (8).

3.2 ENSO

El Niño events last about 12 to 18 months every 2 to 7 years with maximum warming in the Eastern Pacific in December and January, the time of seasonal maximum rainfall in Southern Africa. Wave dynamics (Rossby and Kelvin) along the equator

gives ENSO a quasi-oscillatory character. Rossby and Kelvin waves propagate the energy and momentum received by the wind stress. We discuss these waves later in the report. The atmosphere takes about 10 days to respond to SST changes but it takes a few months for the ocean to respond to wind stress changes. The memory of the system is in the ocean. ENSO is irregular in intensity and spatial extension. Warming in the Pacific Ocean can last longer than the usual ENSO (1990 – 1995 consisted of 3 warm events). The mean states of the oceans have some important variability and the interannual variability is superimposed on the mean state, thus changing the impact of ENSO on the weather. Change of properties since the 70's have been noted with periodicity of about 5 years and longer amplitudes than previously. Low frequency changes can be attributed to change in the mean state. There have been more warm than cold events during the past 25 years. There could also be a tendency to have longer periods with a warmer mean state.

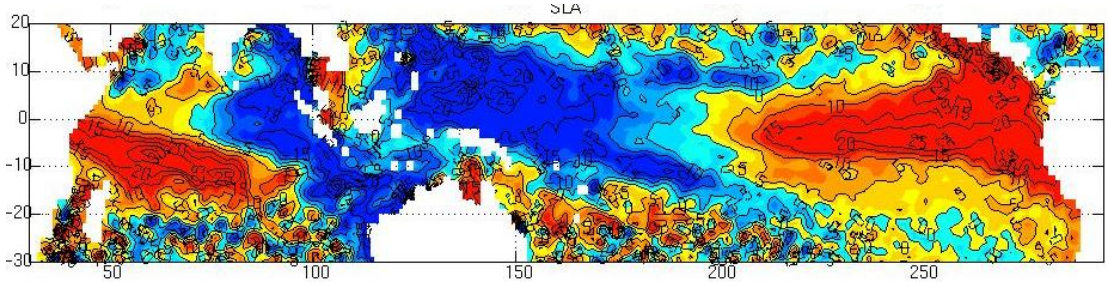

Figure 7: Sea level anomaly (SLA) estimated from altimetry in January 1998 during the mature phase of El Niño. Higher than normal SLA (in red) corresponds to abnormal heat content of the upper ocean above the thermocline.

Sea-level anomaly is the difference between the total sea-level and the average sea-level for a given time of year and is a good proxy for the estimated upper ocean heat content. The accuracy is about 2 to 3 cm. In the Pacific, El Niño is evident as higher than normal sea-levels in the east (in red), and lower than normal sea-levels in the west (in blue). The high sea-levels in the Indian Ocean reflect the impact of El Niño in the Indian Ocean Pacific and some variability internal to the Indian Ocean. In general, and as a first approximation, variations in the depth of the main thermocline can be associated with variations in the sea level anomaly field, where the sea level anomaly is the value of the sea surface height at a fixed location with respect to a mean value in that same location. The sea level anomaly fields used here are a blended altimeter product that combines data from several altimeters (TOPEX, JASON, EUMETSAT, ERS) and that provide weekly and monthly data since 1992 at a 30 km resolution. Figure 7 illustrates sea level anomalies for January 1998 during the mature phase of El Niño. The SST anomalies for January 1998 (Figure 8) partially reflect the SLA in Figure 7.

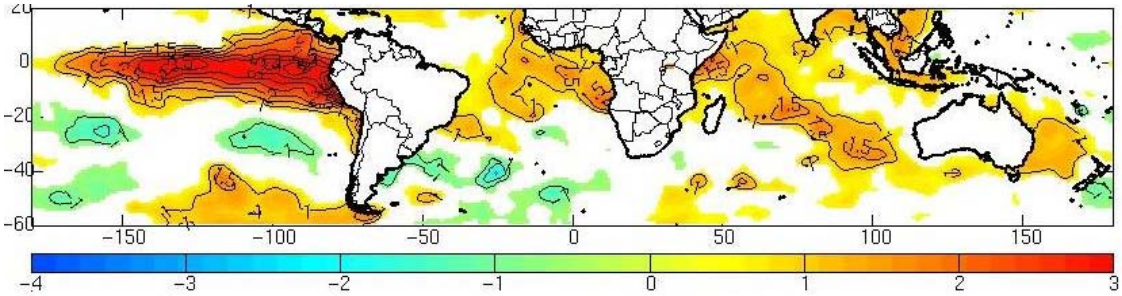

Figure 8: SST anomaly from the 1950-2004 January mean in January 1998 with the Hadley SST dataset.

3.2.1 Normal condition

During normal conditions, winds blow from east to west, due to differences in the atmospheric pressure. A high pressure system sits over the eastern Pacific, while a low pressure system sits over the western Pacific. Because of the low pressure system in the west, there is increased upward convection and these results in more rainfall in the west than in the east. At the same time, the surface currents along the equator generally move east to west. This transports water warmed year round by the sun to the western Pacific, where it tends to pile up before flowing north and south as other currents. This pushes down the thermocline and further warms the upper ocean. In the east, cold water upwells, or rises up from great depths to replace the warm water which flowed west, and the thermocline is shallow. All of this will cause a certain sea-level signature, since sea-level is a measure of the integrated water density. Warmer water has a lower density than colder water, and takes up a greater volume. Thus, sea-level is higher where the thermocline is depressed and the upper waters are warm, and sea-level is lower where the thermocline is raised and upper water is cool.

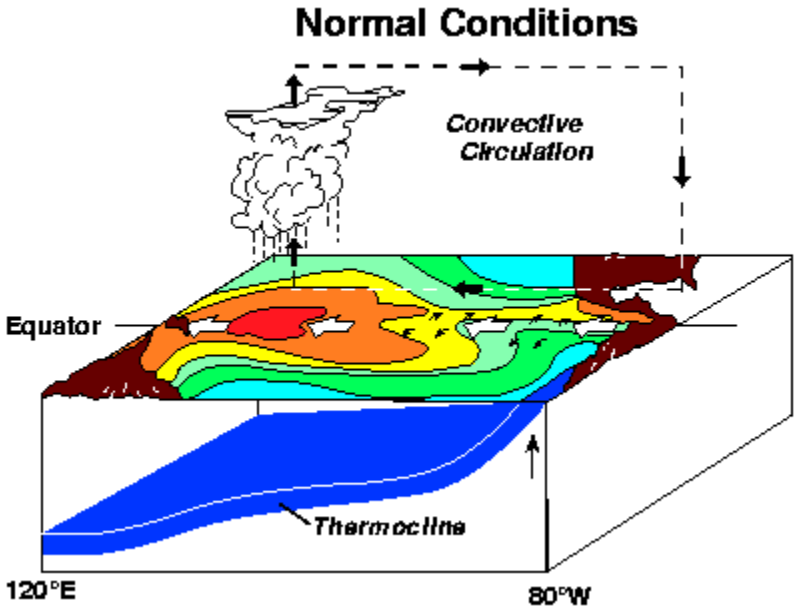

Figure 9: In normal conditions the trade winds blow eastwards across the tropical Pacific. These winds pile up warm surface water in the west Pacific. The sea surface is about 1/2 meter higher at Indonesia than at Ecuador. The sea surface temperature is about 8 C higher in the west, with cool temperatures off South America, due to an upwelling of cold water from deeper levels. Rainfall is found in rising air over the warmest water, the east Pacific is dryer (Figure courtesy NOAA)

3.2.2 El Niño

Several weeks to several months before El Niño begins to manifest in the eastern Pacific, a change occurs in the atmosphere over the Pacific. The pressure over the western Pacific increases while the pressure in the east decreases. This causes a change in the wind pattern and the convection, as shown in the Figure 10. This atmospheric change is called the Southern Oscillation. The trade winds decrease or even reverse and blow west to east. The equatorial surface current slows, and a subsurface current increase. This undercurrent has a core at about 100 meters depth and always flows west to east. Most of the time it dies out in the central Pacific. During El Niño, though, the current is strong all the way to the Galapagos Islands off the coast of South America; it sometimes surfaces. Thus, there is a change in the

ocean associated with the Southern Oscillation. In the west, the thermocline rises and warm water flows east. In the east, months after the initial wind changes, the thermocline gets deeper. The upper water column warms, and the sea-level rises. However other phenomenons are at work. The ocean takes some time to adjust to the wind changes. One of the primary ways it adjusts during El Niño is through the creation of Kelvin waves.

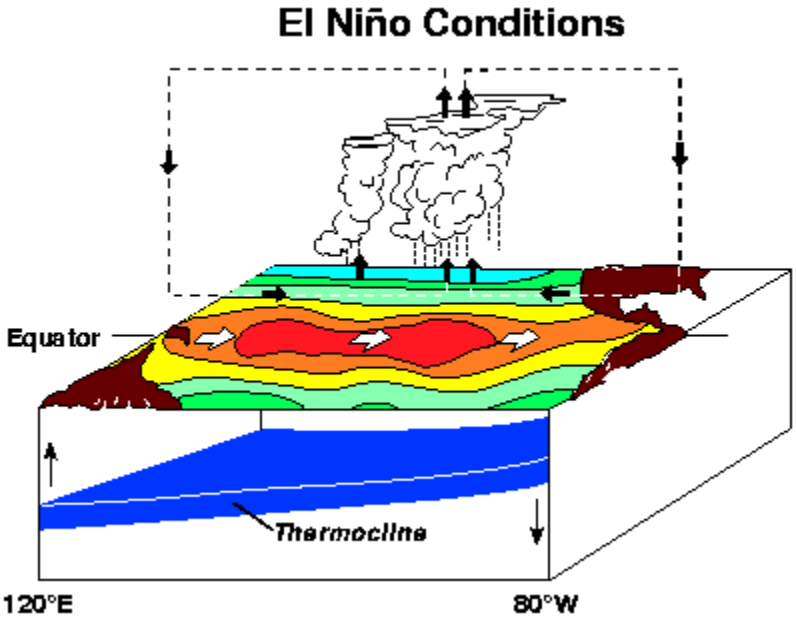

Figure 10: During El Niño, the trade winds relax in the central and western Pacific leading to a depression of the thermocline in the eastern Pacific, and an elevation of the thermocline in the west. This reduces the efficiency of upwelling to cool the surface. The result is a rise in sea surface temperature. Rainfall follows the warm water eastward, with associated flooding in Peru and drought in Indonesia and Australia. The eastward displacement of the atmospheric heat source overlaying the warmest water results in large changes in the global atmospheric circulation, which in turn force changes in weather in regions far removed from the tropical Pacific (Figure courtesy NOAA).

3.2.3 La Niña

La Niña is characterized by unusually cold ocean temperatures in the Equatorial Pacific, compared to El Niño which is characterized by unusually warm ocean temperatures in the Equatorial Pacific.

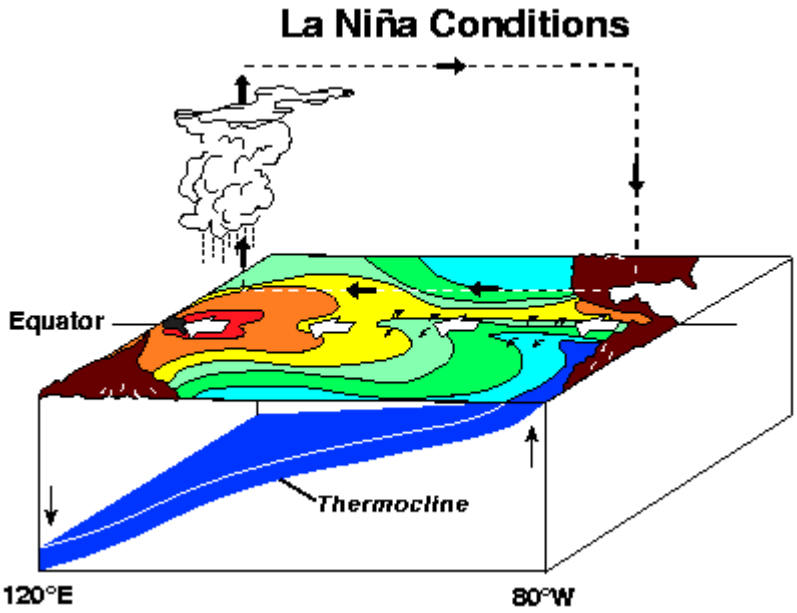

Figure 11: Condition during La Niña (Figure courtesy NOAA copyright AMS)

3.3 Indian Ocean and El Niño

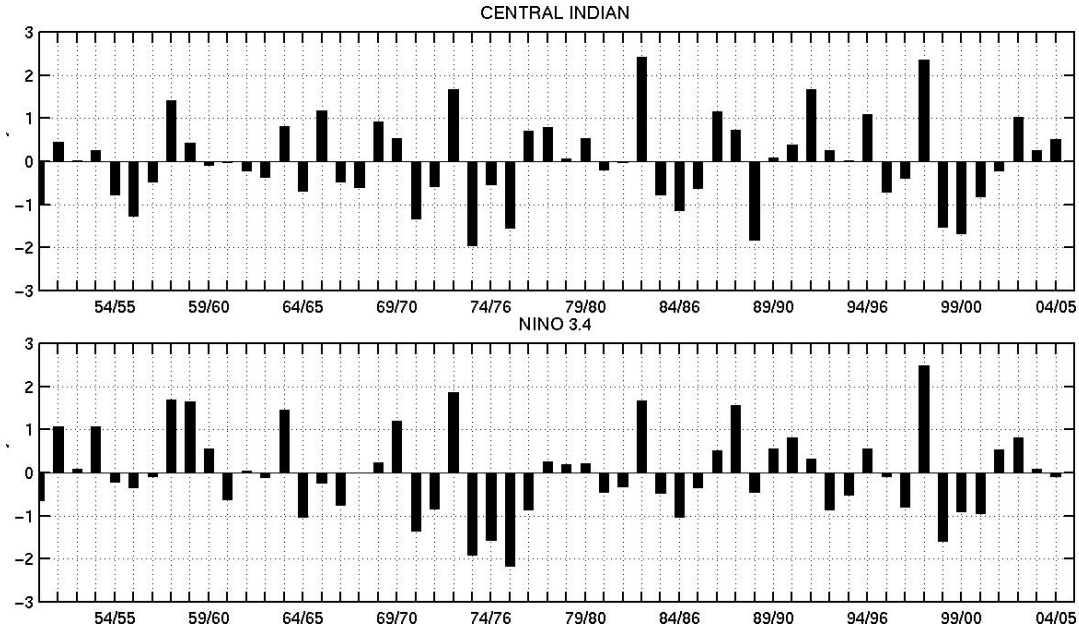

Figure 12: Mean of December January and February sea surface temperature NINO 3.4 index and Indian Ocean index since 1950. Indices are normalized sea surface temperature anomalies (DJF anomalies from the 1950-2004 mean divided by DJF standard deviation) in the same size domains in the Pacific and in the Indian Ocean. The correlation between the two is 0.8 underlying the important influence the Pacific Ocean has on the Indian Ocean. The SST in the Indian Ocean was detrended due to a clear warming trend that Richard et al. (2001) demonstrated to be the cause of the increase in the spatial extension of droughts since the since the 80's

Recently, several studies have looked at SST warming in the southwestern Indian Ocean and the eastern Pacific, and have found that there is a significant correlation between anomalous warming in the Indian Ocean and El Niño (Figure 12) , although SST signals in the eastern Pacific are much larger. These studies (Tourre and White, 1995; Nicholson, 1997) have found correlations between the Indian Ocean and the Pacific for almost every El Niño back to 1946. Chambers et al. (2000) has looked at the T/P altimeter data and see a similar correlation, but the extreme sea-level values are closer to the same magnitude. By combining all of these observations with the high resolution maps made from the TOPEX/Poseidon data, one can begin to see how the Indian Ocean warming is related to El Niño. ENSO has a big influence on the Indian Ocean. A basin wide SST anomaly triggered by ENSO is the dominant mode of variability and the mechanisms linking the two are not well understood. Many observational studies show that the El Niño–Southern Oscillation (ENSO) induces substantial sea surface temperature (SST) variations in other tropical oceans. For example, the Indian Ocean witnesses a basin wide warming in boreal winter that peaks in the following spring after the mature phase of El Niño. Klein et al. (1999) and Murtugudde and Busalacchi (1999) find that surface heat flux is the major mechanism for ENSO-induced warming in the north Indian Ocean. In particular, Klein et al. (1999) showed that changes in atmospheric circulation accompanying El Niño induce changes in cloud cover and evaporation that, in turn, increase the net heat flux entering the remote oceans—the concept of an “atmospheric bridge” that connects SST anomalies in the central equatorial Pacific to those in remote tropical oceans. That mechanism, however, does not explain the SST fluctuations over the southwest Indian Ocean (SWIO) where the anomalies typically reach a maximum (Klein et al., 1999). Xie et al. (2002) and Huang and Kinter (2002) demonstrated that much of SWIO SST variability is not locally forced but is due instead to oceanic Rossby waves that propagate from the east. They showed that such a subsurface effect on SST in the SWIO is made possible by the simultaneous presence of mean upwelling and a shallow thermocline dome and further demonstrated that ENSO is the dominant forcing for the SWIO thermocline variability. Xie et al. (2002) noted that, when an El Niño event occurs, anomalous easterlies appear in the equatorial Indian Ocean, forcing a westward-propagating downwelling Rossby wave in the southern Indian Ocean. In summary, both through atmospheric and oceanic processes, El Niño accounts for the basin wide SST variations observed over the tropical Indian Ocean (TIO).

3.4 Role of wave dynamics

Although surface currents along the equator typically flow east to west, the net transport of water in the equator occurs deeper and is away from the equator as shown above. This is called the Ekman transport. The transport is caused by the winds and the Coriolis force, which is caused by the rotation of the Earth. The net water transport is below the surface and perpendicular to the wind direction; to the right of the wind in the north, and to the left of the wind in the south. Thus, since the trade winds tend to blow east to west in the equatorial region, the net transport is away from the equator. Notice the much deeper thermocline, or the boundary between the warm and cold water, in the west than in the east.

During the Southern Oscillation, winds are weaker in the west; thus the wind anomaly, or deviation from an average wind for that time of year is from west to east. This causes a change in the Ekman transport in this region. Instead of flowing away from the equator, it flows toward the equator. To balance this anomalous influx of water, the warm water in the upper layer downwells to the lower layer. However, the warm water is lighter than the cooler water, and is naturally more buoyant. The forcing of the warmer water into the cooler water will cause an oscillation, normally at

the steepest density gradient, in the thermocline. These oscillations will propagate away from the source of the wind anomaly as very long waves. Along the equator these are called Kelvin waves and they change the thickness of the warm water in both the west and east, which causes a change in the heat content of the upper ocean, large sea-level changes and leads to El Niño

Kelvin waves can cross the Pacific in two months. They can only exist near the equator due to the Earth's rotation. The amplitude of the Kelvin wave is several tens of meters along the thermocline, and the length of the wave is thousands of kilometers (1 degree of longitude = 111 km)

Figure 13 shows a time longitude Hovmoller plot of SLA along the Equator. The time is from January 1997 at the bottom to December 1999 at the top.

The yellow/orange lines which slope across the Pacific beginning in January 1997 indicate Kelvin waves. Eastward movement is indicated by the slope in time from west to east. These waves set up a change in the warm water thickness of the Eastern Pacific beginning in March. Other Kelvin waves are visible after El Niño developed; the first two, indicated by arrows, were early indicators that an El Niño would probably occur this year. Because a Kelvin wave is associated with density fluctuations inside the ocean, it can be seen in the sea-level measurements made by altimeters, although with a reduced magnitude. Notice the amplitude of the two Kelvin waves, from 10 to 15 cm at sea-level compared to 30 and 40 meters in the thermocline change. A depression in the thermocline is associated with an increase in sea-level.

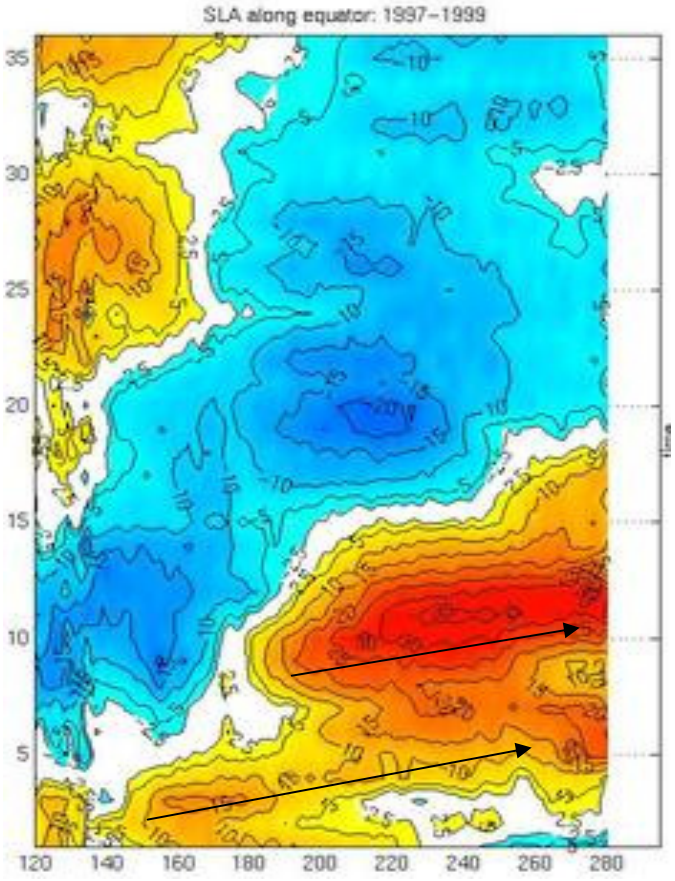

Figure 13: Time longitude Hovmoller plot of sea level anomalies along the Equator in the Pacific Ocean during El Nino. The time is from January 1997 at the bottom to December 1999 at the top.

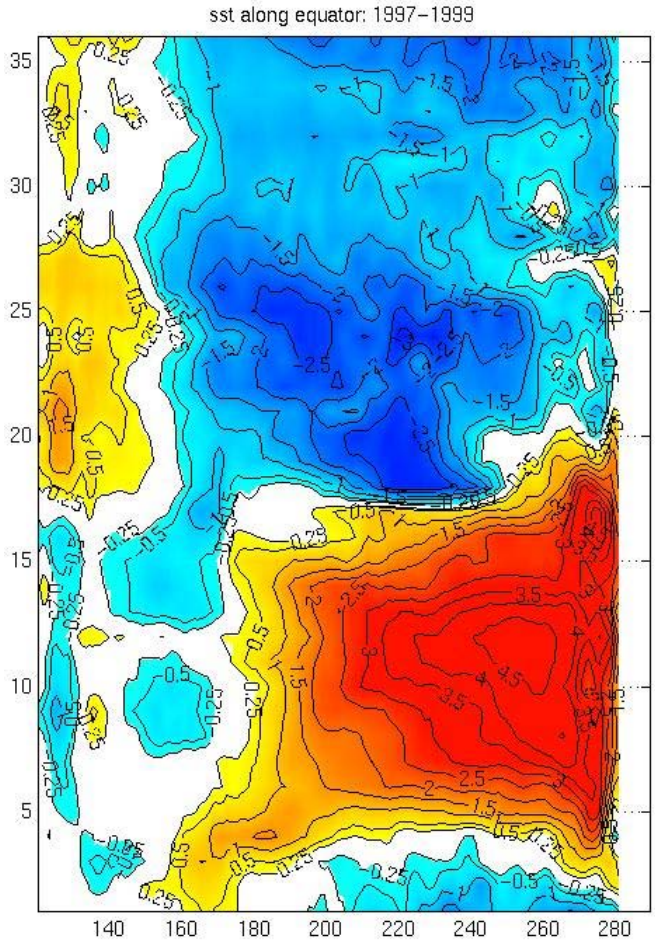

Figure 14: Time longitude Hovmoller plot of sea surface temperature anomalies along the Equator in the Pacific Ocean during El Nino showing the delayed response to SLA anomalies of the SST. The time is from January 1997 at the bottom to December 1999 at the top.

The Kelvin waves travel east and set up changes in the eastern Pacific that lead to El Niño by depressing the thermocline there. We have used the all 1992-2005 SLA data to look at propagative feature in the Pacific and Indian Ocean. There are smaller Kelvin waves in 1995 and 1996. These are seasonal, and do not cause El Niño events. However, large Kelvin waves, such as those observed in early 1997, almost always lead to El Niño events.

However, there are significant differences. Ignoring for a moment the sea-level effects of currents, winds, and other forces, much of the early El Niño signal occurs below the ocean surface. It takes some time for heating at 100 m to reach the surface. However, the changes will be seen in the sea-level measured by altimetry or the moored buoys which monitor temperature to a deep level as they are happening. This means that altimetry (Figure 13) can see El Niño signals slightly before the SST measurements (Figure 14) can. The difference in time is only slight, about two weeks to a month. However by combining the two measurements one can get a more complete picture of how El Niño evolves.

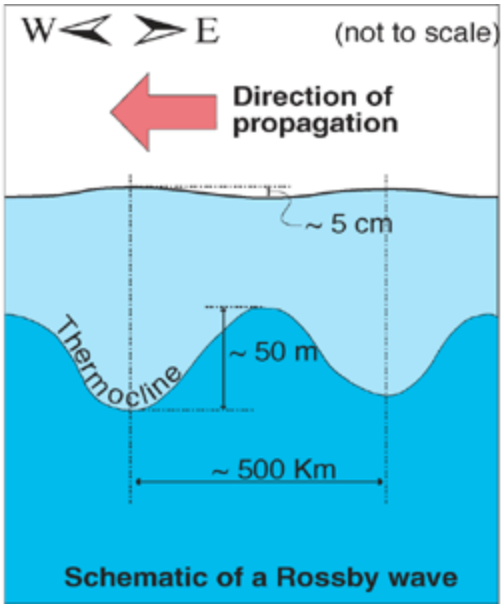

Figure 15: Schematic of a Rossby waves (courtesy SOC)

The deeper thermocline in the west forms due to strong Eckman pumping and Rossby wave mechanisms (Figure 15). Cold SST anomalies near Java propagate along the West coast of Australia. The ENSO signal in the western Pacific intrudes into the Eastern Indian Ocean through the coastal wave guide around Australia. SST in the Eastern Indian Ocean in the Australian spring and summer is influenced by ENSO. Upwelling and evaporation increase the cooling and thus increase the temperature gradient, further enhancing the atmospheric response due to the SST contrast between west and east.

SST is strongly coupled to upper ocean temperature and the depth of the thermocline especially in the domain important for South African rainfall. Rossby waves are forced by the wind stress curl along the Rossby wave pathway. Rossby waves play an important role in the ocean atmosphere interaction of the Southern Ocean where the doming of the mean thermocline allows subsurface anomalies to affect SST. Those Rossby Waves can be forced by ENSO or by local phenomenon and the relative importance of the forcing varies with latitude. In the central and western Indian Ocean the contribution of the wind field to SST anomalies is very large (Konda et al., 2002; Soyi et al., 1999; Webster et al., 1999). Westward wind anomalies in the East during ENSO (Reason, 2000) create a strong wind curl anomaly from East to the central region. The anomaly of tropical SST changes almost simultaneously in the central and western area, mostly explained by meridional Eckman transport. The western part is affected by wind driven Eckman transport and Eckman pumping.

Rossby waves (Figure 15) are generated by atmospheric forcing from winds and buoyancy effects from solar heating and are the principal means by which localized climatic effects drive the global response of the ocean. Waves propagate at only a few cm/s, have wavelengths of up to hundreds of km and result in only a few cm elevation at the sea surface. However, their passage can result in displacements of the thermocline of the order of many meters. It is believed that Rossby waves play an important role in generating the SLA anomalies and some of the SST anomalies observed in the Indian Ocean after the impact of El Nino. The SLA propagates eastwards South of the Equator. The speed varies with latitude and increases equatorward, but is of the order of a few km/day. This means that at mid-latitudes

(say, 30 degrees N or S) one such wave may take several months - or even years - to cross the Pacific Ocean.

3.5 Role of heat content

3.5.1 Introduction

The Mozambique Channel is a wide strait, being 370 km at its narrowest and 1600 km at its widest. The circulation in the Channel itself has become better known by direct observations during the past decade. Instead of the presence of a continuous, intense western boundary current, the presumed Mozambique Current, it has now been shown (De Ruijter et al., 2002) that the circulation is dominated by a train of warm, anti-cyclonic eddies progressing polewards along the western side of the channel. These eddies have cross sections of about 350 km, maximum surface velocities of 2 ms^{-1}, and extend all the way to the sea floor. About 4 are formed per year (Ridderinkhof and de Ruijter, 2003). There is some evidence of the occasional presence of weak, colder, cyclonic features.

Tropical lows, associated with the Inter-tropical Convergence Zone (ITCZ), are characteristic atmospheric features of the region during the austral summer. Roughly 60% of tropical lows reach cyclone intensity here, i.e. they attain surface wind speeds exceeding 33 ms^{-1}. Less than 5 % of the total numbers of south west Indian Ocean (SWIO) tropical cyclones make landfall on the southern African mainland mainly due to the role of mid-level (500 hPa) winds in the eastward propagation of tropical cyclones (Vitard et al., 2003; Reason and Keibel, 2004). Those that make landfall in Mozambique usually are in category 4 of the Saffir and Simpson (Saffir, 1974) scale, with sustained winds up to 70 ms^{-1} and causing extreme damage. Only a few cyclones per decade form over the Mozambique Channel itself. Tropical cyclones develop over waters warmer than 27ºC (Anthes, 1982) and high surface temperatures in the Mozambique Channel may therefore conceivably act as an energy source for passing cyclones or to generate cyclone there. Shay et al. (2000) have demonstrated that hurricanes (cyclones) can rapidly intensify when passing over warm eddies, gaining greater energy than over adjacent ocean regions. Failures in cyclone prediction have consequently been blamed on the lack of incorporating subsurface thermal structure and heat content of the ocean into models. What effect may Mozambique eddies therefore have on cyclone intensification?

We have analysed merged altimetric data from TOPEX-Poseidon, Jason1 and ERS (Ducet et al., 2000) to identify Mozambique eddies and estimate sea surface temperatures based on measurements from the microwave sensor on the Tropical Rainfall Measuring Mission (Stammer et al., 2002). This latter system has also been used to obtain information on precipitation. Scatterometer estimates of wind speed came from the QuickScat satellite from 1999. We present results for three characteristic cyclones: Hudah, that crossed the Channel in 1999; Eline, formed east of Madagascar in 2002 and Japhet that was generated over the Mozambique Channel in 2003.

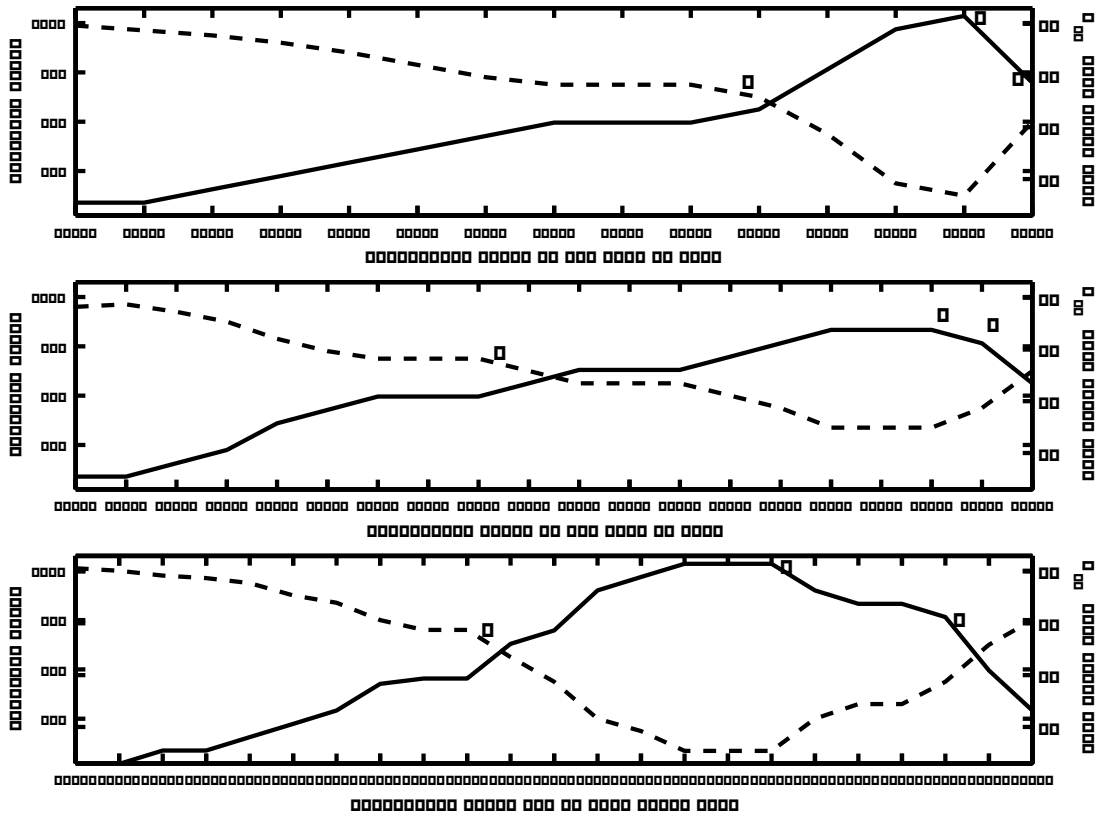

Figure 16: The intensification of tropical cyclones Eline (upper panel), Hudah (middle panel) and Japhet (bottom panel) during their passage across the Mozambique Channel. Solid lines indicate winds speeds averaged for 10 minute periods; broken lines atmospheric pressure. AB indicate the presence of warm eddies below the cyclone's track and C indicates landfall.

3.5.2 Cyclone intensification

Cyclone Hudah originated in the ITCZ near Australia, moved zonally over the width of the South Indian Ocean and made landfall on the north-east of Madagascar as an intense cyclone destroying a large part of the town Antalaha with the deaths of 24 people and 30 000 disaster victims. Over the land mass of Madagascar cyclone Hudah weakened significantly (viz. Figure 19), but started intensifying again over the channel (Figure 16) particularly on moving south-westward over a warm eddy in the eddy street of the channel. It was upgraded to a tropical cyclone on 5 April, reached peak intensity (Figure 16) during 7 April and made landfall on 8 April near the town of Pebane causing the deaths of 4 persons. It then rapidly lost its intensity over land (Figure 16).

Cyclone Eline started as a moderate tropical storm 250 km south of Bali on 4 February 2000. It moved more or less zonally across the Indian Ocean and crossed over Madagascar to the Mozambique Channel on 19 February. Over the channel cyclone Eline moved in a south-westerly direction, slowly gaining in wind speed and decreasing in pressure (Figure 16). By 21 February, as it entered the warm eddy street [Schouten et al., 2003] on the western side of the channel, it exhibited a rapid increase in wind speed from about 30 ms^{-1} to 52 ms^{-1} accompanied by an even more marked decrease in pressure (975 hPa to 930 hPa in less than 18 hours; Figure 16). It thus changed from a tropical depression to a category 3 hurricane during this short period. It subsequently started moving at about 30 km/day, now in a west-north-westerly direction. It made landfall 90 km south of the city of Beira in Mozambique

(Figure 16) on 22 February and its intensity dropped strongly (Figure 16) at the same time, as would be expected. It generated very rough and high seas along this coastline within a radius of 90-120 km from its centre. By 23 February the cyclone was to be found well over land, 200 km south-east of the city of Harare, Zimbabwe. Although it is expected that cyclones weaken when passing across Madagascar, the presence of a warm eddy in the channel could have played a role in the intensification.

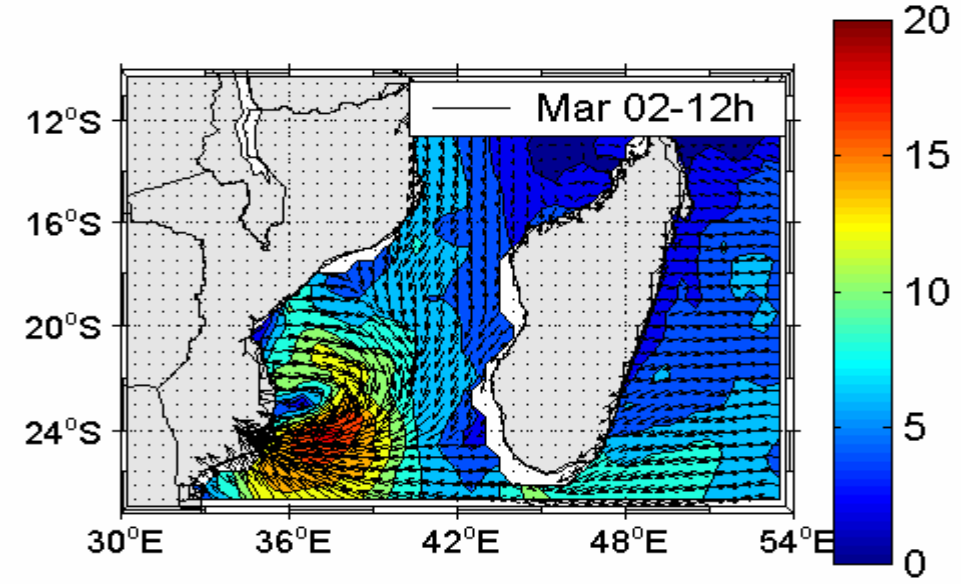

Figure 17: Strengthening of surface winds in tropical cyclone Japhet as it moved across the Mozambique Channel on the March 2 2003. This wind field ($m.s^{-1}$) is from the scatterometer on the QuickScat satellite. Arrows denote wind direction at grid points 25 km apart; colour gives wind speeds in ms^{-1} according to the colour scale.

By contrast, cyclone Japhet was formed as a weak feature off the south-western coast of Madagascar on 25 February 2003, drifting slowly southward (viz. Figure 18). A transitory ridge, approaching from the south-west, altered the cyclone track to the west. On the ridge weakening, the track changed to the south-southwest and the cyclone moved in this direction at a high speed of about 40 km/day. The cyclone had been steadily intensifying (Figure 16) the winds having reached an estimated 28 ms^{-1} by 28 February. On 1 March cyclone Japhet suddenly changed direction to a north-westerly course (viz. Figure 3), its wind speed started increasing rapidly reaching a maximum of 52 ms^{-1} within less than 24 hours. This marked change occurred, as in the case of cyclone Eline, over the average pathway of warm Mozambique eddies.

Subsequently its intensity declined slightly (Figure 16) so that by the time it made landfall on the coast, its maximum speeds had been reduced to 41 ms^{-1}. How representative are these traces of maximum wind speed for the cyclones as a whole?

The example of cyclone Japhet is given in Figure 17. Inspection of twice daily Quickscat wind speed for March 2 2003 shows the intensification pattern of Figure 16. By 2 March when the cyclone was over the western side of the channel (viz. Figure 18) a tight cyclone-shaped storm was evident exhibiting a clear annulus of speeds far in excess of 20 ms^{-1}. The development of cyclones Eline and Hudah (not shown here) was, in most pertinent respects, very similar. Could one assume that part of the energy required for the intensification of these cyclones came from the input of Mozambique Channel eddies? Satellite images of sea surface temperatures before and after the passage of the cyclones may be indicative.

3.5.3 Surface cooling by cyclones

It has been shown that the passage of a cyclone may leave a surface scar of considerably reduced sea surface temperatures in its wake [e.g. Price, 1981; Stramma et al., 1986]. There is general consensus that by far the major cooling effect is the consequence of wind mixing [Greatbatch, 1985]. In the case of the cyclones under discussion, cooling is clearly seen in satellite images of the sea surface temperature (e.g. Figure 18). These microwave observations are not affected by persistent cloud cover and are therefore ideal for studying the results of the passage of a cyclone. Only the results of cyclone Japhet are shown here; those of cyclones Eline and Hudah being sufficiently similar. The upper panel of Figure 18 – for the period 22-28 February, i.e. before the passage of the cyclone – shows typical sea surface temperatures for the Mozambique Channel during austral summer months. Large parts of the region were warmer than 30ºC with a characteristic zonal front spanning the southern mouth of the channel. After the passage of cyclone Japhet (lower panel, 8-14 March 2003) the sea surface temperatures were markedly altered. Over the greater part of the southern channel temperatures now were below 29ºC while along that part of the track taken by the cyclone after it had intensified temperatures had decreased by 2º to 8ºC. This implies vertical mixing of the water column in that part of the Mozambique Channel to a depth of up to 100 m (vertical temperature sections for the region are given by De Ruijter et al. [2002]). The wind direction being contrary to that required for coastal upwelling (viz. Figure 17) these lower temperatures must be due largely to mixing in the upper layers. The signal of all three cyclones in surface temperatures lasted for one to two weeks.

3.5.4 Interaction with Mozambique eddies

From the above there are strong indications that the intensification of all three these tropical cyclones was greater in the corridor where warm Mozambique eddies would be expected. Although other factors could lead to the intensification, the question therefore arises what quantifiable contribution these eddies might make to the intensification of passing cyclones. The eddies are not easily distinguishable in sea winds in the region. At a depth where mixing due to the passage of a tropical cyclone would be prevalent, say 50 m, the temperature difference in an eddy and outside it might be about 5ºC [De Ruijter et al., 2002] making these eddies potentially a rich source of energy for cyclone strengthening.

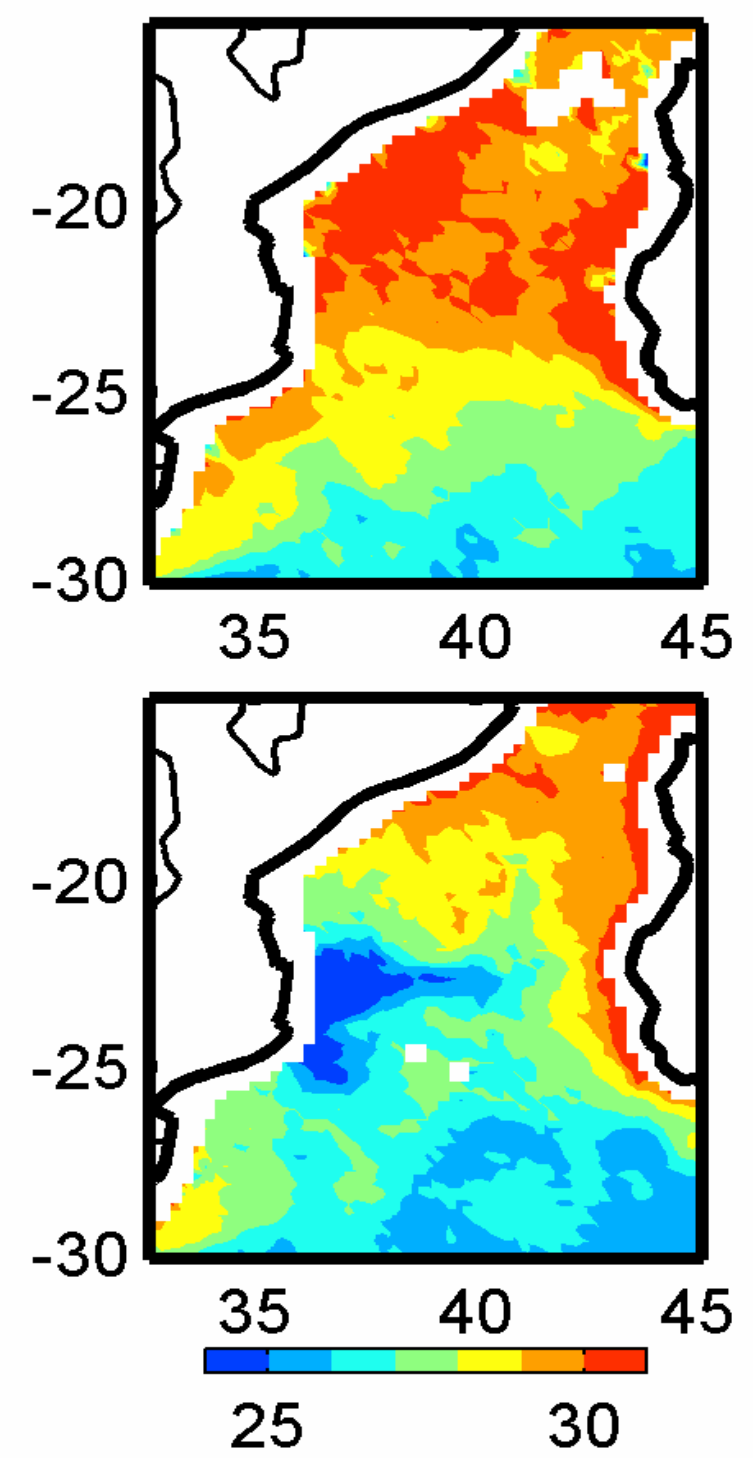

Figure 18: Changes in sea surface temperatures of the Mozambique Channel due to the passage of tropical cyclone Japhet. Top: weekly mean centered on February 23, bottom: weekly mean centered on March 4. The daily temperatures (°C) are derived from TRMM microwave imager. The upper panel is for the week preceding the surface temperatures due to continuous surface warming and the prevalence of light

The track of cyclone Hudah relative to warm eddies, as located from satellite altimetry, is given in Figure 19. These eddies exemplified here have a positive heat content anomaly relative to their general environment. This heat storage was calculated using altimetric observations and the methodology of Chambers et al. [2000]. The track of the cyclone shows that it moved directly over the eddy located at

16ºS, 42ºE (Figure 19). This eddy exhibited a heat content anomaly of 100 KJ.cm^{-2} before the passage of cyclone Hudah that was reduced to less than 50 KJ.cm^{-2} after its passage. During this period the intensity of cyclone Hudah, as measured by wind speed, increased substantially (viz. Figure 16). Although it could be coincidental there is a possibility that the passage of cyclone Hudah caused the diminution in the heat content of this Mozambique eddy and part of that energy fed the cyclone.

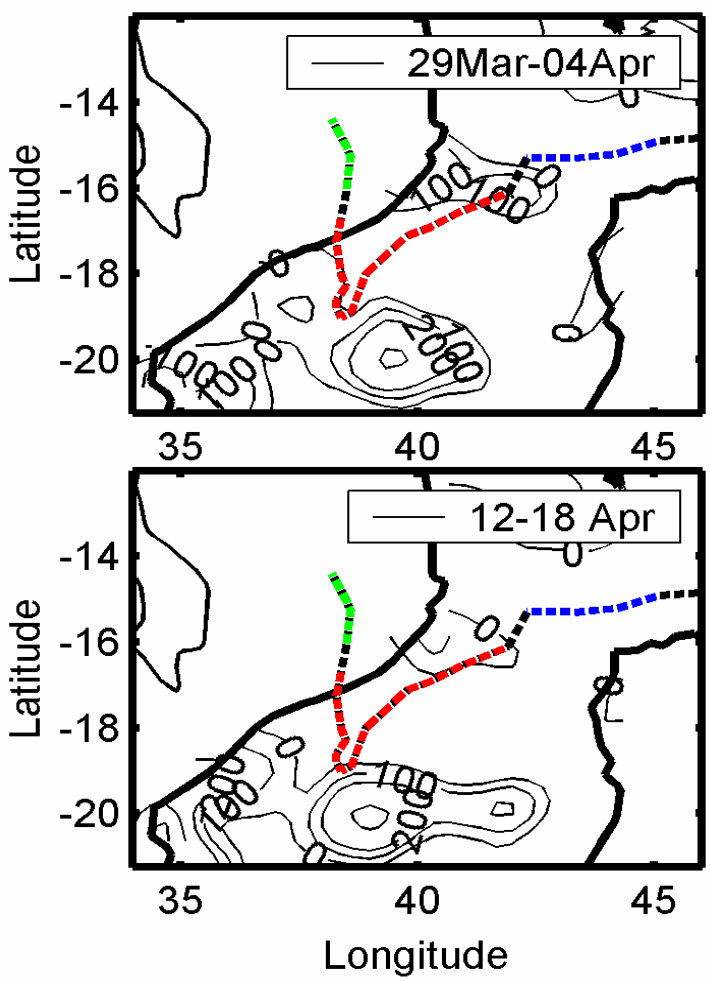

Figure 19: Ocean eddies in the Mozambique Channel as exemplified by anomalies of their heat storage (KJ.cm^{-2}) before (upper panel) and after (lower panel) the passage of cyclone Hudah. The track of the cyclone is given in blue preceding intensification, in red after and green after landfall. Notice the reduction in heat content for the eddy at 16ºS, 42ºE.

The development of cyclone Japhet was comparable. The temperature of the surface waters of the Mozambique Channel was a more-or-less uniform 30ºC at the time. On reaching a warm eddy (not shown here), centred at about 20ºS, 40ºE, the cyclone rapidly intensified (viz. Figure 16) from a category 1 to a category 4 hurricane. It has been shown [Shay et al., 2000] that such hurricane intensification can occur within 24 to 36 hours after passing over a warm eddy. By 2 March cyclone Japhet started passing over a cold, cyclonic feature and its intensity then began declining (Figure 16).

The behaviour of cyclone Eline on passing over a warm eddy was similar. This particular eddy was considerably smaller and with a lower heat content than that over which cyclone Japhet passed and the intensification of cyclone Eline was commensurately slighter (viz. Figure 16).

3.6 Role of ocean-atmosphere interaction

Developments in microwave radiometry and altimetry allow making observations in the Southern Ocean with unprecedented spatial and temporal resolution. Clouds and water vapour for instance do not inhibit SST estimation by the AMSR-E onboard the Aqua satellite. This is a real advantage in the latitudes between 35º to 50º S south of Africa where persistent cloud cover previously was a perennial problem in this regard. Since July 2002, AMSR-E SST has presented global coverage of the ocean at about 56 km resolution (Chelton and Wentz, 2005). Furthermore, the merging of measurements by several altimeters (TOPEX/Poseidon, ERS-2 and Jason-1) allows a better description of mesoscale ocean features in highly energetic regions such as the southern Agulhas Current (Ducet et al., 2000). In addition, wind estimates from the SeaWinds scatterometer onboard the QuikSCAT satellite are since July 1999 (Chelton et al., 2004) at a quarter of a degree resolution along a wide swath.

The latter product, combined with SST estimates from the Tropical Microwave Imager (TMI) onboard the Tropical Rainfall Measuring Mission (TRMM), allowed the demonstration of the impact of mesoscale oceanic features on the overlying atmosphere (e.g. Xie, 2004; Chelton and Wentz, 2005). Chelton et al. (2000) have combined wind stress estimates from QuikSCAT and TMI SST in the eastern tropical Pacific to study the impact on the atmosphere of tropical instability waves, oceanic features with periods of 20 to 40 days and wavelengths of 1000-2000 km. Chelton et al. (2004) used 4 years of filtered QuikSCAT data to show an ubiquitous picture of mesoscale ocean atmosphere interaction linked to SST heterogeneity such as fronts, western boundary currents and tropical instability waves, with the wind increasing (decreasing) when the SST increases (decreases).

Several mechanisms can explain the phenomena that encompass a high range of SST (from 12 C to 30 C) and wind speed (from low to high wind speed). The increase or decrease of surface wind speed along SST gradient and the associated change in the latent and sensible turbulent heat fluxes changes the surface atmospheric stability and adds an extra buoyancy fluxes upwards. Consequently there is a substantial modification of the height and structure of the marine atmospheric boundary layer above the surface layer. According to the numerical study of Samelson et al. (2006) this creates a change in atmospheric conditions leading to the observed wind increase or decrease at the surface. Another possible effect is that change in the stability parameter of the surface layer can lead to a modification of the logarithm profile that characterizes the wind speed in the surface layer. This could also increase the downward mixing of momentum (Wallace et al., 1989). The change in pressure along the SST gradient is also thought to drive secondary circulations (Wai and Stage, 1989)

Closer to Africa, O'Neill et al. (2005), used filtered AMSR-E SST and QuikSCAT data to show that the wind increases and decreases as it goes over warm and cold meanders of the Agulhas Return Current. Rouault and Lutjeharms (2000) measured high values of latent and sensible heat fluxes above a warm eddy in the subantarctic during the SAAMES 3 cruise. High latent and sensible heat fluxes were also measured above an Agulhas ring in summer during the MARE-1 cruise (van Aken et al., 2003) contributing to cool the ring.

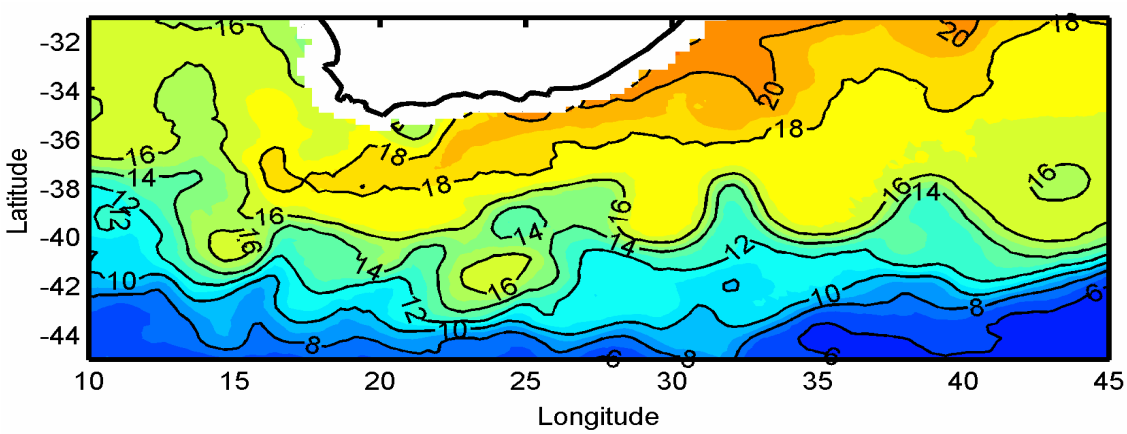

Figure 20: Mean sea surface temperature in August 2003 south of Africa estimated with the Advanced Microwave Scanning Radiometer (AMSR) on board the satellite Aqua. Two warm eddies with temperature of about 16-17°C can be seen centered on 40°S 15°E and 42°S 24°E. They create a strong sea surface temperature gradient with the surrounding ocean. Cold eddies are visible at 38°S 43°E and 39°S 25°E and an eddy is being shed from the Agulhas current at 37°S 17°E. The meander of the Agulhas Return Current is also evident from 25°E along 39°S

Figure 20 shows the mean SST in August 2003 south of Africa obtained by averaging the weekly AMSR-E SST for that month. The Agulhas Current can be seen to follow the eastern coastline of South Africa closely (temperatures exceeding 18ºC) and seems to be in the process of shedding a ring at 37°S, 17°E. Two well-defined warm eddies with temperatures of about 16-17°C are evident at about 40°S,15°E and 42°S,24°E, respectively. They create a strong gradient in SST with the surrounding ocean. Cold eddies are visible at 38°S 43°E and 39°S 25°E. The meanders of the Agulhas Return Current, the object of O'Neill et al.'s study (2005), are also evident along 39°S from 25°E eastwards.

The Agulhas Retroflection has an average loop diameter of 340 km and can be found between 16°E and 20°E (Lutjeharms and Van Ballegooyen, 1988). On average, five anticyclonic rings are shed each year from the occlusion of the retroflection loop (Schouten et al., 2000) and move in a northwestward direction into the South Atlantic Ocean (Gründlingh, 1995; Byrne et al., 1995; Schouten et al., 2000). Apart from these distinct Agulhas rings a number of other eddies are also formed in this region. Lutjeharms and Valentine (1988a) observed eddies with a range of sizes at the termination of the Agulhas retroflection loop. Particularly evident are warm eddies shed southward across the Subtropical Convergence into the colder waters of the subantarctic (Lutjeharms and Valentine, 1988b). Unlike rings those eddies offer distinct SST gradients. Eddies and rings transport warm and saline water from the Southern Indian Ocean into the South Atlantic and therefore have an influence on the thermohaline circulation and the global climate (Gordon et al., 1992; de Ruijter et al., 1999). They have a long lifetime and although they lose their SST expression within a few months, they can cross the entire South Atlantic into the North Brazil Current.

The objective of this part of our study was to explore the interaction between the atmosphere and eddies south and west of the Agulhas retroflection following the preliminary investigations by Rouault and Lutjeharms (2000) of air-sea interaction above a warm eddy in this region. We took advantage of the satellite products, especially the AMSR-E SST, TMI not measuring south of 38ºS. Eddies were identified with a combination of AMSR-E SST and altimetry. Gridded wind speed estimates from QuikSCAT were examined above six eddies and various rings from

July 2002 to June 2004. The implication for the latent and sensible turbulent heat fluxes above Agulhas eddies is discussed.

3.6.1 Eddy detection

Our period of study was July 2002-July 2004 and the geographic domain of the study is defined by Figure 20. We systematically analyzed all weekly SST and altimetry data in this region and for this period to find eddies that had a significantly different thermal expression at the sea surface compared to ambient waters. Such eddies could in all probability interact strongly with the atmosphere as first noted by Rouault and Lutjeharms (2000).

SST was derived from the AMSR-E, launched in 2002 by NASA. It carries a passive microwave radiometer with 6 frequencies that measures brightness temperature at 6.9 GHz, for a 90 % complete global ground coverage within a day, with an accuracy of 0.4 K (Chelton and Wentz, 2005). In this investigation we use weekly data produced by the Remote Sensing System at a resolution of 56 km. As mentioned above, an important advantage of microwave SST retrievals is that they are not altered by cloud cover and water vapor. For instance, due to persistent cloud cover, the data return is about 30 % for infrared estimated SST but about 90 % for microwave SST in the Agulhas Current system (Chelton and Wentz, 2005).

Weekly sea level anomalies (SLA) and geostrophic current were obtained from CNES. They are given on a one third of a degree grid (Ducet et al., 2000), based on merged observations of TOPEX/Poseidon, ERS-2 and Jason-1. We took as an eddy definition a SLA of +15 cm. However, the intense mesoscale variability in SLA generated at the Agulhas Retroflection and in the Agulhas Return Current, make the observation of eddies using satellite altimetry only somewhat ambiguous. This is especially true near the shifting or meandering current. However, the combined use of SST and altimetry allows one to isolate recently formed eddies with less ambiguity than with altimetry alone. The selected eddies shed from the Agulhas Retroflection and the Agulhas Return Current, were identified in an area ranging from 35°S to 45°S latitude and 15°E to 25°E longitude. For most of the cases, the period of unambiguous observation therefore does not exceed a couple of months but for some it exceeds a year. Also, some eddies were reabsorbed by the Agulhas Retroflection or the Agulhas Return Current; they interacted with other eddies or filaments and their SST expressions as a result disappeared or were modified in these ways. In fact most of those eddies stayed quite close to the Agulhas Return Current for a few months before being absorbed by the current or interacting with other eddies. This phenomenon of re-absorption has been observed before (e.g. Boebel et al., 2003); so has the disintegration of warm Agulhas eddies south of the Subtropical Convergence (Lutjeharms, 1988). AMSR-E SST was therefore instrumental in corroborating the location of warm eddies and their trajectories. Please note that the main object of this exercise is not to document fully the formation and tracks of all eddies during the study period, but to identify a sufficient number of eddies with a clear surface expression to give a first clear indication of their impact on the atmosphere.

Eddy 1

The first eddy was pinched off from a big mass of warm water moving westward through the Agulhas Retroflection, early in June 2002, at about 16°E 41°S The eddy had an observed SLA of about +30 cm during the five first months of its existence. Its diameter was an estimated 130 km. During its first month, the eddy moved southward to 15°E, 44°S. By mid-July 2002 the surface temperature of the eddy core was over 14°C, and distinctly warmer than the 8-10°C for the surrounding water.

From mid-July 2002 to early December 2002 the eddy kept moving northwestward to 13°E 41°S. In October 2002, the SST expression had effectively disappeared, but an SLA of about +20 cm was still visible over a smaller surface. For the analysis of the influence of this eddy on the atmosphere we have focused on the periods when the eddy presented significant SST gradients with surrounding waters in July and August 2002.

Eddy 2

This particular eddy was shed from the Agulhas Return Current in mid-July 2002 at 24^{o}E, 42^{o}S. The shedding was not fully complete until the end of August 2002. The eddy was quite energetic. The maximum SLA observed was about +90 cm with a 4^{o}C temperature difference between the edge and the core of the eddy. The eddy surface area was estimated to be 25 000 km^2. During October 2002, several warm filaments and other anticyclonic features interacted with the eddy. At the end of October, Eddy 2 seemed to have united with another eddy and the SST expression increased for the month of November 2002. In December 2002, the eddy was re-absorbed by the current and disappeared in terms of both SLA and SST. The period of study for this eddy is therefore September to November 2002.

Eddy 3

Eddy 3 formed as a small eddy at the Agulhas Retroflection around mid-January 2003 at 17°E, 43°S, with a maximum SLA of +20 cm and a diameter of only about 200 km. The eddy moved rapidly southwestward to reach 15°E, 44.5°S at the end of March 2003. The temperature difference between the edge of the eddy and its core then was about 3°C. By mid-April 2003, the SST expression of the eddy had disappeared. The period of observation for the third eddy is February and March 2003.

Eddy 4

The fourth eddy was shed from the retroflection in the first week of July 2003 at 15°E, 40°S. The SLA at the center of the eddy was about +65 cm and the diameter was estimated to be 230 km. The eddy had a maximum SST of over 16° C at its core. The surrounding water temperature was between 12° to 14° C. At the beginning of September 2003, the eddy was re-integrated with the current and its signal disappeared even as a SLA. Eddy 4 presented a strong gradient of temperature with the surrounding ocean in July and August 2003 and in many respects was similar to the eddy studied intensively in June/July 1993 by Rouault and Lutjeharms (2000). The period of observation for this eddy is July and August 2003.

Eddy 5

Eddy 5 had probably existed since May 2003, but the strong variability in SLA at the Agulhas Retroflection has not allowed us to isolate it properly until the beginning of July 2003. The eddy had clearly been shed by mid-July at 24°E, 41°S with a maximum SLA of +80 cm and an elliptic surface area of about 17 000 km^2 . The SST ranged from 12° C at the edge to 16° C at the center of the feature. The eddy barely moved during the next four months. It seemed to interact with other mesoscale features, such as little eddies and filaments from the Agulhas Retroflection. At the beginning of November 2003, there remained no distinctive SST expression for the eddy and it became reattached to the Agulhas Retroflection a few weeks later. This eddy had a well-defined SST expression that lasted from July to October 2003.

Eddy 6

Eddy 6 had clearly been pinched off the Agulhas Retroflection by the last week of December 2003. It is possible that the eddy was in fact formed a few months earlier, as in the case of Eddy 5, but the spatial resolution of the data (a third of a degree) is

not sufficiently high to isolate it properly during that period. At the end of December 2003, the eddy was about 230 km in diameter and centered on 16°E, 41°S, with an observed maximum SLA of +75 cm. It was clearly separate from the Agulhas Current at the end of January 2004 at 15°E, 43°S and exhibited a strong gradient with the surrounding ocean. It was the strongest of the 6 eddies. The SST of the eddy was 18° C at its core and 10° C at the edge. The eddy was still visible as a SHA at the end of July 2004 which was the end of our study period. Eddy 6 was then located at 12°E, 41°S.

	Jul-02	Aug-02	Sep-02	Oct-02	Nov-02	Dec-02	Jan-03	Feb-03	Mar-03	Apr-03	May-03	Jun-03	Jul-03	Aug-03	Sep-03	Oct-03	Nov-03	Dec-03	Jan-04	Feb-04	Mar-04	Apr-04	May-04	Jun-04
Ed1																								
Ed2																								
Ed3																								
Ed4																								
Ed5																								
Ed6																								

Table 1: Period of ocean-atmosphere interaction study for each eddy

3.6.2 Wind acceleration above eddies

For the two years period from 2 July 2002 to 2 July 2004, we managed to isolate 6 eddies south of Africa that presented strong thermal contrasts with the surrounding water. Rings north of 35 S did not present clear SST gradients partially due to the resolution of SST but also because they quickly lose their surface expression compared to their lifetime that can be several years. The eddies were found in an area between 35°S to 45°S latitude and 15°E to 25°E longitude. The record represents a total of 22 months of clear-cut, identifiable eddies.

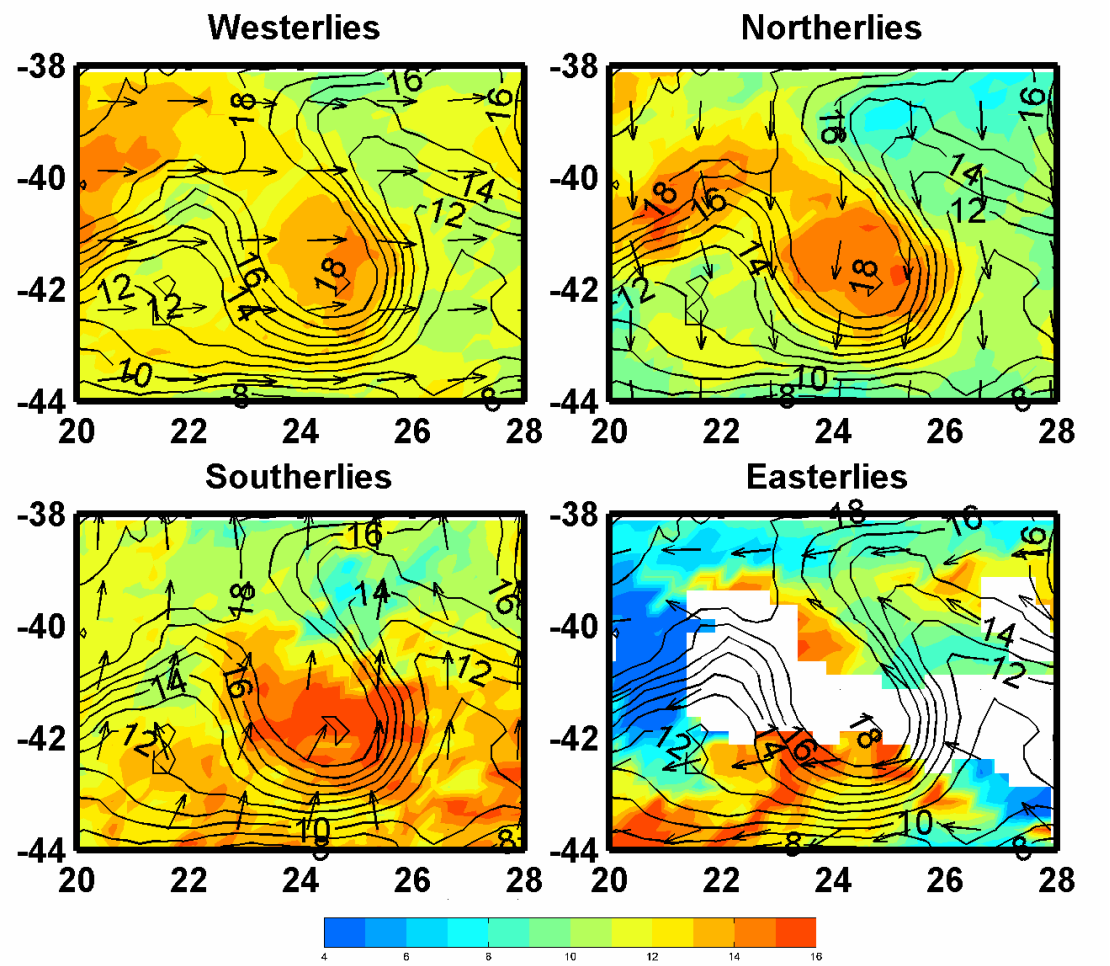

Figure 21: Mean monthly wind speed (color) and direction (arrows) and sea surface temperature (contour) above eddie 5 estimated from twice daily Quickscat wind estimate for westerly (36 cases), northerly (18), easterly (1) and southerly wind (6) in July 2003.

We have plotted the ¼ degree SeaWinds wind speed and direction for morning and evening passes and corresponding weekly SST and SLA. The increase in wind speed above warm eddies was a common feature for all seasons. However, for some cases there were no such clear increases. For these instances, the weather patterns were usually dominated by frontal conditions associated with low pressure systems and this already created a strong wind gradient. In many of the scenes where the SST seems to have had no effect on the winds over the eddies, the wind pattern was representative of powerful cyclonic systems. 10 % of the scenes were contaminated with rainfall and had no valid data. The wind data were provided with a rain flag.

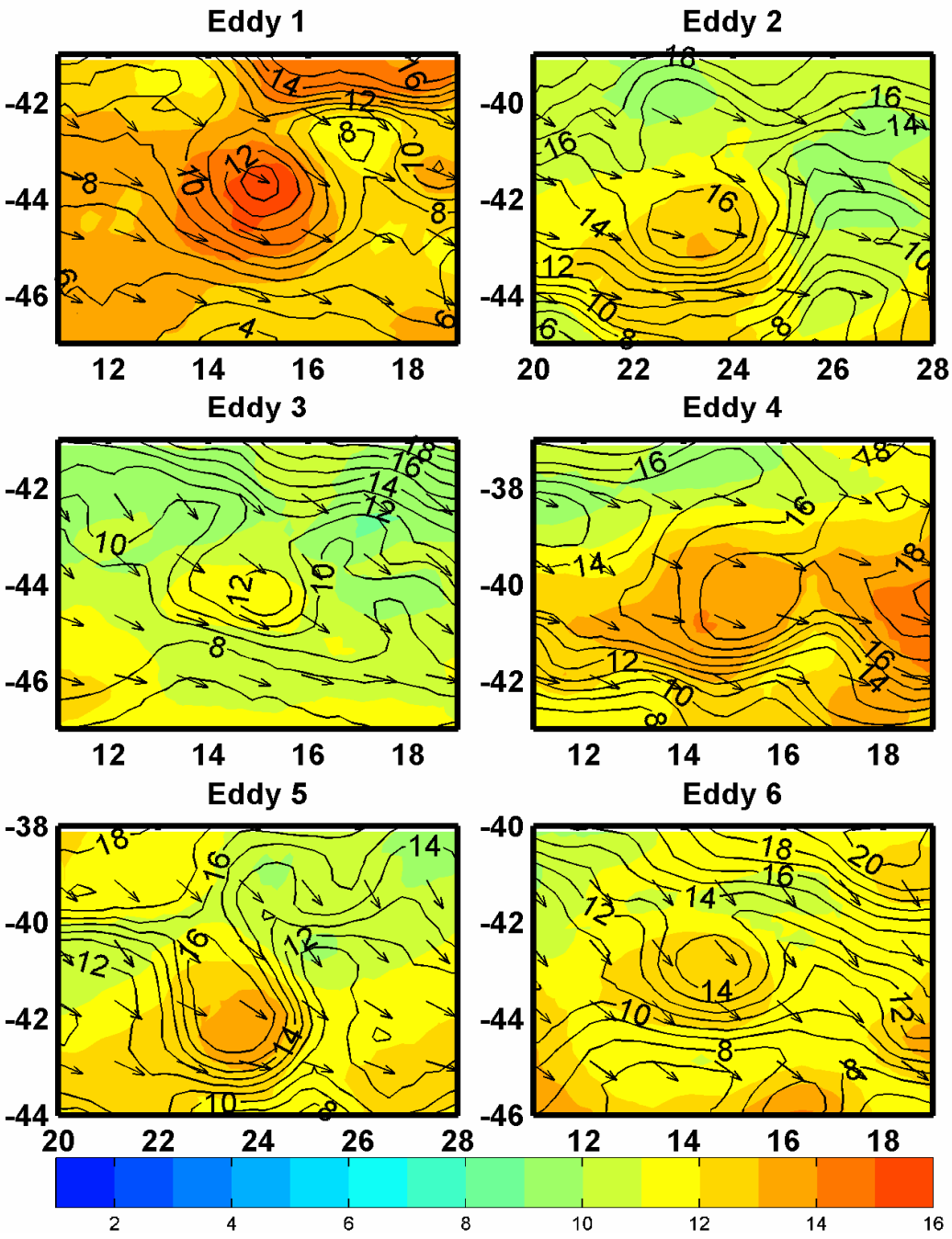

Figure 22: mean monthly wind speed (color) and direction (arrows) and sea surface temperature (contour) above the six eddies.

The high variability of the weather patterns in this region prompted O'Neil et al. (2005) to filter the QuikSCAT data in their study of wind acceleration and deceleration over the Agulhas Return Current. Our study using unfiltered data confirms the relationship shown by O'Neil et al. (2005) as well as that of Chelton et al. (2004) in the Agulhas Current system. In fact, the wind increases (decreases) in any region of positive (negative) SST gradient above the Agulhas Current, at the Agulhas Retroflection, along large filaments, warm and cold eddies and in the Agulhas Return Current.

A monthly average in July 2003 of the two daily QuikSCAT wind speed above eddy 5 for various wind directions is presented in Figure 21. We have separated the data

according to 4 directional quadrants (West, North, East, and South) and vector averaged the result. Wind speed shows clear increases above the eddy for all the directions of the wind. For that month, the westerly selection provided 36 cases, the northerly, 18, the easterly, 1 and the southerly wind, 6. Missing data for the easterly case results from rain interference and is a common occurrence in the dataset and accounted for no data for 9 scenes. The wind strengthening is substantial with an increase from about 10 m/s to 15 m/s above the eddy during wind from all directions. The wind seems also to react rapidly to other features that create a SST gradient, such as the Agulhas retroflection itself or any warm and cold features. Looking at the full set of identified eddies during all seasons, the effect of SST is particularly obvious for the duration of prevailing westerlies or northerlies, but there were several notable cases of southern or eastern winds that also strongly accelerated over the eddy.

Figure 22 shows the mean monthly wind speed this time for all scenes of the month as well as SST above the six eddies. Wind is mostly westerly, a common feature of the “Roaring Forties”. Figure 22 shows an acceleration of the wind speed ranging from 2 to 5 m/s above all the eddies that seems to depend on the SST gradient. Observations from the twice daily QuikSCATdata confirmed that surface winds accelerate over the warm eddies and decelerate downstream where the water gets cooler again and this effect is almost immediate and very site-specific. The phenomenon takes place over short distances, about a few hundred of kilometers, and from any wind direction. We observed a case with westerly wind accelerating about 3 m/s over a warm eddy, decelerating when it passed the eddy and accelerating again further east when the air masses crossed another eddy, all in less than 400 km. This confirms and extends the work of Rouault and Lutjeharms (2000) and O'Neil et al. (2005).

This study focused primarily on warm anticyclonic eddies pinched off the Agulhas Current and the Agulhas Return Current, but the results can be extended to winds decreasing above cold eddies as well. Monthly wind speed during June 2003 decreased by 3 m/s over a cold cyclonic eddy that was in the Agulhas Current system (viz. Figure 20). Bourras et al. (2004) have documented and modeled a decrease of lesser magnitude above a cold eddy that offered a lesser gradient. They offered the downward flux of momentum hypotheses for the decrease, supported by observations.

To quantify the relationship between SST gradient, wind acceleration, season and eddy duration we looked at the statistics of the all merged datasets. SST and SLA were interpolated into the two-year long two-daily wind speed dataset. For each scene, we extracted SST, SLA, absolute geostrophic current and wind speed at three positions along the wind flow until the SST gradient across the eddy was below 1 C per 100 km: a) At the entrance of the flow at the border of the eddy, b) in the middle of the eddy c) downwind at the other eddy border. On average each point was separated by 1.1 degree with values ranging between 0.5 to 2 degrees. The SST gradient was also calculated.

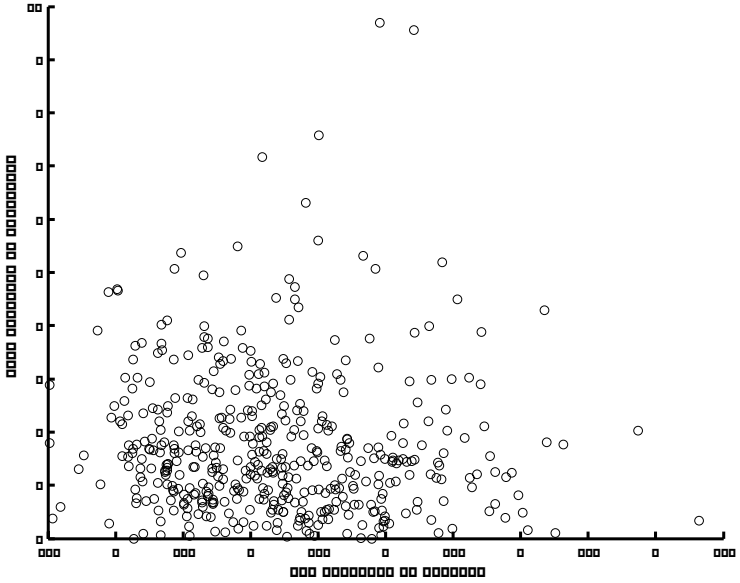

Figure 23: scatter plot of SST gradient in C per 100 /km versus wind gradient in m/s per 100 /km for all case when the wind increased above the eddy and decreased afterwards.

Of the scenes, 30 % show a clear acceleration above the eddy and a deceleration downwind. The mean increase was about 2 m/s for a mean wind speed of 11 m/s at the entrance. Most of selected wind speed ranged between 5 m/s and 20 m/s. The eddy SST centres ranged from 19 C to 12 C and the SST gradient ranged from 1 to 5 C per 100 km for a mean gradient of 2.5 C per 100 km. Figure 23 show scatters plot of the wind speed increase versus the SST gradient, the wind speed at the eddies entrance and the SST at the eddy's centre. There does not seem to be any clear linear relation between those parameters. This could mean that the observed increase is not a direct function of the high turbulent fluxes of latent and sensible heat and the associated stability parameter.

The stability parameter is analogous to the Richardson number, which is the ratio of the work done by the buoyant force to the rate of shear production of turbulent energy. It takes into account both the temperature and moisture dependence of air parcel buoyancy and is affected by the friction velocity. The stability influences the vertical exchange of energy and momentum and thereby the vertical distribution of wind, temperature and humidity in the boundary layer. A positive number of the stability means that the conditions are stable and the stratification will act against the turbulence. Between 0 and -0.3 the stability is neutral. If the stability is less than -0.3 the conditions are unstable with convective activity: the buoyant force begins to dominate the mixing process. Rouault and Lutjeharms (2000) present time series of those parameters above a 16 C eddy, similar to those studied here. Conditions were mostly neutral during the week spent above the eddy during the SAAMES 3 cruises. Only when the wind dropped below 5/ms did conditions became unstable. O 'Neil et al. (2005) have demonstrated that the change in stability at the Agulhas Return Current was not enough to modify the observed wind stress increase there.

However the high turbulent fluxes and mixing can still modify the height and structure of the marine atmospheric boundary layer above the surface layer and create a change in atmospheric conditions leading to the observed wind increase and decrease. This effect has been modeled by Samelson et al. (2006). They also show that the change in stability itself is not enough to create such acceleration. The wind

speed accelerated on average 15 % with a few cases above 5 m/s. This is quite substantial to be explained by surface layer and logarithmic profile considerations.

3.6.3 Impact on turbulent sensible and latent heat fluxes

Turbulent sensible and latent heat fluxes are not measurable parameters. They are calculated from meteorological parameters such as wind speed, air and sea temperature, and air humidity. The turbulent fluxes at the surface of the marine atmospheric boundary layer can be estimated using the bulk aerodynamic method. The turbulent fluxes are estimated with transfer coefficients which relate the fluxes to the mean values of routinely measured meteorological variables. The sensible and latent turbulent heat fluxes are:

$SH=-\rho C_H(U_{10}-U_s)(SST-T_{10})$ (1)
$LH=-\rho LC_E(U_{10}-U_s)(q_{10}-q_{sst})$ (2)

where L is the latent heat of evaporation; ρ is the air density; C_H and C_E are the transfer coefficients for heat and water vapor; U_{10} is the surface wind speed at 10 meter height and U_s the ocean surface velocity; q_{10} is the specific humidity at 10 m height and q_{sst} is the saturated air specific humidity at the temperature of the sea surface. T_{10} is the air temperature. We will assume that the eddies' surface velocities are zero. Although eddy surface velocities of up to 1 m/s were measured before, they are not situated at the centre of the eddy where we do our measurements. With a wind speed of 10 m/s and assuming a relative water velocity of +/- 0.5 m/s to the wind, the error in estimating the turbulent sensible and latent fluxes by neglecting eddy motion would be +/- 5%, only in a small part of the eddy.

Table 2: Mean, standard deviation, minimum and maximum for air-sea interaction parameters for a week of measurements during the SAAMES 3 cruise. These measurements were taken above a warm eddy in the austral winter of 1993. Negative values of the fluxes correspond to a loss of energy of the eddy.

Variable	Mean	Std.	Max.	Min.
Pressure (mb)	1016	10.0	1036	1001
Wind speed (m/s)	12.0	5.80	22.3	1.9
SST (^oC)	15.9	0.51	16.7	13.2
Air temperature (^oC)	13.2	2.35	16.7	7.5
Specific Humidity (g/kg)	7.9	1.50	10.7	4.8
Relative Humidity (%)	82.7	6.95	96.3	67.8
Wind Stress	0.37	0.32	1.2	0.007
Latent heat flux (W/m^{-2})	-122.1	71.7	-365.4	-15.8
Sensible heat flux (W/m^{-2})	-37.8	31.6	-126.3	16.2
Stability parameter	-0.77	1.457	0.61	-10
Visible radiation (W/m^{-2})	41.2	69.2	527.5	0.0
Outgoing Infrared (W/m^{-2})	-397.3	2.8	-402.5	-383.3
Incoming Infrared (W/m^{-2})	337.1	33.0	377.3	251.6
Net heat budget (W/m^{-2})	-181.5	125.2	-595.9	322.9

Thus, in order to calculate the turbulent fluxes in the study region, we can use AMSR-E SST and QuikSCAT wind speed. However, we still need an estimate of the air temperature and its specific humidity. Also, some algorithms need the short and long wave radiation. We therefore make some assumptions for that purpose using cruise data as a baseline. The parameters of interest measured during the SAAMES 3 are presented in Table 2. The MARE cruise (Van Aken, 2003; Table 2) and Rouault

and Lee-Thorp (1997) also provide some useful data. During those cruises, measurements were made of the SST, air temperature, wind speed and direction, short wave radiation and long wave radiation above eddies. This allowed calculating the turbulent fluxes of momentum, sensible and latent heat using the method developed by Fairall et al. (1996).

Based on these cruise data sets, we used a relative humidity of 80% and a difference of temperature of 3^{o}C between the eddy and the air temperature in the turbulent flux calculations above the eddy. These were done using the algorithm of Fairall et al. (1996) for the periods selected in Table 1. In order to quantify the eddies effect on the turbulent latent and sensible heat fluxes, calculations were made for two configurations and compared with NCEP reanalysis:

–With the data observed at the core of the eddy

–With the data just outside the eddy.

Table 3: Monthly averages for sensible (SH) and latent (LH) turbulent heat fluxes for all eddies for: a) case 1: observed situation above the eddy; b) case 2: surrounding waters; c) NCEP

	a) Case 1		b) Case 2		c) NCEP
	SH W/m^2	LH W/m^2	SH W/m^2	LH W/m^2	LH W/m^2
Ed1 Jul 02	62.1	168.3	15.57	80.8	72
Ed1 Aug 02	59.6	151.3	14.35	75	65
Ed2 Sep 02	50.6	164.2	12.55	79.4	120
Ed2 Nov 02	55.1	190.1	14.3	96.5	140
Ed3 Fev 03	48.9	132.2	11.03	61.4	50
Ed3 Mar 03	46.2	117.2	11.67	61	70
Ed4 Jul 03	55.1	190.1	12.14	81.9	150
Ed4 Aug 03	54.4	176.7	14	83.2	145
Ed5 Jul 03	61.3	211.4	14.39	85.5	130
Ed5 Aug 03	54.4	176.7	13.18	83.4	120
Ed5 Sep 03	52.7	171.1	12.46	74	105
Ed5 Oct 03	39.3	127.8	9.52	64.2	65
Ed6 Fev 04	50.8	175.3	11.54	77.83	80
Ed6 Mar 04	56.1	182.3	13.18	83.4	108
Ed6 Apr 04	53.7	164.1	14.26	84.7	95
Ed6 May 04	51.3	147.5	13	72.4	80
Ed6 Jun 04	57	163.7	13.91	77.5	90
Average	52.8	164.5	12.8	77.2	99

The results are presented in Table 3. Over the eddies and for the periods defined in Table 1, the averaged sensible heat flux is about 53 W/m^2 and the averaged latent heat flux is 164 W/m^2 (case 1). For Case 2, when both effects are not accounted for (conditions for the waters surrounding eddies), the fluxes are 40 W/m^2 and 87 W/m^2 less (75 % and 50 % less). Not surprisingly NCEP underestimates the fluxes as demonstrated by Rouault et al. (2003) for the Agulhas Current. This is due to the resolution of the model used by NCEP reanalysis and persistent cloud cover in the “Roaring Forties”. The error made seems to be less when the eddies are close to the Agulhas Current.

Such increases in the fluxes are not unrealistic when looking at the various elements of equation (1) and (2). Greater increases in fluxes at the synoptic scale (factor of 5) were measured during the SAAMES 3 cruise (Rouault and Lutjeharms, 2000) and by Rouault and Lee-Thorp (1997) when sailing across warm eddies. Table 3 also highlights the substantial values of the sensible and latent heat fluxes above the eddy for all seasons, higher when compared with climatology (Josey et al., 1999) of the region.

Of course the value of 80 % used for the relative humidity is somehow arbitrary even if based on the the SAAMES 3 cruise that provided a total of 7 days of high resolution measurements above the eddy in June 2003 but fixing the relative humidity at 90 % also leads to substantial increases above warm eddies. It is interesting to note that during the SAAMES 3 cruise the variation of fluxes were quite substantial when compared with those of the radiative budget. Swath data from ERS-1 during the SAAMES 3 cruise also showed an increase of wind speed above this warm eddy (Rouault and Lutjeharms, 2000). Measurements taken during the MARE cruise (Van Aken et al., 2003) show that even in summer a warm Agulhas ring loses substantial amounts of energy due to strong turbulent heat fluxes.

3.6.4 Conclusion

Modifications to the marine atmospheric boundary layer and ocean-atmosphere interaction across frontal regions were documented during experiments at sea (Sweet et al., 1981; Davidson et al., 1991; Friehe et al., 1991; Rouault et al., 2000b; Bourras et al., 2004) and also modelled (Samelson et al., 2006). Satellite remote sensing confirms and extends in space and time the relationship demonstrated during the SAAMES cruise cruises. Wind speed, wind stress and turbulent fluxes and latent and sensible heat increase substantially when crossing SST gradient.

Ocean-atmosphere interaction above mesoscale eddies is underestimated in reanalysed climate datasets such as NCEP or ERA 40 or in the National Weather Prediction models if the eddy SST are not taken into account. The increase in wind speed substantially enhances the latent and sensible heat fluxes as does the increase in SST gradient. However, Chelton and Wentz (2005) have recently demonstrated that the wind increase in the Agulhas Return Current can be reproduced in atmospheric general circulation models if the spatial resolution of the SST used is upgraded to take into account the mesoscale features.

Using microwave remote sensing from satellite has been beneficial in this regard, as it provides a full global coverage of the Southern Ocean with an unprecedented spatial and time resolution. A combination of merged SLA, geostrophic velocity and AMSR-E SST is a very useful tool for studying the path and track of eddies. This could be easily displayed operationally to provide vessels with early warning and indicate where they are likely to encounter stronger wind. With increases of more than 5 m/s in eddies, the warning should be taken seriously when sailing in the “Roaring Forties”

At least, because of their high heat content, the impact of eddies on the atmosphere can last for many months. The initial decay of eddy heat content observed with altimetry could be influenced by this high loss of energy due to the turbulent sensible and latent heat fluxes and will be the object of further study.

3.7 Role of advection

3.7.1 Data and Method

The new method of combining altimetry, *in situ* observations and an improved geoid model by Rio and Hernandez (2004) provides an improved mean absolute dynamic topography of the global ocean. Rio and Hernandez (2004) applied an iterative process by first subtracting an available geoid from satellite mean sea surface height (SSH), then merging the result with the World Ocean Data Base 1998 climatology (Levitus et al., 2001) to provide smaller spatial scales, and finally combining *in situ* measurements with altimetric data. The *in situ* data include drifter velocities (Niiler et al., 1995; Hansen et al., 1996) and XBT and CTD casts from a 1993 – 2000 data set which possibly includes some of the data already used by Levitus. Error estimates for mean geostrophic velocities resulting from this method are below 10 cm/s at middle and low latitudes. The data are therefore suitable for studying strong currents in subtropical regions.

The data set developed here to characterize the mid-latitude South Indian Ocean is based on absolute geostrophic currents resulting from the sum of the mean dynamic topography (scale 660 km) and sea level anomaly (scale 1/3° or about 35 km) from August 2001 to May 2006. The resolution both in space and in time is higher than in any large-scale in situ observational data set.

3.7.2 Discovering a current in the 21 st century

As reviewed by Stramma and Lutjeharms (1997), the overall upper-layer circulation in the region of study is dominated by the counterclockwise South Indian subtropical gyre. Transport patterns include anticyclonic flow centered in the western Indian Ocean, with mostly westward transports at mid-latitudes between about 15°S and 35°S. It is also well known that long westward-propagating planetary waves can be found in altimetric data (e.g. Chelton and Schlax, 1996; Killworth et al., 1997) and that such waves also exist at mid-latitudes in the southern Indian Ocean. About 4 – 5 westward propagating events per year were noted in this region (Schouten et al., 2002), and it was shown by Birol and Morrow (2001, 2003) that the signals at these latitudes represent approximately semi-annual free Rossby waves originating from the boundary region off West Australia.

When inspecting the current structure at subtropical latitudes, we noted a well-defined zonal band of high mesoscale variability in the latitude range between about 22°S and 26°S. Two examples of geostrophic surface currents are presented in Figures 24a and 24b.

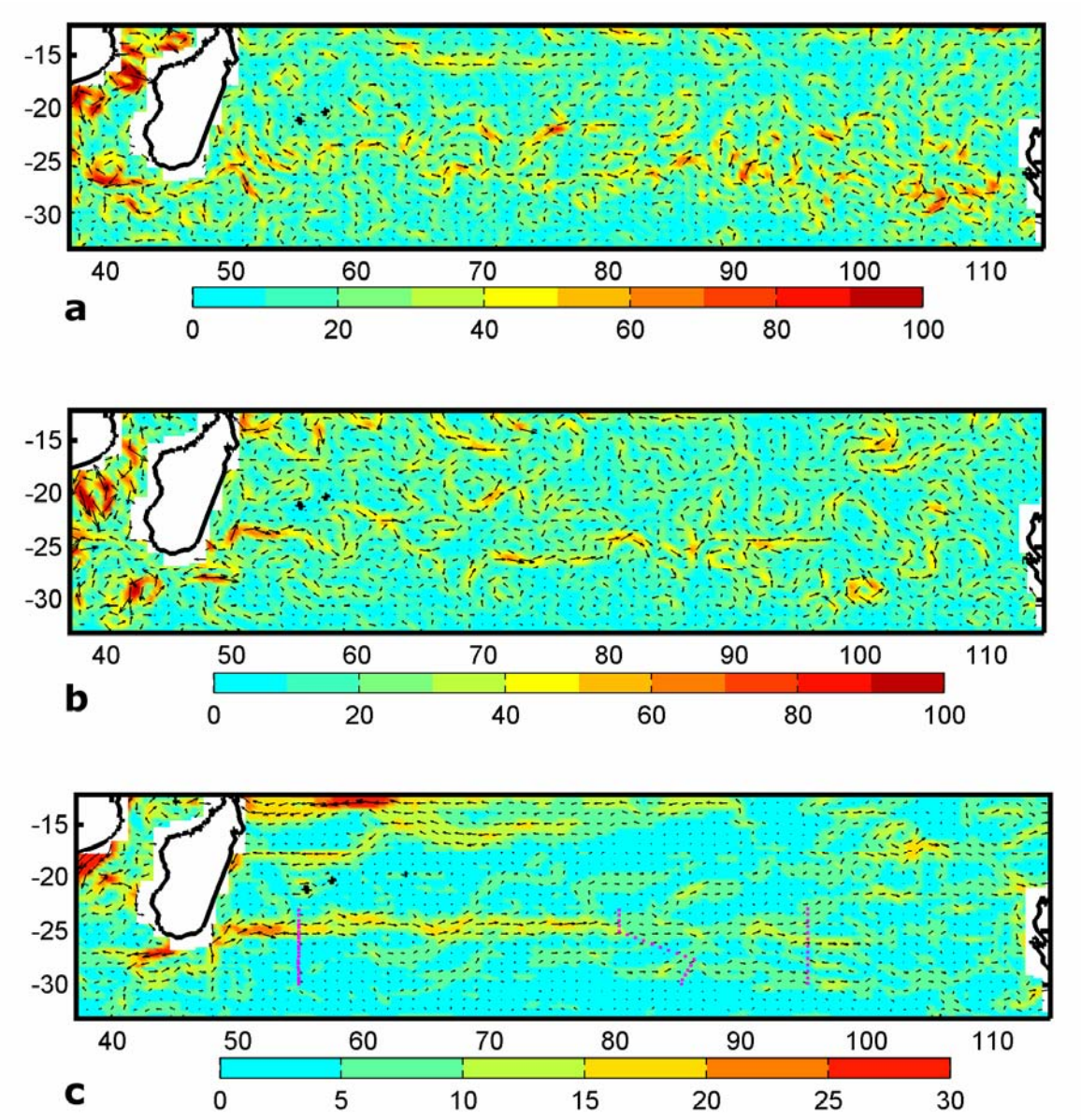

Figure 24: (a) Geostrophic currents on 1 November 2002, (b) on 31 March 2003, and (c) averaged over five years from August 2001 to May 2006 showing the newly discovered South Indian Counter Current. The magenta dots in Figure 24c indicate the positions of the WOCE stations used for transport calculations.

One recognizes wave-like and eddy patterns. The signal properties correspond to those of westward-propagating planetary waves which have been well documented in longitude-time plots (e.g. Birol and Morrow, 2001, Plate 2). With the high resolution of the absolute geostrophic current field, one is now able to identify the current structure within the wave trains. The result is a predominantly eastward narrow geostrophic surface current which is guided within the westward propagating Rossby wave structure that we called South Indian Counter Current (SICC). The typical widths of the eastward flow in the short-time means are between about 50 and 100 km, mostly within the 22-26°S latitude belt and with speeds reaching beyond 0.5 m/s. However, depending on the phase of the planetary waves, weaker westward flow can also be observed.

The mean over the total period of five years is presented in Figure 24c. In much of the latitude belt 22-26°S, the mean velocities are above 10 cm/s and therefore

significant within the error limits of the data set. A continuous mean zonal countercurrent to the east is identified, with a width of about 100 – 200 km. It is particularly strong between the region off Madagascar and about 80°E where the signal weakens and spreads, becoming well-established again between about 90°E and 100°E. When checking the sequence of events in the data set, a related pattern emerges. Particularly strong eddy and wave formation is recognized in a broad latitude range off West Australia, the suggested region of planetary wave generation (Birol and Morrow, 2003). One finds waves and occasional eddies emanating from this region. The eddies with diameters of 200 – 300 km appear to be generated off southwestern Australia, travel westward and approach the eastward current belt from the south between 90°S and 80°S. Having grown to wave scale, they become part of the wave structure. This process may be the reason for the lack of a narrow zonal current in this longitude range.

3.7.3 Volume transports

We used the high-resolution meridional WOCE (World Ocean Circulation Experiment) hydrographic sections from 1995 (see Figure 24c) to study the deeper geostrophic current and volume transport structure in the South Indian Counter Current region. When comparing the positions of these cores with geostrophic surface current patterns estimated from Aviso sea level anomalies (DT-MSLA Merged) within a few days of the WOCE observations (not shown), we found excellent correspondence. Although the main flow exists between the surface and 200 dbar as determined in earlier studies, the eastward currents found here in part reach down to 800 dbar or deeper. At 54°E we find two eastward flow cores between 23.5°S and 26°S, with westward flow in between, representing the eastward countercurrent and an anticyclonic eddy south of it. Only a weaker eastward flow core can be identified at 80°E which is the longitude where the eastward flow in Figure 24c weakens and spreads. At 95°E there is a well-defined core again. The 0 – 800 dbar transports in the eastward flow cores near 24°S are 10 Sv (54°E), 4 Sv (80°E) and 9 Sv (95°E) with an error estimate of $\pm$3 Sv (1 Sv = 10^6 m^3s^{-1}). Because of the smoothing effect due to station distances of about 50 km, the velocities from hydrographic data are somewhat lower than those from the satellite data. The overall transport estimates are not sensitive to station spacing. Since the sections suggest some eastward flow even below 800 dbar, the transport numbers may be on the low side. In a study of transports in the whole water column at 54°E. Donahue and Toole (2003) analyzed the same data and also displayed a deep-reaching current band between about 24-25°S with transports of similar size in the upper ocean.

What causes the meridional density gradients which are a prerequisite for the front with a geostrophic countercurrent? The wind stress fields of the southeasterly trades in the north and the westerlies in the south push light water southwestward and heavier water northward. The transition in zonal wind direction occurs near 30°S (see Kallberg, 2005) thus generating a subtropical convergence. Surface buoyancy fluxes due to large evaporation minus precipitation in combination with heat flux produces dense water in the eastern South Indian Ocean (e.g. Schott et al., 2002). The region of maximum surface salinity is found between approximately 25°S and 35°S (Wyrtki, 1971; Toole and Warren, 1993; O'Connor et al., 2005; Nauw et al., 2006). The SICC and its related density front coincides with the northern boundary of the maximum surface salinity area and also with the northern boundary of the Subtropical Underwater subduction area (Karstensen and Quadfasel, 2002; O'Connor et al., 2005). We note that one also finds the northern boundary of Subtropical Mode Water formation (Hanawa and Talley, 2001) in that region.

Both Ekman transport convergence and surface buoyancy fluxes apparently contribute to generating the SICC related frontal zone. It is not certain at this point which forcing dominates although regional correspondence of salinity pattern and SICC position would seem to suggest a dominating forcing by buoyancy effects in the central and eastern parts of the region. Understanding the processes which control the transition between the western boundary and the central region will require model studies.

3.7.4 The origin of the countercurrent

The results also address the question on the nature of the termination of the southern limb of the East Madagascar Current (EMC). This has variously been described as a complete retroflection (Lutjeharms, 1988) based on thermal infrared imagery and drifter tracks, and as a free westward jet generating vortex dipoles (de Ruijter et al., 2004) once it overshoots the southern tip of Madagascar. The lack of an eastward current was a critical argument against the existence of a retroflection (Quartly et al., 2006). Westward drifting circulation disturbances passing through the region, considered to be eddies, complicate this picture (Gründlingh et al., 1991; Donahue and Toole, 2003). The prevalence of eddies is indeed supported by an animation of events in the region. However, when averaging of the altimetric signal is carried out over periods much longer than typical eddy scales, a flow pattern emerges with water from a retroflection of the southern branch of the EMC connected to the subtropical countercurrent. Another part is seen to move directly westward (see Figure 24c).

The EMC has its origin in a branch of the South Equatorial Current (SEC), arriving at the northeastern slope of Madagascar (Schott et al., 1988). The long-term mean in Figure 24c shows that branch separation already occurs near 60°E and 18°S above the Mascarene Ridge and that a narrow flow band reaches the Madagascar slope and turns south. The mooring data at 23°S by Schott et al. (1988) documented southward transports of about 13 and 20 Sv between the surface and 750 m along the Madagascar slope to the south. We also note that the southward transport near Madagascar at 20°S and also the eastward transport near 24-25°S given by Donahue and Toole (2003, their Fig. 20) have magnitudes of more than 10 Sv. The altimeter data are not accurate enough near the coastline (the white area in Figure 24c) to describe the EMC itself. Earlier work, however, has shown it to be a narrow current near the Madagascar slope in that area, with a typical width of 100 - 200 km (Schott et al., 1988; Donahue and Toole, 2003). Its turning towards the west in the south of Madagascar was not documented by observations directly. However, when inspecting currents below the Ekman layer (148m) in output from the Simple Ocean Data Assimilation (SODA) package version 1.4.2 (Carton et al., 2000; Carton and Giese, 2006), the EMC can well be followed southward along the east coast and around the southern tip of Madagascar to the west. The model is based on the Geophysical Fluid Dynamics Laboratory MOM 2.b code and assimilates in situ and satellite altimeter data. In all probability the westward flow south of Madagascar seen in Figure 24c therefore represents the continuation of the EMC which partially retroflects and leads into the SICC. The above transport magnitudes mean that the EMC transports would be sufficiently large to provide the source water for the countercurrent. We checked WOCE temperature/salinity diagrams in the core regions of the SEC branch, the EMC and the western SICC (not shown). The curves are variable in the SEC, and the envelopes of distributions correspond and are tight in the EMC and SICC between 150 and 800 dbar, supporting the conclusion that the flows are related.

3.7.5 Conclusions

With its rather large transport of 10 Sverdrup the SICC is an essential component of the near-surface subtropical circulation in the South Indian Ocean. The core of the zonal countercurrent extends to about 800 m. The present study shows evidence for a narrow SICC being embedded in a planetary wave and eddy flow pattern. In addition, baroclinic instability can be expected to play a role in the more central parts of the subtropical South Indian Ocean. Potential vorticity distributions at approximately 250 m and 500 m (McCarthy and Talley, 1999) show a change of sign in the region to the north, between the SICC and the SEC, corresponding to the necessary condition for baroclinic instability (e.g. Kantha and Clayson, 2000).

Based on a 5-year mean we show that the EMC is fed by a well-defined branch of the SEC. At the southern termination of the EMC there is evidence for both the EMC retroflecting and thus feeding the SICC and for moving directly westward. The energetic eddy pattern makes it difficult to recognize a possible dominance of westward jet or eastward retroflection during shorter periods. The countercurrent advects water to the subtropical underwater subduction region, probably influencing the composition of water masses in the subduction process. The dynamics of the frontal zone and the corresponding countercurrent generation remain to be clarified although it can be imagined that surface buoyancy fluxes dominate the wind stress influence.

3.8 Role of the Tropical Atlantic Ocean.

3.8.1 Introduction

Warmer than normal upper ocean temperature events along the Angolan and Namibian Atlantic coastline (5^{o}S to 27^{o}S) can impact the marine ecosystem and the rainfall of the region. When anomalous warm water penetrates southward in the upwelling system of the Benguela Current and has a negative impact on the ecosystem, the warm event is called Benguela Niño (Shannon et al., 1986) by analogy to the southward propagation of warm water along the Equatorian and Peruvian coastline during El Niño. Benguela Niños have a strong impact on the coastal ecosystem as low-nutrient warm Angolan water is upwelled to the surface in place of cold, nutrient rich upwelled water (Shannon et al., 1986). Benguela Niños often lead to floods in Angola and Namibia and abundant rainfall in the usually arid Namib Desert (Shannon et al., 1986; Rouault et al., 2003). When warm events occur in late austral summer, during the maximum of annual sea surface temperature (SST) and rainfall, they have a stronger impact on atmospheric instability and coastal rainfall (Hirst and Hastenrath, 1983), African rainfall (Nicholson and Entekhabi, 1987) and fisheries (Boyer et al., 2001; Binet et al., 2001).

Figure 25 shows a schematic of the major oceanographic features off Angola and Namibia in late austral summer based on cruise data (Gordon and Bosley, 1991; Shannon and Nelson, 1996; Gammelsrød et al., 1998; Stramma and Schott, 1999; Lass et al., 2000; Mercier et al., 2003; Schott et al., 2004).This includes the southward warm Angola Current, the Angola Benguela Front (ABF), the northwestward cold Benguela current and the upwelling areas of the Angola Benguela Current system. The region is fed by tropical water brought about by the Equatorial Undercurrent, the Gabon Current, the South Equatorial Counter Current and the South Equatorial Undercurrent. Other features likely to play an important role are the Angola Dome (Voituriez, 1981; Yamagata and Iizuka, 1995) and the Congo River.

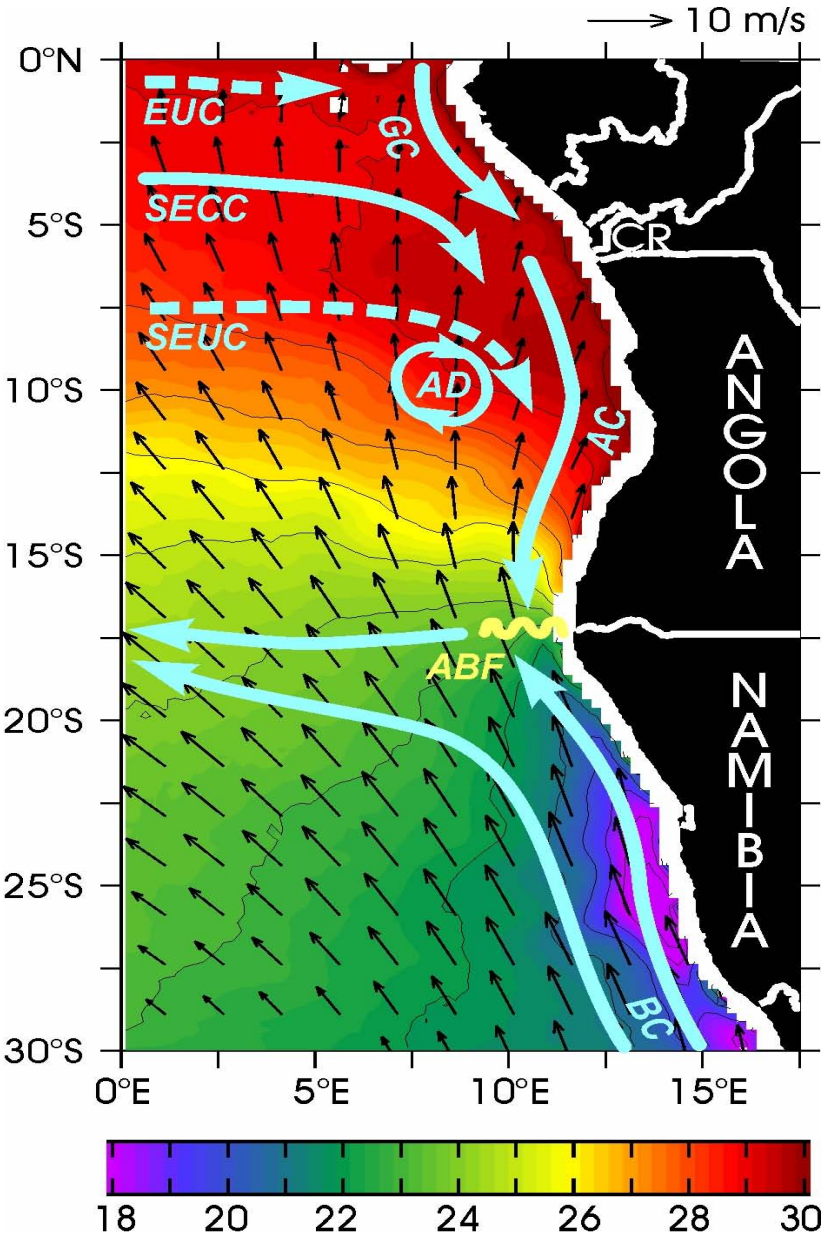

Figure 25: Schematic of the major oceanographic features in the South East Tropical Atlantic in late austral summer with mean March TRMM TMI SST and QuikScat wind speed and direction. Major feature are Equatorial Undercurrent (EUC), South Equatorial CounterCurrent (SECC), South Equatorial Undercurrent (SEUC), Congo River (CR), Angola Current (AC), Angola Benguela front (ABF) and Benguela Current (BC). SST is plotted every degree from 18 to 30 C. Maximum wind speed is 8 m/s in the south and minimum wind speed is 3 m/s north of the ABF. Wind arrow scales are in the top right corner

Figure 25 also shows the 1998-2004 mean of March SST estimated with the Tropical Rainfall Measuring Mission Microwave Imager (TMI SST) together with the 2000-2004 mean March wind speed and direction inferred from scatterometer SeaWinds onboard the QuikScat satellite. The position of the Angola Benguela Front (ABF) is found at about 17°S in March, its southernmost annual position. The region is subject to the seasonal displacement of the South Atlantic Anticyclone that influences the changes in the location of the ABF (Meeuwis and Lutjeharms, 1990). The mean wind is mostly southerly, i.e. along-shore, and stronger south of the Angola Benguela

Frontal zone where it drives strong upwelling. Along the equator, the seasonal relaxation of easterly wind in austral summer especially in the west of the Tropical Atlantic reduces the zonal pressure gradient, decreases the slope of the thermocline and contributes to the late austral summer seasonal warming of the upper ocean in the north of the domain shown in Figure 25 (Philander and Pacanowski, 1986; Carton and Zhou, 1997).

3.8.2 Warm event in the Tropical Southeast Atlantic

During Benguela Niños, intrusion of warm water can reach as far as 25°S (Shannon and Nelson, 1996) about 8° south of the ABF. The 1984 and 1995 Benguela Niños happened in late austral summer and were remotely forced by reduced trade winds in the western equatorial part of the Tropical Atlantic (Philander, 1986; Carton and Huang, 1994; Vauclair and du Penhoat, 2001; Florenchie et al., 2003; Florenchie et al., 2004). Periods of sustained eastward propagation of warm anomalies in the Tropical Atlantic due to reduced tradewinds are usually called Atlantic Niños. It is thought that during an Atlantic Niño, relaxation of trade winds in the western part of the Tropical Atlantic triggers Kelvin waves, propagating eastwards towards Africa. These propagations induce a deepening of the thermocline and a warming of the equatorial upwelling system in the eastern equatorial part of the Tropical Atlantic (Hisart, 1980; Philander, 1990; Zebiak, 1993; Carton et al., 1996; Illig et al., 2004).

The influence of the Tropical Atlantic Ocean on Brazilian and West African climate has been the subject of numerous studies but less has been done to understand the effect of tropical Atlantic variability on Southern, Central and Eastern Africa during the peak sea surface temperature (SST) and rainfall season of austral summer and autumn. Using data from 1940-1975, Hirst and Hastenrath (1983) established a positive correlation between tropical southeastern Atlantic SST and Angolan coastal rainfall and wind pattern for late summer (March–April). The SST and rain anomalies were correlated to the variability of trade winds along the equator mainly off Brazil. Subsequently, Nicholson and Entekhabi (1987) showed that during warm South East Atlantic events, above average rainfall occurred along the Angolan (6°S to 17.5°S) and Namibian (17.5°S to 29°S) coasts as well as inland. Rouault et al. (2003) have updated Hirst and Hastenrath (1983). Mc Hugh (2004) has also shown the importance of the tropical Atlantic moist air to Eastern African rainfall in austral summer.

Rouault et al. (2003) also documented the impact of the recent oceanic warm events of late austral summer 1984, 1986, 1995 and 2001 on Southern African rainfall. During these events, positive anomalies reached a maximum during March/April with monthly mean SST reaching as high as 30°C along the coast of Angola. Cold events (1982, 1992 and 1997) are met with below average rainfall. Figure 26 plots the precipitation anomalies divided by the standard deviation at each grid point and highlights the relatively homogeneous rainfall responses above the warm events. Seasonal anomalies of up to 2 standard deviation occur above the SST anomalies and neighbouring areas of Angola and Namibia. This translates in floods in Angola with terrible societal impact. For instance 50 people died in a flood that displaced 50 000 people in March 2001 according to the OFDA/CRED International Disaster Database

During the 1995 event, ocean temperature anomalies of up to 8°C were measured below 30 m. Cruise data showed these anomalies extending 300 km offshore with a southward extension to 27°S (Gammelsrød et al., 1998). This, and other warm events, has had a strong influence on local fish distribution and abundance in

Angolan and Namibian waters (Binet et al., 2001; Boyer et al., 2001). The 1984 1995 and 2001 warm events off Angola and Namibia were part of a large scale basin phenomenon in the tropical Atlantic (Philander, 1986; Carton and Huang, 1994; Delécluse et al., 1994; Vauclair and du Penhoat, 2000; Florenchie et al., 2003, 2004; Rouault et al., 2007). Development of warm anomalies simulated with the Ocean general circulation model OPA suggest that these warm events are remotely forced and they follow a sudden relaxation of the trade winds along the equator and especially off Brazil. This trade wind relaxation lead to a change in the slope of the thermocline and also sometimes to the generation of equatorial Kelvin waves. This produces a depression of the thermocline along the equator that could lead to a strengthening of the South Equatorial Counter Current (SECC) (Philander and Pacanowski, 1986; Rouault et al., 2007). Warm waters then accumulate in the eastern South Atlantic along the coast and the poleward Angolan Current could intensify and transport the anomalies southward along the coast. The origin of the 1984, 1995 and 2001 event seemed to happen one or two months before appearance of the anomalies at the coast and it seems to have been triggered by the abnormal westerly wind in the eastern part of the basin or all along the equator. A link between the equatorial variability and Angolan Current has therefore been established but mechanisms need to be further understood as well as the impact of local wind on the modulation of the warm events in the upwelling area of Namibia. Benguela Niños seems to happen before Atlantic Niños and could be their precursors. Atlantic Niños are linked to major climate disruption in West and Central Africa and Brazil, making the variability in that area relevant to all countries bordering the Tropical Atlantic.

Besides having a direct impact on rainfall off Angola and Namibia it may be possible that ocean conditions off Angola are also important for many Southern African countries. Although the western Indian Ocean is the principal source of moisture for summer rainfall over southern Africa, a secondary source is situated in the Atlantic Ocean off Angola. During January and February the mean flux is westerly off the tropical SE Atlantic, converging over Zambia with the mean easterly flux originating in the tropical Indian Ocean. In 1995, the SE Atlantic SSTA was largest but the inflow into Angola / Namibia from the Indian Ocean was weaker than average. Rainfall was enhanced only by the Atlantic source. For 2001, there was a convergence in southern Zambia / northern Zimbabwe between the enhanced moisture flux from the SE Atlantic SSTA and that coming from the western Indian Ocean. Hence, the largest precipitation anomalies occurred over central southern Africa with those in western Angola / Namibia influenced only by the SE Atlantic moisture flux. By contrast, the moisture flux from the western Indian Ocean across low latitude southern Africa was enhanced in 1984 and 1986 with relative convergence over western Angola / Namibia. This, together with the increased unstable lower atmosphere and increased evaporation (i.e. latent heat flux) over the warm SE Atlantic SSTA, led to relatively large precipitation anomalies in this region. It is therefore important to quantify the local evaporation and atmospheric instability in the region of the SE Atlantic that could act to augment the precipitation derived from the Indian source. Again an ATLAS mooring is perfectly suited for that task.

In order to address the role of radiative or surface flux forcing vs. the role of ocean dynamics for SST anomalies and the preconditioning of the surface in response to flux anomalies, we did a study of NCEP turbulent fluxes, 10 m wind, surface pressure, Hadley SST and GPCP rainfall in the domain study 20º S-10º S and 8º E-coast for the mean of February March and May (Figure 26). The latent heat flux is quite substantial (mean 90 $W.m^2$ standard deviation: 13 $W.m^2$) and dominates the turbulent heat fluxes, winds are moderate and steady (mean 4.85 m/s STD 0.25) and mostly southeasterly (mean U= 0.75 mean V=4.8). Mean SST is 25.6 C and standard

deviation = 0.9 C. We calculated for each year since 1979 the anomaly divided by the standard deviation for the February, March and April average of sea level pressure, rainfall, SST, latent heat flux, wind speed, meridional wind and zonal wind. Outstanding oceanic events are those inferior to -1 STD (cold events) or superior to 1 STD (warm events). Events of 1984, 1995 and 2001 stand out as warm events. The 1995 and 2001 events have the highest latent and sensible heat fluxes and 1984 is not far behind. The reason for those high fluxes is because the difference between the specific humidity of the air and the sea surface increases quickly when the SST increases during Benguela Niños leading to more evaporation (latent heat flux). Colder and drier air is advected from the South (Benguela Current, Namibia) by the Santa Helena high at that time of the year.

The unexpected result is that the latent and sensible heat fluxes contribute to cool the warm events in 1984 1995 and 2001. In fact given the magnitude of the wind speed and its weak variability off Angola, specific humidity variability and SST rather than wind speed variability dominate the latent heat flux variability. Likewise the three major cold events of 1982, 1992 and 1997 have weaker than normal latent heat flux, even with stronger wind in 1992 or 1997. In conclusion the latent heat fluxes have a rather passive role and seem to act as a thermostat to regulate cold and warm event at the surface. They definitively did not create the higher than normal SST in 1984, 1995 and 2001. Moreover since the rain was greater than normal the reduced solar radiation was probably having a cooling effect during warm events and a warming effect for cold events (below normal rainfall), acting in concert with the latent and sensible heat fluxes. Local upwelling and wind curl probably had a role in producing cold SSTs in 1997 and 1992, but wind does not play the major role in that region. The 2001 warm event had upwelling-favourable meridional wind and the cold 1982 event had weaker than normal meridional wind. In fact, 1982 also had weaker latent heat flux, so the explanation for that cooling must come from ocean dynamics. This illustrates the complexity of the surface heat budget for that region. The flux data used have their limitations and we did not attempt to integrate the radiative budget from NCEP in the net heat budget due to the questionable validity of the dataset.

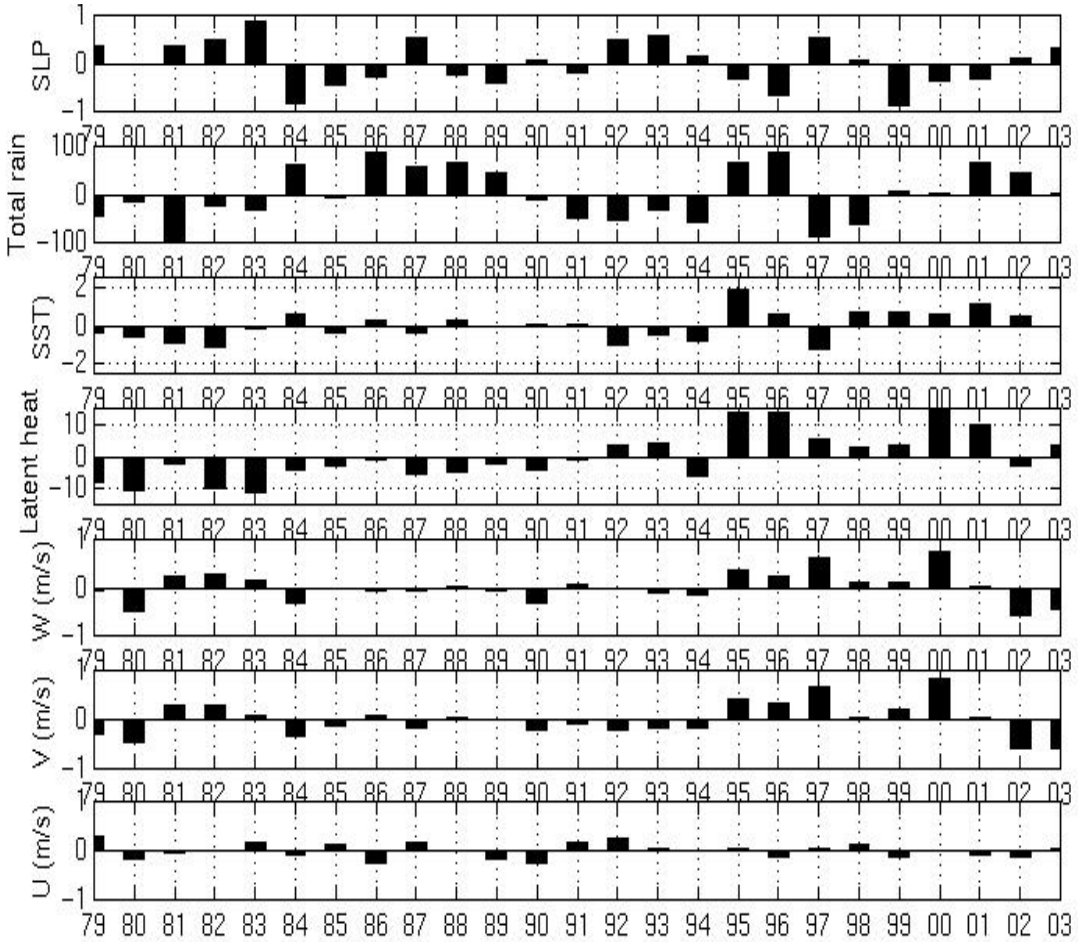

Figure 26: From top to bottom: normalized anomaly (anomaly of the mean of February March and April of each year relative to the 1979-2003 mean of FMA divided by the standard deviation of 1979-2003 FMA) for GPCP-V2 total rainfall, Hadley SST, NCEP latent heat flux, NCEP meridional (V) and zonal (U) surface wind speed, averaged between 8 E to the coast and between 20 S to 10 S.

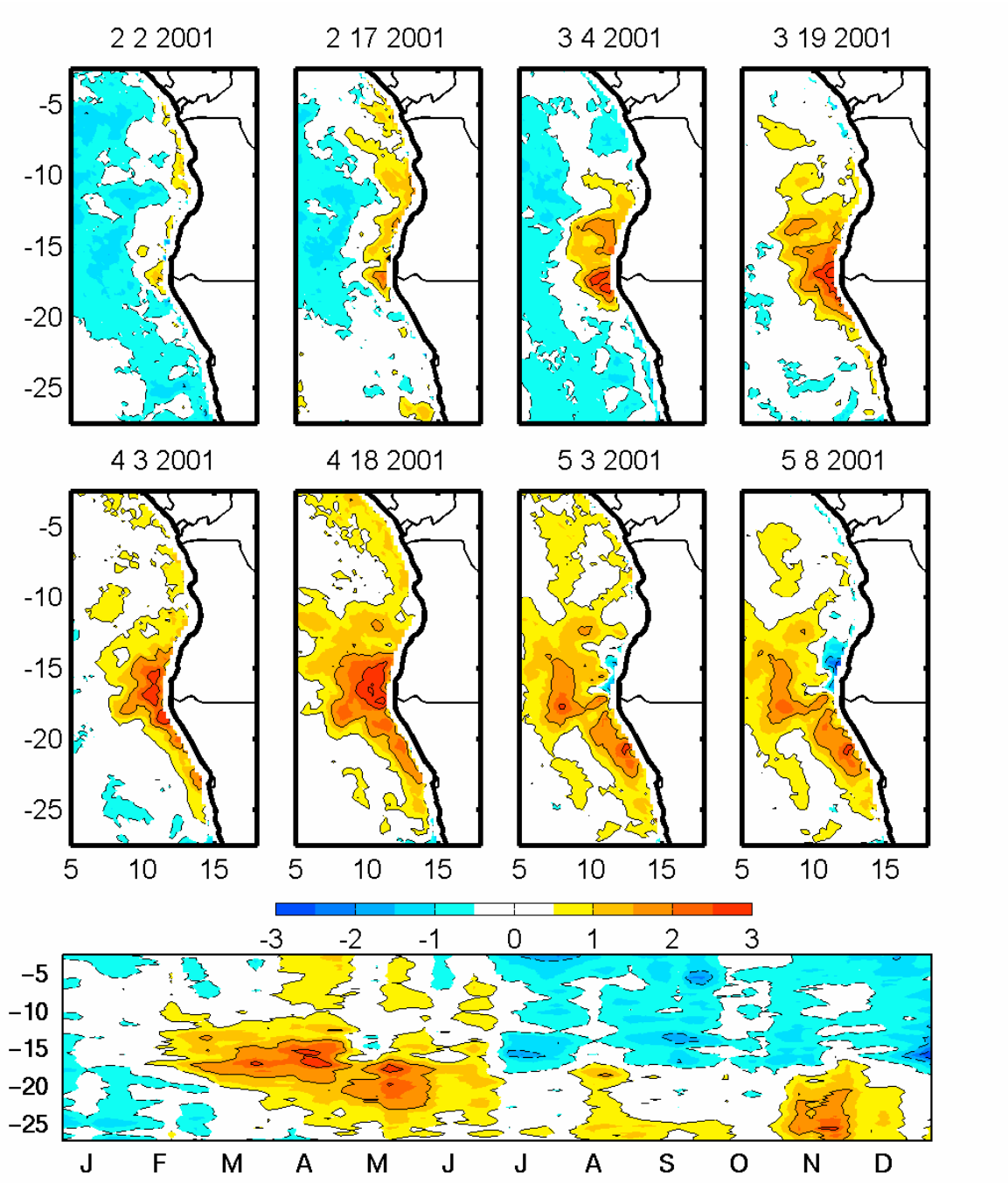

Figure 27: Top: maps of weekly mean TRMM TMI SST anomaly showing poleward propagation of above normal warm water from Angola to Namibia from February 2001 to May 2001. From left to right and top to bottom, the data are displayed every two weeks. The dates displayed correspond to the middle of the week. Bottom: time-latitude Hovmöller diagram of the weekly mean TRMM TMI SST anomaly. SSTA are averaged from the coast to 3 degree longitude offshore. Unit is °C. Contour Interval is 1°C. Interannual anomalies are estimated with respect to weekly climatology computed over the 2000-2005 period

Warmer than average sea surface temperatures were observed by the Tropical Rainfall Mission Microwave Imager in the Angola Benguela Current system in late austral summer 2001 and persisted for about three months. These coastal anomalies extended offshore by 1 to 4 degrees and were not due to local ocean atmosphere

interaction or relaxation of the mean upwelling-favourable southerly winds. Instead, they were remotely forced by ocean-atmosphere interaction in the Tropical Atlantic. Satellite remote sensing and a linear ocean model suggest that relaxation of trade winds along the equator triggered a Kelvin wave that crossed the basin within a month in early 2001 with a phase speed value of 2.3 m/s. Westerly wind anomalies were also observed in December 2000 and January 2001 over most of the Tropical Atlantic contributing to an enhancement of the oceanic seasonal cycle. This led to abnormal sea level heights near equatorial Africa that propagated southwards along the coast towards Angola and Namibia. Ocean general circulation models confirm the equatorial origin of the warm event and suggest a strengthening of the seasonal currents in the South East Tropical Atlantic. This process would have induced an increased penetration of warm water in the Angola Benguela upwelling system.

3.8.3 The 2001 warm event.

Figure 27 shows the southward propagation of warm SST anomalies along the Angola and Namibian coastlines at two-weekly intervals from February 2001 to May 2001. We calculated the weekly anomalies from weekly TMI SST minus a 1998-2004 monthly average centered on the week of interest. Anomalies are plotted only every 2 weeks from February 2001 to April 2001. Positive SST anomalies first appeared at the end of January at the Angolan coast between 5^{o}S and 17^{o}S raising Angolan water temperature from about 28^{o}C to 30^{o}C as far south as 15^{o}S. It seems that this anomalous warm water started accumulating and intensifying in February at the Angola Benguela Front (ABF) before propagating southwards in March in the coastal upwelling system of the Benguela Current to reach 26^{o}S at the end of March. The anomaly stayed positive in April from 13^{o}S to 26^{o}S. Analysis of the SST charts shows that those anomalies extended offshore by 2 to 4 degrees longitude at the ABF and about 1 degree longitude at the southern limit of the event. In total the warm anomaly was sustained for about 3 months, regardless of the local wind conditions, which were on average upwelling favourable between 15 ^{o}S and 25 ^{o}S. The 2001 persistent thermal anomaly can be likened to the 1984 and 1995 Benguela Niños. They occurred at the same time of the year (Shannon et al., 1986; Gammelsrød et al., 1998) but the surface expression of the 2001 event was not as strong (Rouault et al., 2003, Figure 27).

Variability in the wind usually determines SST variability south of the ABF which is situated at about 17 ^{o}S in late austral summer (Kostaniov and Lutjeharms, 1999; Shannon and Nelson, 1996; Colberg and Reason, 2006). Warm events south of the ABF at 15 South in the upwelling area are usually related to a weakening of the southerly wind or a spell of northerly wind (Shannon and Nelson, 1996). In the absence of long time series of daily wind speed in the domain, we investigated the variability of Quikscat wind stress in and compared it with the mean of 1999-2006.

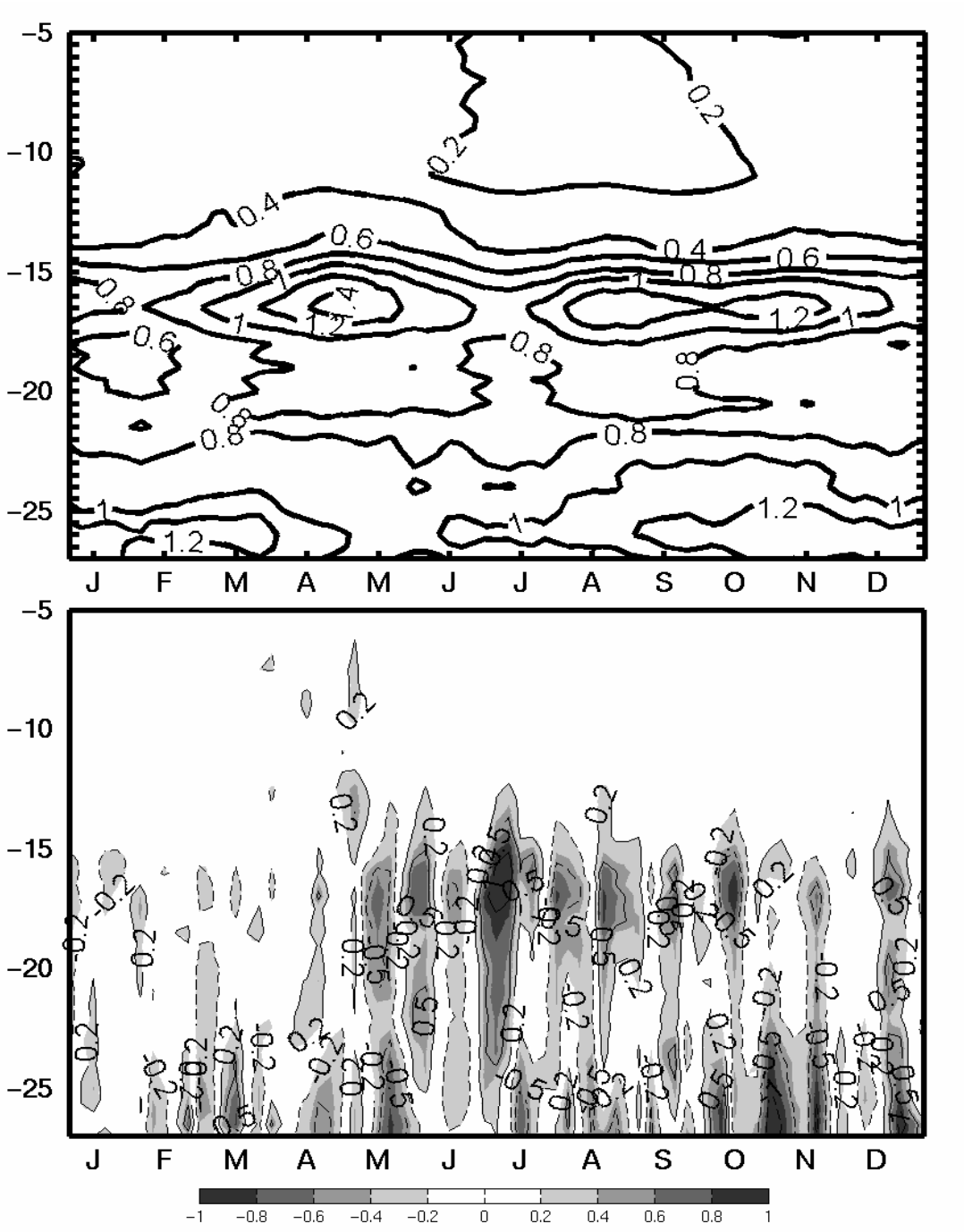

Figure 28: Time-latitude Hovmöller diagram of the daily QuikSCAT meridional wind stress (TY) climatology (a) and interannual anomalies in 2001 (b) along the African coasts. Data are averaged from the coast to 2 degree longitude offshore. Unit is dyn/cm^2. Contour Interval is 0.2dyn/cm^2. The climatology is computed over the 2000-2006 period and the interannual anomalies are estimated with respect to this climatology.

Figure 28a shows the climatology of the meridional wind stress averaged from the coast to 2 degree longitude offshore inferred from Quikscat (1999-2005). Wind favourable to upwelling is mostly found south of 15 S. The Quikscat climatology corresponds well to the climatology of Shannon and Nelson (1996) and Hardman-Mountford et al. (2004) even with no data roughly within 50 km from the coast. There is a good match between the Quikscat wind stress climatology and the major

upwelling cells at Cape Frio, and Luderitz (Demarc et al., 2004; Veitch et al., 2006). A relaxation of the wind is observed in January-February in our domain study from about 23 S to 15 S that is linked to the seasonal polewards migration of the South Atlantic anticyclone and associated trade winds.

Figure 28b presents a time-latitude Hovmöller diagram of Quikscat meridional wind stress anomalies from a 1999-2006 monthly mean centered on each week of interest off Angola and Namibia for the year 2001. Wind stress anomalies are averaged from the coast to 2 degree longitude offshore and indicate that the wind stress was mostly normal from January to April 2001 with the first substantial relaxation of upwelling-favourable wind in late April/May 2001. Although the wind stress anomaly was negative in February, it was not strong and long enough to be able to perturb the system for the 3 month period of the event. Figure 28b show that south of the ABF, only more intense and longer decreases in wind stress in October-November 2001 and in August 2001 can be linked with SST increases at the same period. However, increase and decrease of wind speed seems to slightly modulate the event. The first important wind stress anomaly happened at the end of April 2001 and probably contributed to extend the 2001 warm event. Time series for each year since 2000 of TMI SST and Quickscat wind speed anomalies averaged from 19 S to 25 S in the upwelling system south of the ABF confirm that the warming in 2001 was sustained and did not respond much to the relatively weak increase or decrease of early 2001. Additional material shows Hovmöller of SST and wind stress anomalies from 200 to 2005 and confirm the lesser role of local wind speed there.

3.8.4 Origin of the warm anomalies

To find the origin of the event, we analyzed merged sea surface height (SSH) altimetric data and Quikscat wind data for the entire Tropical Atlantic and we used a linear model to investigate wave dynamics along the equator. SSH are usually calculated against a mean annual reference In the Tropical Atlantic, the seasonal variability is much stronger than the interannual variability (Philander, 1990). It is therefore important to remove the seasonal signal to detect abnormal events in the Tropical Atlantic in SSH, especially if they are merely an enhancement of the seasonal cycle.

Figure 29 shows time/longitude Hovmöller diagrams along the equator and along the African coast of SSH anomalies estimated first with respect to the annual mean (Figures 29a, b) and then with respect to the seasonal cycle (Figures 29c, d). Figure 29c shows evidence of rapid propagation of higher than normal positive SSH from January 2001 to March 2001 across the equatorial Atlantic, which is associated with an intensification of the observed SSH seasonal cycle (Figure 29a). Note that Figure 29c also suggests that a preconditioning took place in January 2001 in the eastern equatorial part of the tropical Atlantic; where above normal positive SSH is observed in early 2001. At the African coast, the altimetric data clearly show that this equatorial propagation of positive SSHA is coherent with a relatively slower southward propagation of SSHA along the African coasts (Figure 29d). The above normal SSHA reached 20°S in March 2001, which is consistent with the SSTA propagation observed along the African coasts. We propose that the warm anomalies observed in the Angola Benguela upwelling system in late austral summer 2001 originate from this equatorial propagation, which in turn propagates southward so that the upwelling favourable winds off southern Angola / northern Namibia bring warm sub-surface water to the surface.

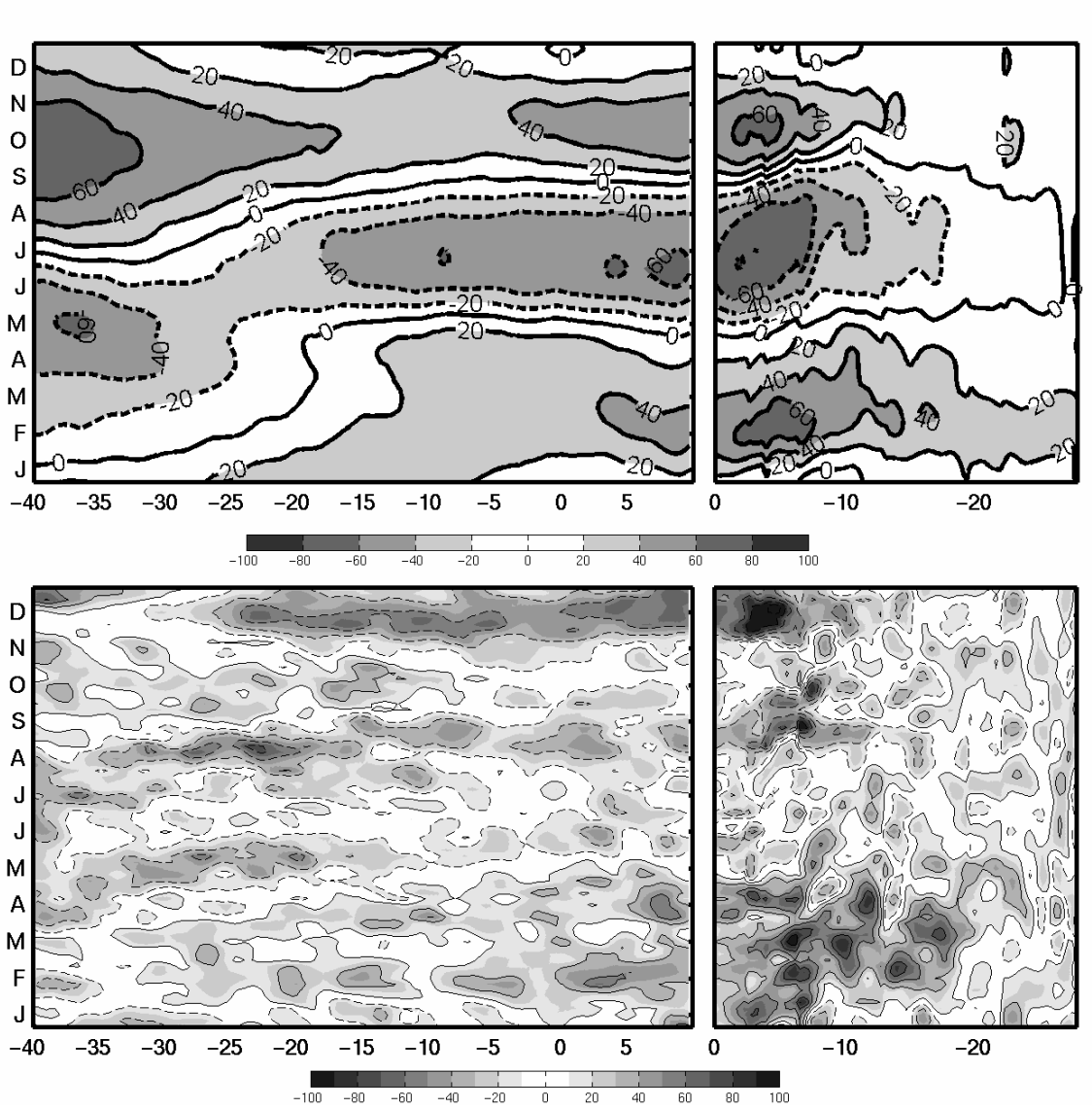

Figure 29: a) Longitude-time Hovmöller diagram of the weekly observed altimetric SSH seasonal cycle (SSHC) along the equator. b) Latitude-time Hovmöller diagram of the weekly SSHC along the African coasts. Weekly seasonal cycle is estimated relative to the 1999-2004 yearly mean. Panels c) and d) are similar to the panels a) and b) respectively, but for the observed altimetric SSH interannual anomalies. Anomalies are computed with respect to the weekly climatology estimated over the 1999-2004 period. Unit is cm. Contour Interval is 2 cm

In order to investigate the eastward equatorial propagation evidenced by the altimetric data, we used the Ocean Linear Model (OLM) forced by QuikSCAT wind stress anomalies. This model provides evidence of the significant role of the long equatorial wave propagations (Kelvin and Rossby) in the tropical Atlantic interannual variability whose signatures, by comparison to the tropical Pacific, are more difficult to determine in the observed altimeter data because of the reduced size of the basin and the contribution of several baroclinic modes (Illig et al., 2004). Nevertheless, this model is an efficient tool to interpret the altimetric signal along the equator and enabled Illig et al. (2006) to investigate the long equatorial wave contribution to the observed equatorial Atlantic 1996 warm event.

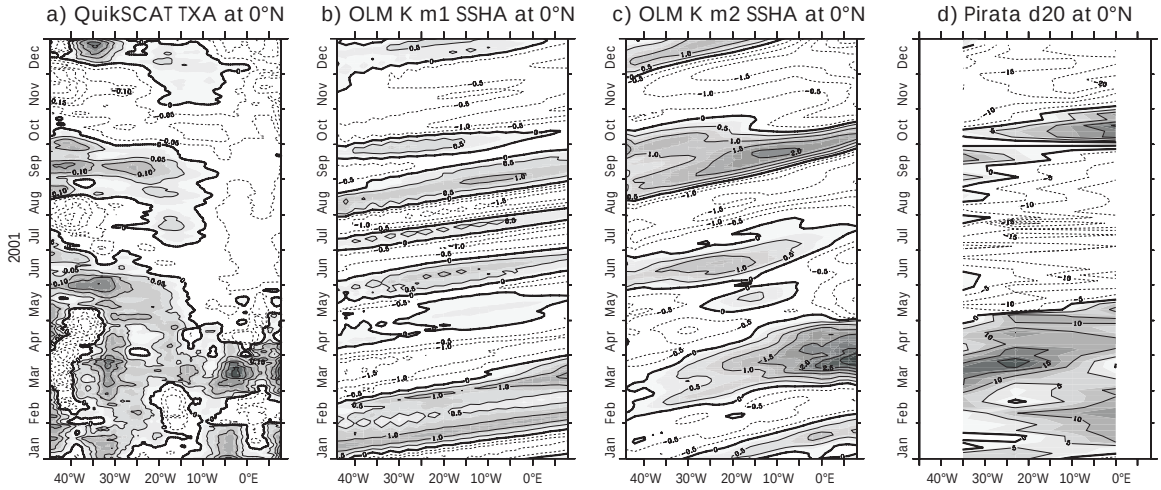

Figure 30: Longitude-time Hovmöller diagrams along the equator of the daily a) QuikSCAT Zonal wind stress anomalies (TXA), b) the Ocean Linear Model (OLM) first baroclinic mode Kelvin (K) contribution to SSH anomalies (SSHA) and c) the OLM second baroclinic mode K contribution to SSHA. Unit are dyn/cm^2 and cm respectively. Contour intervals are 0.1 dyn/cm^2 and 1 cm respectively. Anomalies are relative to the 2000-2005 seasonal cycle. For a better representation a 15-day running mean filter has been applied. Longitude-time Hovmöller diagrams along the equator of the anomaly of the depth of the 20 C isotherm inferred from the PIRATA array of mooring showing propagation of Z20 anomaly starting mid February.

QuikSCAT zonal wind stress anomalies along the equator are displayed in Figure 30a, along with the OLM first and second baroclinic mode Kelvin wave contributions to SSHA along the equator (Figure 30b, c). The OLM results allow us to identify a first baroclinic mode Kelvin wave that crosses the basin in January-February 2001, which is in agreement with the altimetric signal presented in Figure 30c. According to the OLM dynamics, this Kelvin wave is forced in early 2001 by the anomalous zonal wind stress in the western equatorial part of the Tropical Atlantic shown in Figure 30a, associated with a local trade wind relaxation. It propagates eastward with a phase speed value of 2.3 m/s, the same order of magnitude as those measured by Katz et al. (1997) or estimated by Delecluse et al. (1994). The analysis of the OLM second baroclinic mode Kelvin contribution to SSHA highlights a propagation from February 2001 to April 2001. It was triggered by anomalous zonal wind stress along the equatorial band, and intensified by intense anomalous zonal wind stress in eastern basin in early March 2001. This slower propagation can also be determined in the altimetric signal and takes slightly less than 2 months to cross the basin, in agreement with the theoretical phase speed of a second baroclinic Kelvin wave (1.34 m/s). The summed contribution of the first two baroclinic Kelvin wave to SSHA (not shown) closely resembles the altimetric signal, and explains the spreading in time of the propagation seen in Figure 30c. Moreover, the signature of the eastward propagations can also be observed in the equatorial Atlantic sub-surface, as shown by the Z20 anomaly estimated with the 1998-2006 PIRATA data (Figure 30d).

The eastward propagating Kelvin waves reach the African boundary from February 2001 to April 2001 in agreement with the altimetric signal. Examination of charts of weekly SSH anomalies from the seasonal cycle (not shown) show that higher than normal SSH appeared east of the Greenwich meridian during the second week of January 2001. According to the OLM results (Figure 30c), these anomalies are associated with a second baroclinic mode Kelvin wave, triggered by anomalous zonal wind stress in the centre of the basin in December 2000 and January 2001. Due to

local anomalous zonal wind stress, this anomaly intensified slightly during January before spreading southward. The SSH anomalies along the coast intensified and propagated gradually southwards in February and March 2001 linking the 2001 warm event to the equatorial region and suggesting an intensification of the mean annual cycle by the event.

The trade wind relaxation and westerly wind along the equator from late December 2000 to February 2001 seems to have played an important role in the onset of the 2001 warm event, as was the case for the 1984 and 1995 Benguela Niños (Carton and Huang, 1994; Florenchie et al., 2003, 2004). However, it is not clear if the 2001 warming was due to the abovementioned Kelvin wave triggered by the relaxation of the trade winds in January between 35 W and 25 W near the Equator, by the abnormally strong westerly wind in the east in December 2000 and January 2001 or by the resulting higher than normal integrated westerly wind component for December and January over all the equatorial region. However, it could be that the timing of an equatorial Kelvin waves relative to the annual cycle is the key for the penetration of warm anomaly south of the Angola Benguela Frontal Zone.

The results presented here demonstrate that the 2001 warm event was remotely forced. It seems that higher than normal SSH have propagated to the Front at 17 S. We now discuss a possible scenario where higher than normal SSH were the results of wave dynamics and exaggeration of the seasonal cycle all the way to the ABF. This would have deepened the thermocline, then warmed up the upper ocean and created stronger than normal poleward geostrophic current that would have strengthen the Angola Current. Advection could have then propagated the anomaly from the front to about 25 S. However, wind fluctuations could have modulated the events especially at the end of April 2001.

The intrusion of warm water in the northern Benguela current along the coast and the associated displacement of the ABF is indeed a seasonal feature (Boyd et al., 1986). Although little is known about the Angola Current, several cruises in the Angola Benguela current system (Moroshkin et al., 1970; Bubnov, 1972; Bubnov et Egorikhin, 1980; Lass et al., 2000; Morholtz et al., 2001) measured current speed of 0.5 to 0.7 m/s in the Angola current. They found that the Angola Current is weaker in winter and stronger in summer, weaker off the north of Angola and stronger to the south. It has a depth of about 200 meters and a width of about 200 to 300 km. A comprehensive survey done in April 1997 at the ABF and in the Angola Current by Lass et al. (2000) showed that most of the water feeding the Current at the time was coming from the northwest and was composed of Tropical Atlantic upper ocean water. Their results suggest that the South Equatorial Atlantic Counter Current along the northern limb of the Angola Gyre fed the Angolan Current. The model study of Carton and Huang (1994) and the analysis of Philander (1986) have also noted an increased South Equatorial Atlantic Counter Current during the onset of the 1984 Benguela Niño. Mercier et al. (2003) sampled along two lines in January 1995 along 9 W and in April 1995 along 5 S. They measured an eastward moving South Equatorial Counter Current and South Equatorial Undercurrent contributing to the northern limb of the Angola Gyre. They concluded that the circulation through the Angola Gyre was responsible for half the transport calculated for the Angola Current. A southward pulse of warm Angolan water was sampled at the Angola Benguela front during a cruise in April 1999 (Morholtz et al., 2001; John et al., 2004) with similar results. Note that Illig et al., 2004 suggested Kelvin waves in February March 1999 with timing consistent with the April 1999 warming. According to TMI SST the 1999 warming was not as intense as 2001, only lasted a month and propagated to 20 S only (Rouault and Lutjeharms, 2003).

Since the winds in the Benguela Current region south of the ABF were not weaker than average during, or prior, to the development of the 2001 warm event, we assume that the Benguela Current northwestward surface transport and the upwelling system itself were not weaker than usual. The 2001 warming as well as the 1984 and 1995 Benguela Niños and the 1999 warm event occurred at the same time of the year and this suggests a phase locking of Benguela Niños to the late summer when the ABF is further south. Figure 25 shows that the coastline starts to veer in a southeastwards direction at about 17 S, near the southernmost position of the Angola Benguela front that happens to occur in March. The seasonal southerly winds are weakest in the northern upwelling system when the South Atlantic Anticyclone is furthest south in early summer. All these factors imply that the 2001 warm event and perhaps the 1984 and 1995 Benguela Niños and the 1999 warm events may be related to an intensification of the annual cycle that then leads to a stronger than normal penetration of the Angola Current in the northern upwelling system.

A phase locking of Benguela Niños to late austral summer could explain why Kelvin waves in the Tropical Atlantic are not necessarily followed by Benguela Niños. For instance, the TRMM SST dataset shows several warm events off Angola that did not penetrate in the upwelling system (Rouault and Lutjeharms, 2003). We have noted several warm events of minor intensity that happened in other seasons and were linked to wind shifts in the Tropical Atlantic. They did not penetrate as far south as for the 1984, 1995, 1999 and 2001 warm events.

3.8.5 Conclusion

Warm SST anomalies propagated in the northern Benguela region from February to April 2001 in a similar fashion to the 1984 and 1995 Benguela Niños, although it was not as intense and the warming was shorter. Substantial SST anomalies started to appear at about 5 to 10 S and propagated along the coast to about 25 S. Ocean-atmosphere interaction acted to cool the event that was slightly modulated by the local wind stress. The origin of the warm event can be traced to anomalous behaviour in the Tropical Atlantic along the equator. This could have increased the accumulation of warm water along the Angolan coast and/or deepened the thermocline through the action of wave dynamics leading to an intensification of the Angola current with a timing that favored the intrusion of warm water in the northern upwelling system south of the Angola Benguela Front at 17 S. There is also a strong indication that Kelvin waves acted to propagate the anomalies along the Equator. In any case, the equatorial origin of the event has been demonstrated in this study, as it was for the 1984 and 1995 Benguela Niños. However, stronger than average westerly winds east of the Greenwich meridian could also have contributed to the event by enhancing the seasonal appearance of high SSH near Africa in austral summer 2001. The lack of *in situ* data motivates the extension of the PIRATA array in the South East Tropical Atlantic (Servain et al., 1999), which will be well suited to monitor Benguela Niños upstream of the event and link the Angola Benguela Current system to the Tropical Atlantic. Tide gauges are also needed along the coast together with a fine resolution ocean model for the South East Atlantic in order to help determine the relative roles of Angola Current advection of the signal and coastally trapped waves. Such a system will also help assess the potential contribution of the Congo River outflow which is not well understood.

4. Winter Rainfall

4.1 Principal mode of variability in the South Hemisphere.

Mo (2000) shows that the main modes of atmospheric and sea surface temperature variability in the South Hemisphere are ENSO and the Antarctic Annular Oscillation (AAO). The latter is also called the South Hemisphere annular mode (SAM) or high latitude mode (Kidson, 1999; Kiladis and Mo, 1998; Gong and Wang, 1999; Thomson and Wallace, 2000). In the Southern Hemisphere high latitudes, ENSO's impacts are mostly felt in the South Pacific, Bellingshausen, Amundsen and Ross Seas (Mo et al., 2000; Kwok and Comiso, 2002; Genthon et al., 2003). In its positive phase, the AAO is characterized by a southwards shift of the jet stream with an increase of westerly wind around the Antarctica ice cap near 60^{o}S and decrease of westerly wind, increase of northerly wind and increased subsidence near 40^{o}S (Thomson et al., 2000; Hall and Visbeck, 2002). The midlatitude pattern of the AAO is asymmetric with zonal 3 wave structure (Mo, 2000). The AAO is the dominant pattern of non-seasonal tropospheric circulation variability south of 20^{o}S, and it is characterized by pressure anomalies of one sign centered in the Antarctic and anomalies of the opposite sign centred at about 40-50^{o}S. The AAO is apparent throughout the year, but tends to be more active in austral spring (Thompson and Wallace, 2000). These authors defined the AAO as the leading principal component of 850 hPa geopotential height anomalies south of 20^{o}S; whereas Gong and Wang (1999) defined the Antarctic Oscillation Index (AOI) as the difference of the zonal mean level pressure between 40^{o}S and 65^{o}S. The U.S. Climate Prediction Center uses the leading principal component of the 700 hPa height field to define the AAO. Changes in the AAO since the 1970's have been linked to changes in the semi-annual oscillation (SAO) (van Loon et al., 1993; Burnett and McNicoll, 2000), to Antarctic ozone decrease (van Loon et Tourpali, 1995; Thomson and Solomon, 2002; Shindell and Schmidt, 2004), changes in SST gradient in the midlatitudes (Meehl et al., 1998) and increases in low latitude SST (Hurrell and van Loon, 1994). In addition, Jones and Moberg (2003) reported a Southern Hemisphere warming of the air temperature of 0.165 ^{o} C per decade for the 1977-2001 period. Casey and Cornillon (2001) present a non-uniform warming of slightly lesser magnitude in sea surface temperature for most of the Indian, South Atlantic and Southern Ocean for the period 1942-1995. At middle and high latitudes in the Southern Hemisphere, the annual cycle of mean sea level pressure is dominated by a strong half-yearly cycle called the semi-annual oscillation (SAO). The amplitude of the SAO peaks from 45S to 50S, reaches a minimum near 50-60S, and reaches a second peak over Antarctica. This feature is driven by the differing marches of tropospheric temperature over the southern oceans and the Antarctic continent (e.g. van Loon, 1967; Meehl et al., 1998). Van Loon (1967) noted a twice-yearly intensification of the mid-tropospheric temperature gradient between 50S and 65S.

Given that the AAO is a fundamental part of the subtropical to high latitude Southern Hemisphere atmospheric circulation, it is natural to ask whether it influences South African precipitation. In our study, we show evidence of links between the AAO and winter (JJA) rainfall over the southwestern Cape (SWC) region of South Africa. This region of the country contains the second largest city (one of the world's top tourist destinations) and significant irrigated agriculture as well as being very prone to drought, yet the variability in its climate has not been widely studied. It is a semi-arid region receiving most of its rainfall in winter via cold fronts and whose economy depends critically on the adequate storage of these winter rains in large dams. The rapidly growing population is frequently subjected to water restrictions during the summer half of the year when the winter rains have been inadequate. Better understanding of its climate variability is therefore a high priority.

Given this evidence of large scale warming and the importance of the SAO and the AAO for mid- to high latitude Southern Hemisphere climate, The causes of the climate change at Marion Island since the 1960's were also explored as links with variability of the mid and high latitude of South Hemisphere climate. We have analyzed the trend in meteorological parameters and sea surface temperature at Marion. We then investigate relationships between the trend and the change in the SAO and AAO.

4.2 Decrease in winter rainfall

4.2.1 Data and methods

Station data from the South African Weather Service (SAWS) and the gridded monthly 0.5^{o} resolution gridded CRU rainfall data (New et al., 2000) averaged over the SWC region of South Africa (17-21^{o}E, 30-35 ^{o}S) are used to investigate winter (JJA) rainfall. Winters with 0.8 or more standard deviations above (below) average rainfall in the 1948-2004 period are defined as wet (dry). In addition to the substantial interannual variability studied herein, a wavelet analysis of the rainfall time series using the Morlet wavelet indicates quasi-decadal variability with highest power during the 1930-1980 period. This quasi-decadal variability in winter rainfall has been examined by Reason and Rouault (2002) and was related to ENSO-like decadal variability.

Wet year: 1996, 1991, 1986, 1981, 1977, 1974, 1962, 1957, 1956, 1955, 1954

Dry year: 2004, 2003, 1998, 1984, 1978, 1972, 1969, 1965, 1960, 1959, 1958

To define an index for the AAO, the leading EOF of the austral winter (JJA), 700 hPa geopotential height from the NCEP re-analyses (Kalnay et al., 1996) computed for the entire Southern Hemisphere south of 20^{o}S, is used. Since a strong tendency exists in the AAO for positive polarity in recent decades (e.g. Thompson and Wallace, 2000), the index is de-trended and then normalised using the standard deviation to determine winters with positive or negative AAO phase. It is found that 9 out of the 11 wet (8 out of the 11 dry) winters correspond to negative (positive) AAO phase suggesting a connection between this circulation pattern and SWC anomalous winter rainfall. Composites of NCEP re-analysis variables for the 9 negative and 8 positive AAO phase winters are used to investigate the associated anomalies in regional atmospheric circulation that may impact on SWC rainfall. The 1962 and 1956 wet (1972, 1965, 1959 dry) winters that do not correspond to negative (positive) AAO phase are investigated separately to determine if different mechanisms are responsible.

4.2.2 Links between the AAO and winter rainfall

A correlation at zero lag between the AAO time series and the SWC winter rainfall index derived from the New et al. (2000) 0.5^{o} gridded data for the overlapping period of the two datasets of 1948-1998 shows values of 0.2-0.4 (95-99.5% statistical significance) over the west coast region of South Africa. The correlation region broadens to include a much larger region of western South Africa at 1 (not shown) and 2 month (Figure 1) lead suggesting that circulation patterns associated with the AAO may influence late winter/spring rainfall over this part of the country.

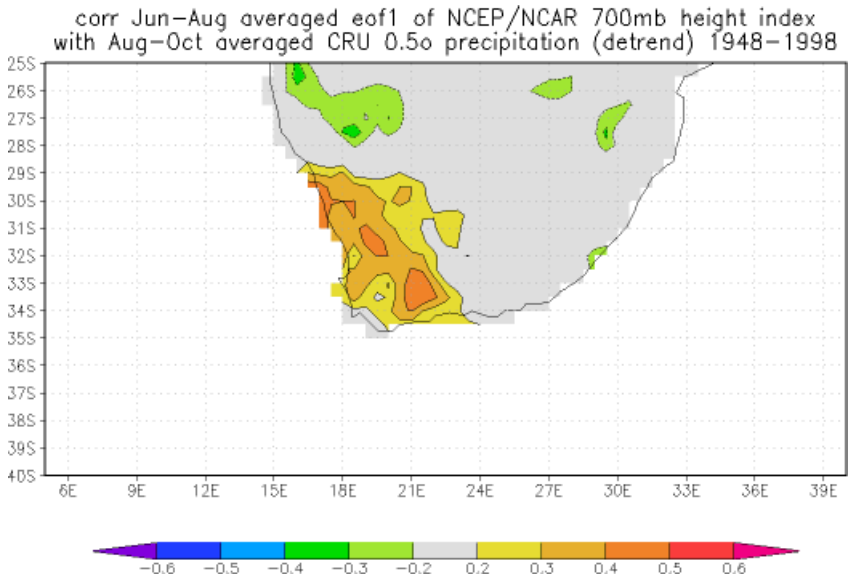

Figure 1: Field correlation between winter (JJA) rainfall and the AAO index at two month lead.

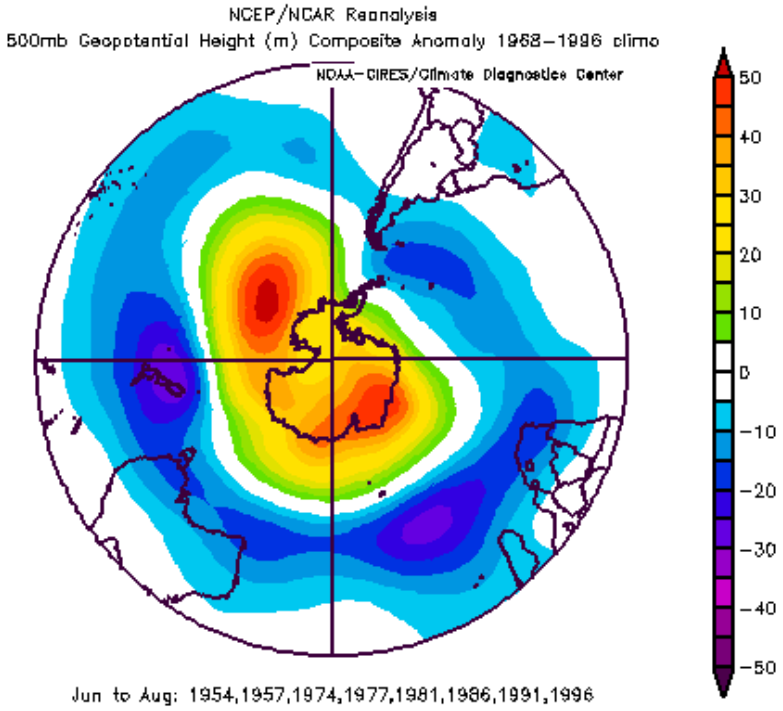

Figure 2: Composite of wet winter 500 hPa geopotential height anomaly for the 9 out of 11 wettest winters with negative AAO phase (1954, 1955, 1957, 1974, 1977, 1981, 1986, 1991, and 1996). Contour interval is 5m.

Winter/spring rainfall is mainly brought about by cold fronts, with lesser contributions from cut-off lows and other westerly disturbances. To consider potential mechanisms, Figure 2 shows the composite wet winter 500 hPa geopotential height over the Southern Hemisphere indicating that, in addition to the annular mode, there is a wave 3-4 pattern in the midlatitudes. An area of low pressure anomaly stretches from the climatologically important cyclogenesis region in the far SW Atlantic (Jones and

Simmonds, 1993) across the South Atlantic midlatitudes and subtropics to southern Africa and the SW Indian Ocean. Negative anomalies in the far SW Atlantic are favourable for the genesis of more and stronger depressions tracking towards the SWC. Figure 2 also suggests that wet SWC winters are associated with weaker South Atlantic and South Indian anticyclones, decreasing the typical winter subsidence over South Africa and favouring a more northward track of frontal systems in the region. The pattern shown in Figure 2 is robust in the sense that all the wet winters show an area of low pressure anomaly stretching west from the SWC with another cyclonic anomaly in the SW Atlantic. The non-AAO wet winters (1962 and 1956) also show significant low pressure anomalies over the SWC and stretching westwards over the South Atlantic; the difference from Figure 2 is that they do not show sufficiently positive height anomalies over Antarctica to be classified as negative AAO phase. The connection between these cyclonic anomalies, the AAO, and SWC rainfall is supported by Figure 3 which shows a region of positive correlation between the AAO index and NCEP surface latent heat flux stretching from areas of cyclogenesis in the SW Atlantic across the midlatitudes towards the SWC.

The dry winter composite (not shown) is roughly opposite to Figure 2 with high pressure anomalies extending over the SWC and subtropical to midlatitude South Atlantic and negative over Antarctic. Of the three non-AAO dry winters, 1972 also displays high pressure anomalies over the SWC but extending more to the south / southwest rather than west / southwest as in the composite. For 1959, the main feature is a large cyclonic anomaly centred across the South Atlantic well to the south of South Africa indicating that westerly storm tracks were anomalously far south during that winter leading to relatively dry conditions over the SWC. The 1965 winter shows cyclonic anomalies over and northwest of the SWC but high pressure anomalies over most of the midlatitude South Atlantic, particularly in areas of high cyclogenesis (Jones and Simmonds, 1993). Thus, although local conditions were relatively favourable for winter rainfall, those over the ocean areas upstream where cyclonic systems are generated were not, and hence this winter was dry.

Since the winter rainfall is mainly frontal, one might expect shifts in the subtropical jet just upstream of the region during anomalously wet or dry winters. Figure 3 shows that this is indeed the case for the wet winters with the jet shifted equatorwards and stronger than average by about 15 %, consistent with a northward shift of the storm track and stronger westerly troughs. For the dry composite, there is a weakening and slight southward shift of the jet (not shown), unfavourable for good rains. These suggested shifts in the storm tracks are supported by a strengthening (weakening) of the low level westerly flow over southern South Africa (the ocean near 40-50^{o}S) for the wet composite (not shown) and the reverse for the dry composite. This result together with the surface evaporation correlation suggests that more (less) low-level moisture is transported towards the SWC from the subtropics / midlatitudes of the South Atlantic during wet (dry) winters. The 1000-500 hPa thickness has also been examined (Figure 4) and indicates a region of reduced thickness over the SWC and upstream across the South Atlantic. Since reduced thickness implies a denser and colder atmosphere, and therefore one less able to contain water vapour, the implication of this result is that during wet SWC winters, more of the lower atmosphere moisture is precipitated out over and upstream of the SWC, consistent with the increased rainfall. For the dry composite (not shown), increased thickness exists over western South Africa and the neighbouring South East Atlantic.

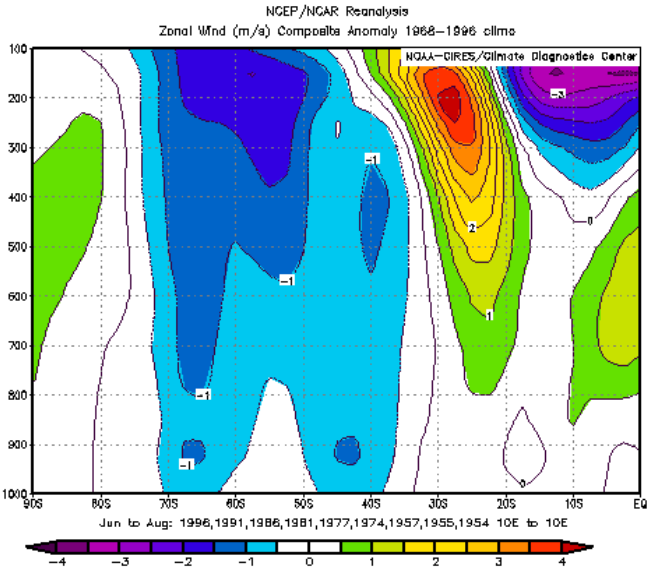

Figure 3: As for Figure 2 except zonal wind at 10°E, just upstream of southwestern South Africa. Contour interval is 0.5 m/s.

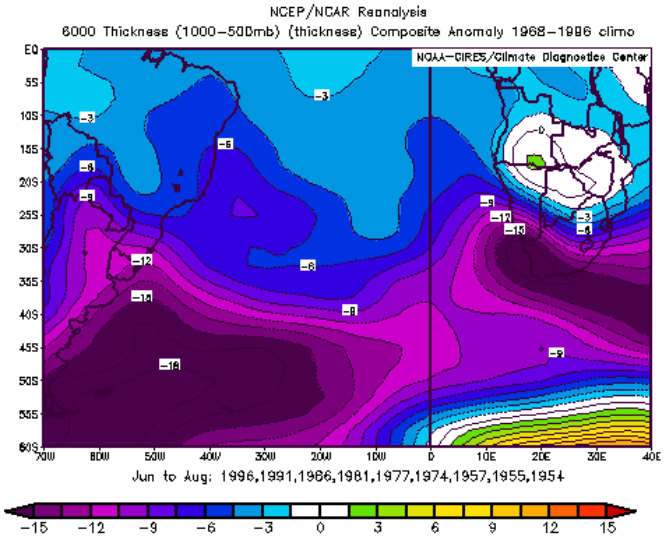

Figure 4: As for Figure 2 except thickness of the 1000-500 hPa layer (contour interval is 1.5m).

Other re-analysis parameters indicative of changes in frontal rainfall were examined and found to be consistent with the suggestion of a stronger and northward shifted storm track during the wet winters. Figure 5 shows enhanced uplift at 500 hPa over the region and neighbouring ocean areas in the wet composite with roughly the reverse pattern for the dry winters (not shown). Additionally, low-level cyclonic vorticity and relative convergence (anticyclonic vorticity and divergence anomalies) exist over the SWC and adjacent ocean for the wet (dry) composite (not shown). As a result, conditions are favourable for local strengthening (weakening) of approaching frontal systems during wet (dry) winters.

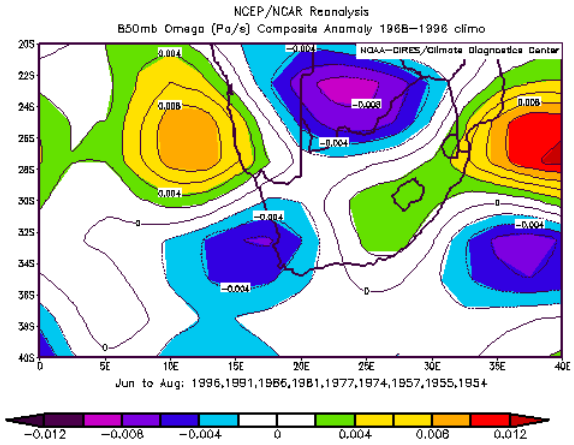

Figure 5: As for Figure 2 except vertical motion at the 500 hPa level (contour interval is 0.002 Pa/s). Negative (positive) values correspond to anomalous uplift (subsidence).

Previous observational and modelling work (Reason et al., 2002, 2003) has suggested that South Atlantic SST anomalies may be related to SWC winter rainfall variability such that warm (cool) SST anomalies in the west (central) subtropics / midlatitudes of the South Atlantic tend to be associated with wet winters. A similar SST pattern is found for the wet composite while the SST anomaly pattern for the dry composite is characterized more by cool anomalies in the central-west South Atlantic and large warm anomalies southeast of South Africa. This result suggests that the AAO-surface evaporation link is not directly related to changes in SST but rather to changes in surface wind and specific humidity induced by the AAO circulation anomalies. In addition, the mix of neutral and ENSO winters in the list of anomalously wet and dry winters suggests that there may be also an ENSO relationship as well as an AAO influence on SWC winter rainfall.

4.2.3 Potential ENSO influence

Several of the high and low phase AAO seasons are also ENSO seasons. It is well known that there is an impact of ENSO on the SST and atmospheric circulation of the South Atlantic region via the Pacific South America (PSA) pattern (e.g. Mo and Paegle, 2001; Colberg et al., 2004) and therefore there may also be an ENSO influence on SWC rainfall. Of the 11 wettest (11 driest) winters in Table 1, 3 are El Niño and 4 are mature phase La Niña (1 is a La Niña and 3 are mature phase El Niño) years. By mature phase, it is meant that the winter in question from Table 1 follows the JFM of the mature El Niño or La Niña event (e.g. the 1958 dry winter or the 1996 wet winter). If the winter is re-defined to also include May and September, then the numbers of wet or dry winters corresponding to ENSO years decreases. The mix of ENSO and neutral years in Table 1 suggests that any influence on SWC winter rainfall is likely to be subtle. Indeed, a field correlation of the Niño 3.4 SST index with winter rainfall over the SWC shows values smaller than –0.2 for zero lead which increase to –0.2 to –0.3 at one or two month leads. These values are somewhat smaller than those derived earlier for the AAO index.

In an attempt to remove any ENSO influence, the AAO time series was re-calculated with the 1957, 1963, 1965, 1972, 1982, and 1997 strong El Niño winters set to special values and correlations with SWC winter rainfall repeated. At zero lead, the

correlations are almost identical to that obtained for the original AAO index but extending over a slightly larger area. For one month lead, the increased area of correlations of 0.2-0.4 is also larger than for the original index but the most substantial increase is seen at two month lead where some areas exceed 0.5. A similar result was obtained if the winters corresponding to strong La Niña events are removed from the original AAO index. Thus, it appears that the AAO relationship with SWC winter rainfall is robust and is not significantly contributed to by any ENSO influence on SWC rainfall.

4.2.4 Summary and conclusions

The Antarctic Oscillation (AAO), Southern Annular or "high latitude" mode (Kidson, 1988) is the dominant pattern of tropospheric circulation variability south of 20^{o}S, and it is characterized by pressure anomalies of one sign centered in the Antarctic and anomalies of the opposite sign centred at about 40-50^{o}S. Evidence has been presented that there is a statistical relationship between the AAO, defined as the leading EOF of the NCEP re-analysis 700 hPa geopotential height field over the Southern Hemisphere south of 20^{o}S, and rainfall over southwestern South Africa for the austral winter (JJA). Note that the majority of the annual rainfall in this region occurs in winter. Since there is a tendency towards increasing polarity of the AAO in recent decades, both the AAO index and the rainfall have been detrended before analysis. Of the 11 wettest (11 driest) winters in this region during the 1948-2004 period, 9 (8) correspond to negative (positive) AAO phase. A weak relationship also exists between the winter rainfall of this region and ENSO, as measured by the Niño 3.4 SST index. When this weak relationship is removed, that with the AAO index is increased.

Analysis of the circulation anomalies indicates that the mechanisms by which the AAO influences winter rainfall over southwestern South Africa involves shifts in the subtropical jet, changes in the surface evaporation over the midlatitude South Atlantic upstream of the region, and local uplift, low-level convergence and relative vorticity. As a result, negative AAO/wet winters tend to be associated with an equatorward shifted and stronger midlatitude storm track in the South African sector and positive AAO phase/dry winters with the reverse. In addition, there are shifts in the wavenumber 3 – 4 pattern such that cyclonic (anticyclonic) anomalies tend to exist over and upstream of southwestern Africa during wet (dry) winters. Given that the statistical relationship between the rainfall and the AAO index increases with one or two month lead, some indications of late winter/early spring rainfall may be obtained from the state of the AAO index in early winter. This possibility is potentially of great importance to water managers since the region is prone to winter drought, and in the last decade or so, there have been several years in which dry or very dry early to mid-winter months were followed by average or above average late winter/early spring rains.

4.3 Climate change at Marion Island since 1950

4.3.1 Introduction

Marion Island (46°54' S and 37°51' E) is a subantarctic island, situated 1700 kilometers southeast of Africa, whose climate has shown significant changes over the last thirty years. This volcanic island is about 250 km^2 with 72 km of coastline and the highest peak at 1300 m. Since the beginning of the 1970's, the total annual precipitation has decreased by 25%, sunshine hours have increased and mean air temperature has increased by 1.2°C (Smith, 2002). Analysis of sea surface temperature shows an increase of 1.4°C since the 1950s in near shore sea surface temperature measured daily at the island. These variations in local climate have had a substantial influence on the island ecosystem (Smith and Steenkamp, 1990; Chown and Smith, 1993; Smith et al., 2001; Smith and Gremmen, 2001; Pakhomov et al., 2004).

Marion Island is situated in the "Roaring Forties" and, on weather time scales, is subject to a succession of midlatitude depressions, frontal systems and migratory anticyclones (Vowinckel, 1954). Oceanographically the Prince Edward Islands (of which Marion Island forms part) lie in the subantarctic with the Subtropical Convergence to the north and the Antarctic Polar Front to the south. The islands lie in the general path of the Antarctic Circumpolar Current (ACC).

In this study, we argue that regional atmospheric circulation patterns have changed on interannual and longer time scales, thereby leading to the observed variations in precipitation, non rainy days, air temperature, sunshine hours, coastal sea surface temperature and wind speed and direction. Evidence is presented that these changes are linked to modification of the nature of the semi-annual oscillation (SAO), a strong half-yearly cycle in pressure, temperature and wind in the midlatitudes of the Southern Hemisphere which arises from the different timings of the annual cycle between the ice covered high latitudes and the ocean dominated midlatitudes (van Loon, 1967). Changes in the SAO previously reported by van Loon et al. (1993) , Hurrell and van Loon (1994) and Meehl et al. (1998) influence the synoptic systems at Marion Island's latitude, and hence the local climate.

4.3.2 Marion Island time series

Meteorological and sea surface temperature measurements have been made daily at Marion Island since 1950 making it a unique dataset for the sub-Antarctic. In addition to the monthly precipitation, mean air temperature and sunshine hours data already presented by Smith (2002), we study the surface atmospheric pressure, minimum and maximum air temperature, precipitation and sea surface temperature data recorded at Marion as well as surface wind speed and direction and regional circulation inferred from NCEP reanalysis climate data (Kalnay et al., 1996). The Marion Island surface and upper air data are assimilated into the NCEP re-analysis so we have confidence in using these to complement and extend the station data for wind speed and direction. NCEP data should be taken with caution because they are less reliable south of 40°S than elsewhere due to a relative lack of observations available to be assimilated into the NCEP model, especially before the 1970's. This could hamper the interpretation of atmospheric trends and mechanisms in the Southern Ocean (Hines et al., 2000; Kistler et al., 2001; Marshall, 2003; Genthon et al., 2003; Renwick, 2004; Tennant, 2004).

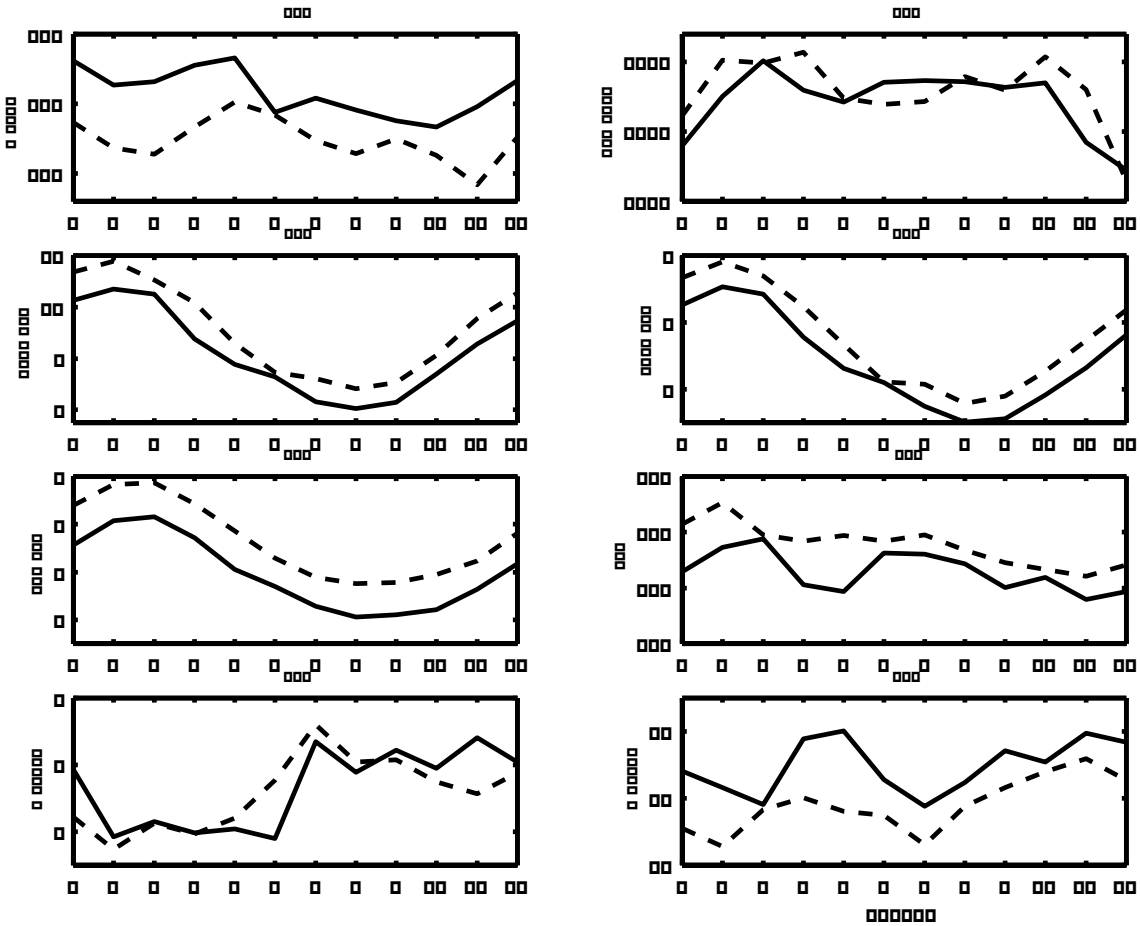

Figure 6: Left to right and top to bottom: yearly mean cycle of precipitation (a), surface atmospheric pressure (b), maximum (c) and minimum (d) temperature, nearshore sea surface temperature (e), NCEP wind direction (f), zonal (g) and meridional (h) wind speed for the period 1960-1980 (black line) and 1981-2001 (dashed line).

Figure 6 shows the mean yearly cycles of a number of climate variables. Note that NCEP surface wind speeds are used because there were several interruptions in the Marion Island wind data that prevents us from using the local data for calculating trends. These interruptions arose with the introduction of an automatic measuring system in the 1980's. There is also a problem of bad wind data from 1966 to 1979 that has not yet been solved. The wind is mostly westerly all year long with maximum in winter and minimum in autumn. Precipitation, pressure, temperature and wind speed and direction show a relatively small annual range in values as expected for a maritime mid-latitude location impacted throughout the year by eastward moving low-pressure systems (Vowinckel, 1954). About 100 low-pressure systems affect Marion Island every year according to Smith (2002). Rainfall tends to peak in summer (December and January) and in May when sea level pressure is low. Pressure is lower in summer than in winter. Rainfall seems to decrease in June but precipitation measurement in winter months (June to September) must be taken with caution since snowfall or hail in the rain gauge bucket can interfere with the measurement. The liquid water content of snow and hail collected in the gauge are melted by the meteorologist working on the island and taken as total precipitation. We will therefore consider the precipitation data only for the October-April period, but the parameter, days without precipitation, is still valid for winter. The two rainfall minima (February-March and October-November) occur when the sea level pressure is maximum and

reflect the semiannual modulations in the meridional temperature gradient associated with the SAO. Figure 6 also illustrates the change in climate of the island that will be discussed further.

A linear fit is used to estimate the trend of the different series for each calendar month (not shown). Since least-square fitting can have undesired sensitivity to outlying points, we used a robust technique based on the minimization of the absolute deviation (Press et al., 1992). There are a few breaks in the records; however, we did not fill these and we calculated the linear fit for the existing data only. The trends, defined here as the difference between the last and first value of the linear fit, are plotted in Figure 7. We performed an analysis of variance to test the significance level of the trends. Under the null hypothesis that there is no effect due to the linear regression fit, the ratio of the mean squares due to the regression and the mean square due to the residuals are expected to follow a F-distribution. Up-pointing triangles in Figure 7 show the months where the trends are significant at the 0.01 level according to the F-test, while down-pointing triangles show those which are significant at the 0.05 level.

Except for March, we observe a significant positive trend of the pressure in spring, summer and autumn and no trend in winter (Figure 7a). Trends will be discussed later. The trends in the precipitation (Figure 7b) and more remarkably, the trends in the numbers of days without rainfall (Figure 7c), agree well with those found in the pressure (Figure 7a). The correlation coefficient between the pressure trend curve (Figure 7a) and the curve showing the number of days with no precipitation trend (Figure 7c) is r =0.7 (significant at the 0.01 level). The largest changes in rainfall occur from November to April with a 20 % reduction in precipitation for the last 20 years. Rainfall seems to have decreased for almost all months but the results for the winter (May to September) must be taken with caution because of the snow problem mentioned above. The change in days without precipitation is significant for all months except March, June and October. Change in maximum temperature is substantial, up to 2.4 C.

We note a northward shift in the NCEP wind direction (Figure 7d). The maximum (Figure 7e) and minimum (Figure 7f) temperature, and the SST (Figure 7g) shows strong positive trends in the summer months and weaker positive trends in the winter months. We also note a decrease of the trend in March for all parameters. This remarkable feature will be explained later. It is interesting to note that even though there is little change in winter in atmospheric parameters, SSTs remain significantly higher all year long.

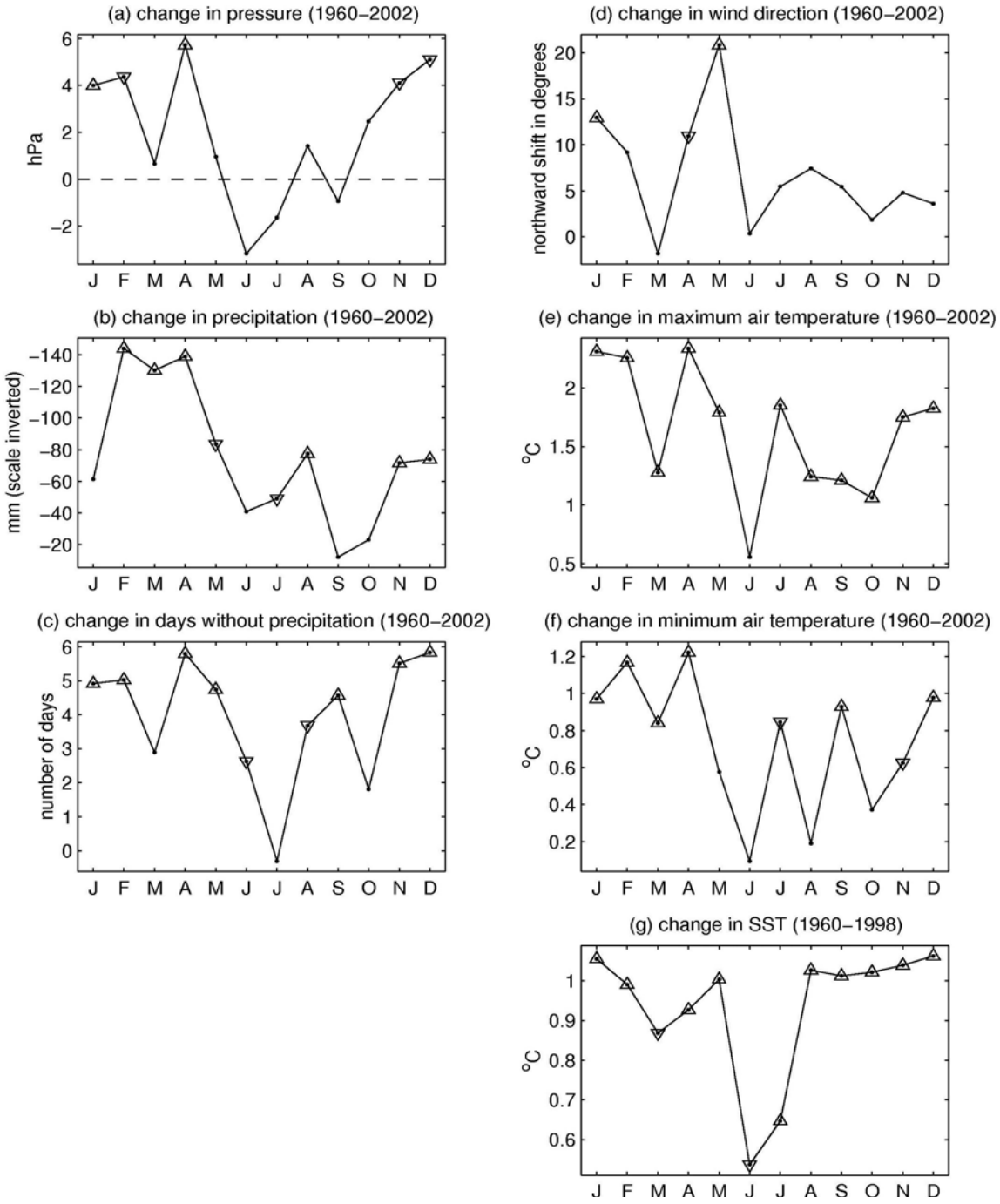

Figure 7: Trend from 1960 to 2002 for each calendar month at Marion Island of surface atmospheric pressure (a), precipitation (b), number of days without precipitation (c), NCEP wind direction (d), maximum air temperature (e), minimum air temperature (f) and the near shore sea surface temperature (g) from 1960 to 2002. The trend is defined as the difference between the last year (2002, for (a) to (f), 1998 for (g) and the first year (1960) of the linear fits. Up-pointing triangles show the months where the trends are significant at the 0.01 level according to the F-test, while down-pointing triangles show those which are significant at the 0.05 level.

4.3.3 Variability of the pressure at Marion and cyclonic activity

The trends observed in Figure 7 show that the increase of the pressure in summer corresponds to a decrease of the rainfall, an increase in the number of days without

precipitation and a northward shift in the wind direction. This suggests a change in cyclonic activity impacting the island. Change in NCEP wind speed for the last 20 years corresponds to a summer reduction in the westerly wind component and an increase in the northerly wind component all year long. The reduction in the westerly wind component is consistent with the increase in atmospheric pressure and the decrease in rainfall, and would imply relatively more anticyclonic conditions over the island or a reduction in low pressure affecting the island in summer.

According to the linear fit of the entire series (not shown), the mean pressure varies from 1006.8 hPa in January 1960 to 1008.6 hPa in December 2002, while the number of non-rainy days increases from 37 days per year in 1960 to 84 per year in 2002. This summer increase in surface pressure and non-rainy days, and the decrease of the rainfall, may tentatively be linked to the decrease in the number of cyclones observed in the Southern Hemisphere and/or to a southward shift in the cyclonic storm track (Simmonds and Keay, 2000; Fyfe, 2003).

In Figure 8, we have plotted the 1960-2001 trend of the NCEP-NCAR sea level pressure at 35 E for latitudes from 40S to 60S for all months. We note an increase in the pressure trend north of 52.5 S and a decrease south of this latitude (Marion lies near 47S). This is consistent with the hypothesis of a southward shift of the cyclonic activity. However, caution must be exercised when dealing with NCEP SLP data south of 45 S, which before 1967 is considered too high by Hines et al. (2000).

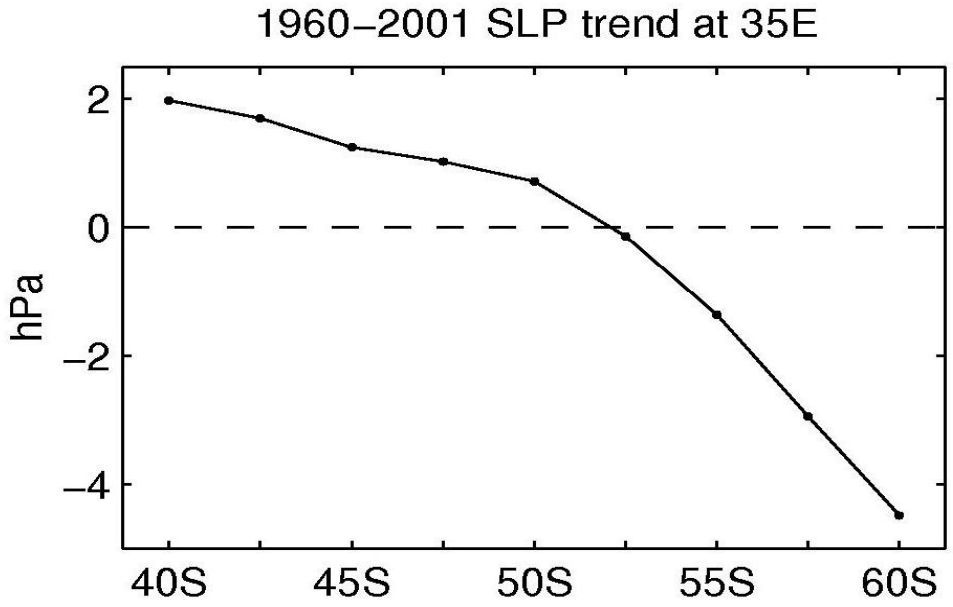

Figure 8: Trend (in hPa) of the 1960 to 2001 sea level pressure at 35°E from 40°S to 60°S.

Finally, the northward shift in the wind direction can be linked to the pressure increase and the decrease in cyclone numbers affecting the island in summer. Examination of the meteorological conditions for non-rainy days show that in between the depressions, Marion Island is usually under the influence of the South Indian Ocean anticyclone with its centre of action to the north east of the Island. This brings warm air from the north and moderate northwesterly to northeasterly wind. It is interesting to note that the northerly component has also increased in winter.

The variations in local climate at Marion Island over the last 40 years are more significant from November to May than in winter. A southwards shift of the low

pressure systems affecting the island or a reduction in their number in that period could have caused an increase in sunshine and non rainy days, a decrease in the westerly wind component and an increase in the northerly component. All these changes would be favorable for an increase in local near-shore SST, as observed. In addition, an increase in northerly wind will bring warmer air from the north, increasing ocean warming through turbulent sensible heat flux. This suggests that these atmospheric changes are responsible for the SST increase. However, we observed a warming in SST for the month of June while there is no change in rainfall or air temperature. Moreover, the change in SST and air temperature is significant at all months while it is not the case for the other parameters (i.e. March). This could either mean that the warming during summer and autumn can persist in winter or that part of the SST warming is explained by changes in the large-scale oceanographic conditions.

4.3.4 Variability of the pressure at Marion and the Semi-Annual Oscillation (SAO)

At middle and high latitudes in the Southern Hemisphere, the annual cycle of mean sea level pressure is dominated by a strong half-yearly cycle called the semi-annual oscillation (SAO). The amplitude of the SAO peaks from 45S to 50S, reaches a minimum near 50-60S, and reaches a second peak over Antarctica. This feature is driven by the differing marches of tropospheric temperature over the southern oceans and the Antarctic continent (e.g. van Loon, 1967; Meehl et al., 1998). Van Loon (1967) noted a twice-yearly intensification of the mid-tropospheric temperature gradient between 50S and 65S. Thus, a useful index of the SAO, first used by Van Loon (1967), is the difference of the zonal mean 500-mb temperature between 50S and 65S. He showed that this index, indicative of the state of the SAO, was associated with the forcing of the phenomenon. The idea is that the twice-yearly intensification of the mid-tropospheric temperature gradient between the ocean-dominated middle latitudes and the polar continental latitudes is associated with a twice-yearly increase of storm activity and thus changes in the intensity of the circumpolar trough. Here, we demonstrate that the variability of the pressure observed at Marion is linked to a change in the phase and amplitude of the SAO index.

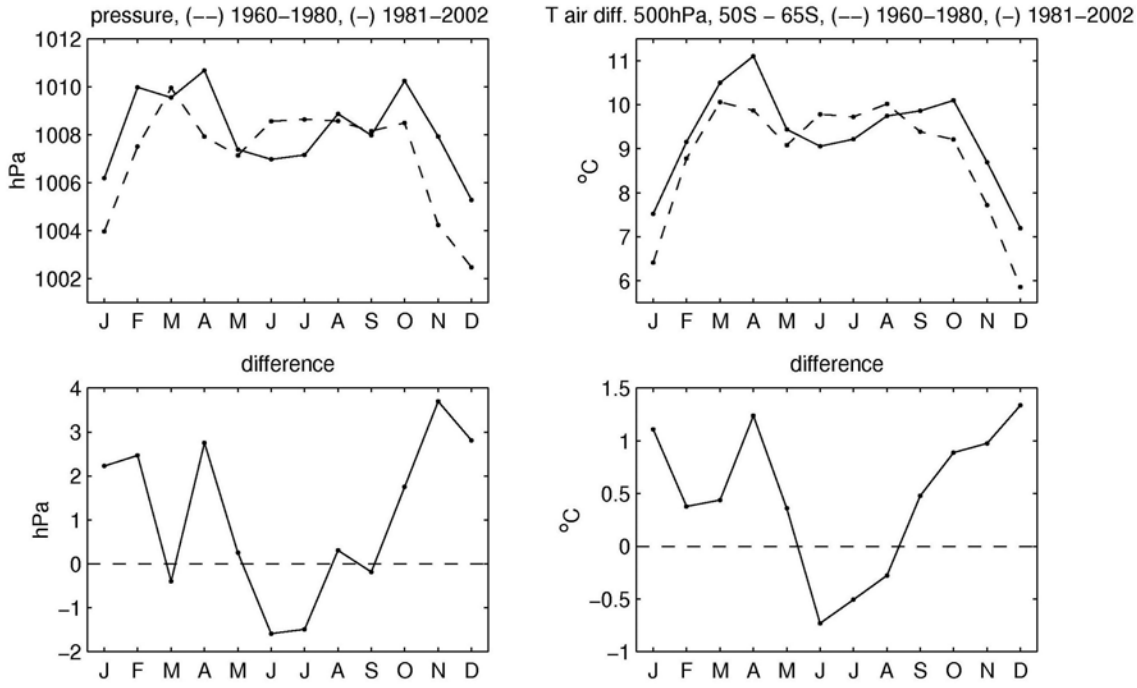

Figure 9: Top left: Observed average pressure at Marion Island for 1960-1980 (broken line) and 1981-2002 (plain line) for each calendar month. Bottom left: Difference between the 1981-2002 mean and the 1960-1980 mean. Top right: Difference between the NCEP air temperature at 50°S and the air temperature at 65°S at 500 hPa and at 37.5E (Marion's longitude). The temperature is averaged from 1960 to 1980 (broken line) and from 1981 to 2001 (plain line). Bottom right: Difference between the 1981-2001 temperature average and the 1960-1980 temperature average.

In Figure 9 (top left), we have plotted the observed mean pressure for 1960-1980 and for 1981-2002. We can clearly see the typical SAO signature in the two curves: there are two maxima (and two minima) separated by about 6 months. But there are also remarkable differences between the two curves. Firstly, there is a change in the phase of the SAO. For example, during 1960-1980, the maximum mean pressure is in March, while for 1981-2002, the maximum is in April. Secondly, as already observed in the trends, the mean pressure in 1981-2002 is higher than in 1960-1980, except for the winter months of June and July. The difference between the two pressure curves for 1960-1980 and 1981-2002 is plotted in Figure 9 (bottom left). As expected, the difference plot mimics the pressure trend (not shown). What is remarkable is the low value observed in March. This low value is caused by the change in phase of the SAO (maximum in March for 1960-1980, maximum in April for 1981-2002).

The mean of the difference between the NCEP 500 hPa air temperatures at 65S and 50S at Marion's longitude is displayed in Figure 9 (top right) for 1960-1980 and 1981-2002. This difference is the definition of the SAO index. As with the pressure at Marion, we observe a shift of the phase of the SAO index: in 1960-1980, the maximum of the SAO index is in March, while in 1981-2002, the maximum is in April. The difference of the two (1960-1980 and 1981-2002) curves of Figure 9 is plotted in the bottom panel. Note that this difference agrees (except for March) with the difference of the two pressure curves plotted in Figure 9 (bottom right). Trends in difference between the 500 hPa air temperatures at 65S and 50S at Marion's

longitude for 1960-2001 agrees well with trends of the pressure at Marion. The correlation coefficient between the two series is r = 0.82 (significant at the 0.01 level).

4.3.5 Interpretation of the pressure changes at Marion in relation with the Antarctic Annular Oscillation (AAO) and the Semi-Annual Oscillation (SAO)

The AAO refers to a large-scale alternation of atmospheric mass between the mid-latitudes and high latitudes of the Southern Hemisphere. The AAO is the dominant pattern of non-seasonal tropospheric circulation variability south of 20 S, and it is characterized by pressure anomalies of one sign centered in the Antarctic and anomalies of the opposite sign centered about 40-50 S. Thomson and Wallace (2000) defined the AAO as the leading principal component of NCEP 850 hPa geopotential height anomalies south of 20 S; whereas Gong and Wang (1999) defined the Antarctic Oscillation Index (AOI) as the difference of the zonally averaged NCEP mean level pressure between 40 S and 65 S. According to these authors, the spatial features of the semi-annual oscillation (SAO), discussed in the previous section, is similar to the spatial structure of the Antarctic Oscillation (AAO). They also point out that the SAO is part of the seasonal cycle, but that the definition of AAO removes the semi-annual oscillation.

The AAO shows a positive trend in recent decades (Thompson et al., 2000; Hall and Visbeck, 2002) although its seasonality and intensity is discussed in Marshall (2003) and Renwick (2004) using observation NCEP and ERA-40 Reanalysis. The correlation coefficient between the AOI and the surface pressure anomalies at Marion Island for 1960-2003 is r = 0.3 (significant at the 0.01 level). Given the definition of the AOI and the location of Marion, it is logical to find such a significant correlation but the pressure changes at Marion are more clearly explained by the changes in the SAO index than by the changes in the AAO.

The trends found in the AAO, and thus in the SAO, have recently been analyzed by Thomson and Solomon (2003). At ~70S, negative trends in the temperature and the geopotential height are observed in the stratosphere with a peak around November, whereas in the troposphere, the trends are observed with two peaks values occurring in December-January and April-May. They argue that the largest and most significant tropospheric trends can be traced to recent trends in the lower stratospheric polar vortex, which are due largely to photochemical ozone loss. They also show that the observed trends in geopotential height over the Southern Hemisphere polar region are consistent with a trend towards high-index polarity of the AAO, which is most pronounced during December-January and April-May but persists throughout the summer months. The associated change in the midlatitude is asymmetric with a zonal wave 3 structure and high pressure increase especially marked in the Indian Ocean in summer time on an area encompassing Marion island (Thomson and Solomon, 2003; Shindell et al., 2004). We note that these trends are also consistent with the trends observed in the SAO, and more remarkably, with the “dual peak” of December-January-February and April observed in Figures 7a and 9a, b.

The 1960-2001 trends of geopotential height (Figure 10) and of temperature at the 500 hPa level, at 50S, and 65S show a dual-peak in December-January and April-May in the 65S trends. We also note that the variability of the trends at 65S is large compared to the variability of the trends at 50S. This indicates that the strongest trends are observed at the latitude where the ozone losses are observed but it can also indicate a region of high variability.

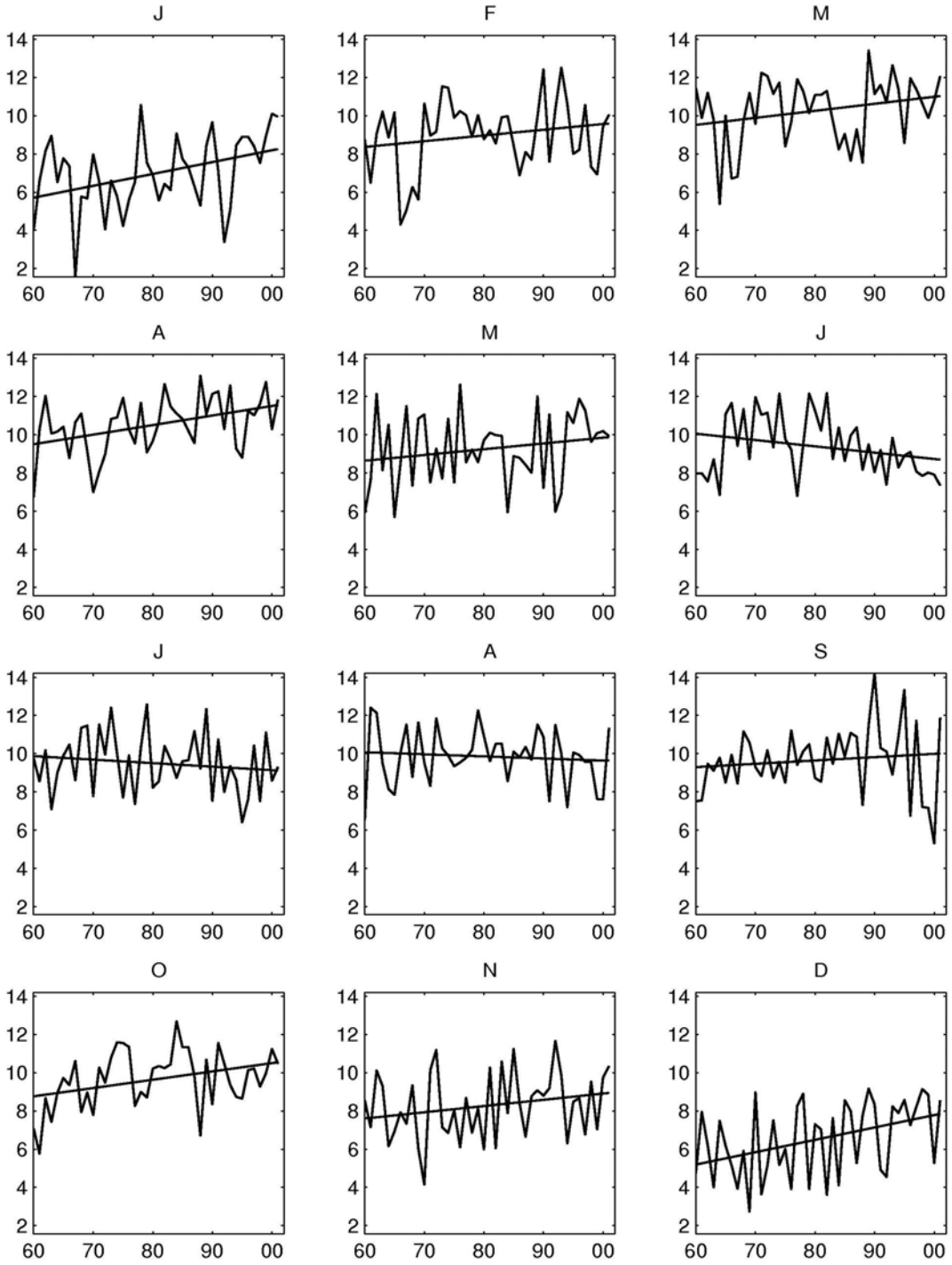

Figure 10: Trend from 1960 to 2002 for each calendar month of the monthly mean of the difference between the NCEP 500 hPa geopotential height at 50°S and at 65°S at 37.5E (Marion's longitude). The trend is defined as the difference between the last year (2001) and the first year (1960) of the linear fits for each calendar month.

Model studies by Gillet and Thomson (2003) and Shindell and Schmidt (2004) confirm the link between ozone depletion and change in South Hemisphere circulation consistent with the changes observed at Marion Island although the change started prior to ozone depletion (Van Loon and Tourpali, 1995; Marshall et al., 2004).

4.3.6 Discussion

It could be argued that a shift in the wind could have created the deficit in rainfall due to the island orography. This shift could have increased the air temperature and SST at the station. The western side of the island is more exposed and experiences higher levels of humidity, cloudiness and precipitation than eastern side of the island where the South African weather station is located. The westerly wind is stronger on the western side but the station is well exposed to the prevailing wind being situated on the northeastern side of the island. Nevertheless, if the change were only due to a shift in the wind and the island orography, this would not have led to the observed change in SLP. In any case, even if the change were due to the orography and a change in wind direction, this change in wind direction (more northerly) is consistent with the effect of change in SAO. Moreover, the change observed since the 1970's in wind speed, geopotential heights and SST is not just confined to Marion Island. For example, a warming in the local climate was also observed for Kerguelen Island (49.3 S, 70 E) (Frenot et al., 1997) suggesting that these changes could be representative of the Indian sector of the Southern Ocean. In fact observational data from other subantarctic Island van Loon et al. (1993), Hurrell and van Loon (1994) and Meehl et al. (1998) show that change of SAO is well represented by Islands at that latitude. Furthermore, changes in the ecosystem due to the decreased rainfall were observed around the island (Smith, 2002; Pakhomov et al., 2003) and not only in the vicinity of the station.

Another point of discussion is the problem already mentioned concerning NCEP data for trend detection (Hines et al., 2000; Kistler et al., 2001; Marshall, 2003; Genthon et al., 2003; Renwick, 2004; Tennant, 2004). This will affect results presented in that paper but also in most of the literature cited here. Nevertheless, Shindell and Schmidt (2004) show with model and reanalysed climate data from 1979 that changes in the South Hemisphere due to a combination of ozone loss and global warming happen mostly in summer with high pressure increase following a zonal 3 wave structure and stronger pressure increase in the Indian ocean spreading over the Marion Island sector. A composite of NCEP geopotential height (not shown) in the South Hemisphere for the summer season (DJF) of the period 1982-2004 minus 1959-1981 shows a substantial increase in sea level pressure, 500 hPa geopotential and surface temperature in the midlatitude Indian Ocean sector with northerly wind increase in summer in Marion Island sector. This fits with our observations. Similar results are obtained when using data for 2004-1992 minus 1979-1991 when data are more reliable. Other studies based on observations (Thomson and Solomon, 2003; Marshall, 2003) show that changes in low latitudes and midlatitudes happen mostly in summer and are consistent with our findings. The winter changes previously reported were overestimated due to the lack of observations prior to the 70's (Renwick, 2004)

Finally, we cannot rule out that some of the change in SST and air temperature at Marion Island may have been caused by large-scale ocean dynamics. Hypotheses related to this possibility are presented by Hall and Visbeck (2002). According to their coupled model, SST increase in midlatitude in the positive phase of the AAO could be caused by a combination of ocean dynamics and decrease in rainfall via increased subsidence (and more short-wave radiation) due to changes in the jet stream position. Moreover, decreases in the wind speed would also reduce the loss of energy from the ocean to the atmosphere via evaporation and induce less upper ocean mixing. Advection of warmer air from the north could also decrease the loss of energy due to sensible heat transfer for the annual mean of zonally averaged ocean and atmosphere parameter. Since Hall and Visbeck (2002) present zonally averaged data for the yearly mean we cannot directly compare their results to ours. They indicated that changes in the South Hemisphere are caused by ocean

atmosphere ice dynamics as suggested by studies done on the SAO. An increase in SST in midlatitude would further impact the SAO and create an interesting feedback where SST increase would lead to a southward shift of the storm track leading to further SST increase. Unfortunately, a lack of long term ocean data in this sector of the Southern Hemisphere prevents us from addressing that question. This calls for the monitoring of ocean and atmospheric conditions between Africa and the Antarctic on a regular basis.

4.3.7 Conclusion

Significant changes in recent decades to the local climate of Marion Island occur from October to May but are more significant from November to May with a substantial reduction in rainfall and increase in sunshine hours, increase in non- rainy days, increase in pressure. Increase in minimum and maximum temperature and coastal SST are significant most of the year. Due to the uncertainties in re-analyzed climate data prior to the satellite era in late 70's for use in assessing climate change in the Southern Hemisphere, the Marion Island dataset represents a unique benchmark against which hypotheses can be tested. Marion Island, located in the southwest Indian Ocean sector of the Southern Ocean, also represents an important natural laboratory for monitoring the impacts of climate change on ecosystems, with scientific expeditions having been organized on a regular basis since the 50's.

Marion Island warming and climate change since the 1970's seem to be consistent with changes in large-scale atmospheric circulation in the low latitudes and the ocean atmosphere dynamics of the Southern Hemisphere, as assessed using observations, reanalyzed climate data and models. Changes are linked to the well documented phase change in the SAO and the recent change in high latitude climate. Since the latter have been linked to a decrease in ozone and global warming, it is tempting to state that the recent changes in the summer climate of Marion Island may be due to human influences. However; changes of circulation in the Southern hemisphere of the same magnitude were reported before the 1970's (Jones and Widmann, 2003).

5. Moisture fluxes from adjacent oceans

5.1 Introduction

Rainfall variability in Southern Africa is influenced by sea-surface temperatures (SST) of the neighboring oceanic basins. The tropical Atlantic is regarded as a secondary source of moisture over the subcontinent. In order to investigate the role played by the tropical Atlantic Ocean in southern African climate and its impacts on rainfall, we investigated the moisture fluxes along the land-ocean interface, using NCEP DOE II re-analysed atmospheric fields that were used to calculate the humidity fluxes at various level. This was done in collaboration with the Centre de Recherche Climatique, University of Bourgogne. A multivariate analysis was done on the zonal humidity flux component (west-east) from 1000 mb to 300 mb levels. It revealed key features of the southern African circulation. Two primary modes of variability were identified together with regions of humidity convergence/divergence and this helped to detect local deep convection mechanisms.

5.2 Data and methods

In this study, we used monthly rainfall data from 1901 to 2000 at a 0.5°x0.5° spatial resolution from the Climatic Research Unit, CRU TS 2.0 dataset (Mitchell et al., 2004) offering. Simultaneously, we used the 2.5°x2.5° degrees monthly Outgoing Longwave Radiation (OLR) from NOAA-NCEP-CPC dataset covering the period from 1979 to 2004.
As an alternative to direct rainfall estimates, moisture fluxes and convergence were computed. We used the newly released 6 hourly NCEP-DOE AMIP Re-analyses dataset (Kanamitsu et al., 2002), also called NCEP R2, offering a various range of atmospheric parameters at 2.5 degrees spatial resolution. Moisture fluxes were computed for the 1979-2003 period, at 8 pressure levels between 1000 mb and 300 mb over an area ranging from 2.5°N to 37.5°S in latitude and from 5°E to 50°E in longitude. Due to ruptures in stability in the data we high-pass filtered the calculated zonal moisture fluxes over the period 1979-2003, and we ran EOF using the co-variance matrix to determine the pre-dominant modes of variability.

5.3 Water vapour transport along the west coast of southern Africa

January-February vector moisture fluxes maps with contours of mean humidity convergence at 850 mb, 700 mb and 500 mb are shown in Figure 1. Pronounced moisture convergence at surface (850 mb) appear to match with marked divergence in mid-tropospheric levels (700 to 500 mb) and help identify three major convective areas in summer over the subcontinent. Deep convection processes are found to take place to the East of the Congo basin (around 30°E) and, as we will see in the following, potentially play an important role on summer rainfall in tropical southern Africa. In southeastern Angola, centered at about 17°S over the Bie plateau, is a local feature known as the Angola low (Mulenga et al., 1998; Cook et al., 2004; Reason and Jagadheesha, 2005). Stronger divergence at 700 mb over south Angola suggests substantial convection mechanisms there, but less deep within the air column. Further south, a third low-level convergence zone is found to the south of Botswana at about 25°E corresponding with the location of the subtropical heat low in summer : when deep this low-pressure cell is known to produce substantial rain over southern Africa subtropics (Preston-Whyte and Tyson, 1988).

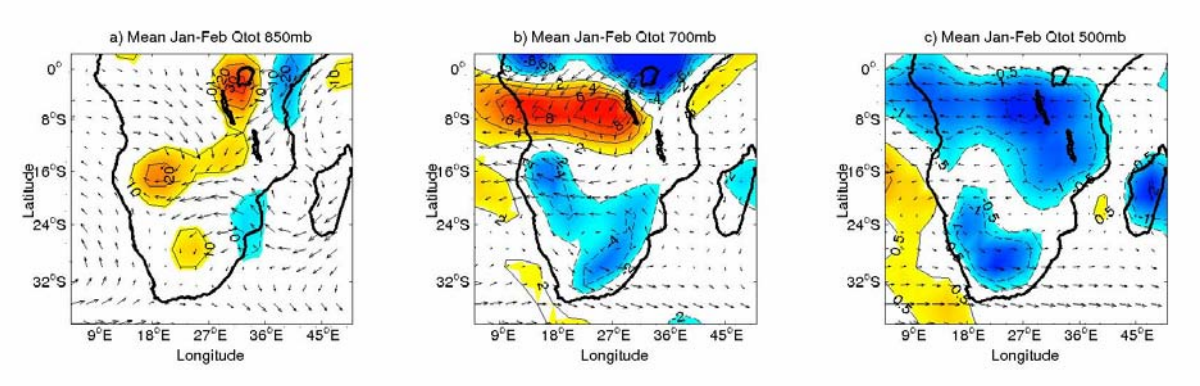

Figure 1: Mean January-February surface moisture fluxes (streamlines in g/kg.m/s with arrows scaled at 1 unit/degree of latitude) together with contours of moisture convergence (in g/kg/s) at 850 mb (a), 700 mb (b) and 500 mb (c). Positive values contour areas of moisture convergence while negative values refer to moisture divergence at given levels

Using a vertical domain along the west coast of southern Africa for zonal moisture fluxes is a way to quantify, at least zonally, the exchange in moisture at the land-ocean interface and thus the role of the tropical Atlantic in modulating southern African climate.

Figure 2 presents the mean January-February climatological structure for zonal moisture flux along the west coast of southern Africa. The contribution of both stationary and transient components in zonal moisture fluxes vary with latitude, reflecting the dual influence of tropical and mid-latitude circulations. In the tropics, the transient term represents less than 10% of the total zonal moisture transport. This agrees with previous studies (Chen et al., 1985; Rocha and Simmonds, 1997; Fauchereau, 2004) stating that the steady component in water vapour fluxes is well suited to represent moisture changes due to large-scale circulation in the tropics.

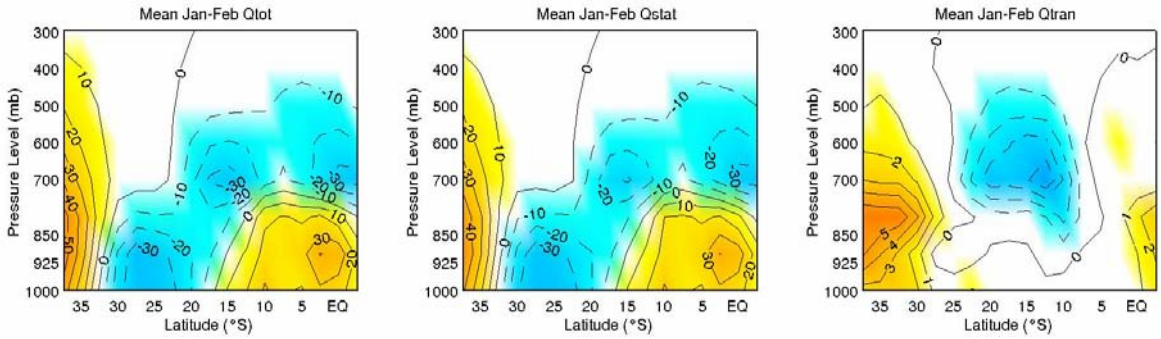

Figure 2: Mean vertical structure of zonal moisture fluxes along the west Southern African coast (in g/kg.m/s) for January-February together with its stationary and transient components. Positive values correspond to westerly fluxes while negative values refer to easterly fluxes.

The key features of summer moisture flux can be summed as follows:

- a westerly monsoon-like flux in the tropics, at the surface and as far south as 15°S, potentially feeding a deep convergence cell over southeast Angola.
- overlying, a southern dependence on the African Easterly Jet (AEJ), between 600-700 mb and located at 12°S in December, feeding a strong mid-tropospheric convergence cell to the north of Angola.
- a surface easterly flux to the south, covering the whole Benguela region and connecting with the southern AEJ in summer.

- further south, the westerly circulation linked with the ST Helena HP, at its southernmost location in summer.

Preparing the data to perform a multivariate analysis, we identified some stationarity breaks (not shown) in the fluxes (typically in 1993, 1996 and 1986). We then ran a Butterworth filter at 96 months scale in order to apply the EOFs through the covariance matrix on the high frequency signal, this, to overcome these instabilities in the re-analyses. In Figure 3 are shown the spatial patterns of the firsts four EOFs of high-filtered (HF) zonal moisture fluxes along the west coast of southern Africa using the covariance matrix. The truncated basis defined by these four primary modes interestingly contributes almost half of the total variance explained. The first mode is the modulation of St Helena high pressure system and westerly circulation in low latitudes. The second mode represents the intensity of the westerly monsoon-like flux from the tropical Atlantic. The last two modes are less clear to interpret but they are definitely linked with the variability of the southern dependence of the African Easterly Jet. Each modes respectively explains about 25%, 11%, 7% and 6% of the total variance. Their spectral signatures show for all strong intra-annual and intraseasonal peaks.

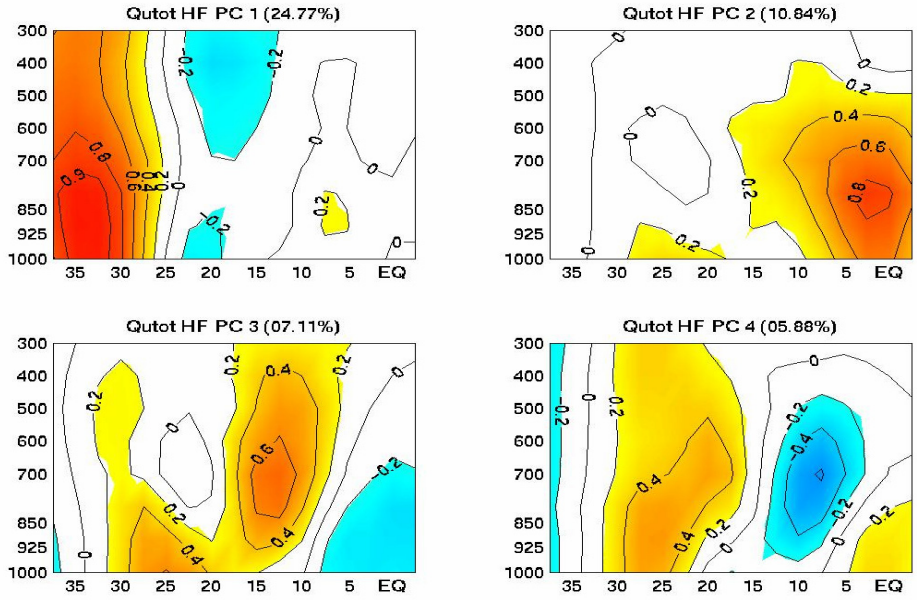

Figure 3: Leading EOF modes of variability in high frequency zonal moisture fluxes along the west southern African coast

Within subtropical areas of Southern Africa, weather and climate are controlled by the mean anticyclonic circulation (Preston-Whyte and Tyson, 1988). D'Abreton and Lindesay (1993) report changes in zonal and meridional transport of water vapour over southern Africa during wet and dry summers, with the neighboring oceans contributing as moisture sources. The first leading EOF mode of zonal moisture fluxes along the west coast of southern Africa is linked to the latitudinal movement of the South Atlantic anticyclone. This mode, referred as the South Atlantic Midlatitude mode, contributes the most to the variability in moisture input from the south Atlantic onto the subcontinent at subtropical latitudes.

Figure 4 presents the January-February time-series for the corresponding south Atlantic midlatitude mode expansion coefficient. A threshold at 0.6 of normalized anomalies deviation from the mean defines significant extreme years. We choose

respectively (1983, 1992 and 1995) and (1981, 1994, and 2000) as positive/negative events, for which the circulation linked with the mid-latitude westerlies and the south Atlantic anticyclone appeared to be significantly shifted northward/southward.

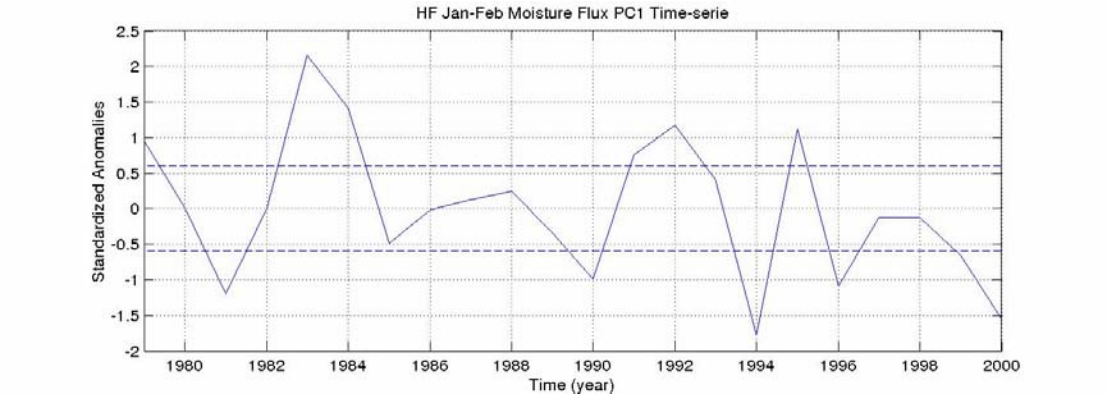

Figure 4: January-February PC1 mode expansion coefficient for high frequency zonal moisture fluxes along the west southern African coast from 1979 to 2000. Dashed lines indicate +/-0.6 levels.

Heterogeneous correlations between January-February South Atlantic midlatitude mode expansion coefficient and CRU TS 2.0 rainfall are presented in Figure 5. High scores for synchronous correlation are found to the south of the uplands surrounding the Congo basin, with maximums over Zimbabwe and Botswana stretching southward west of the east coast escarpment to South Africa and westwards to Namibia. Rainfall composites (not shown) for positive (1983, 1992 and 1995) and negative (1981, 1994, and 2000) years of the January-February moisture flux PC1 time-series (Figure 4) confirm the symmetry of the relation with significant anomalies over these areas of maximum correlation scores. Patterns in OLR for similar composites (not shown) exhibit respectively enhanced/reduced convection broadly over subtropical areas of the subcontinent with extrema located to the southeast where anomalies are statistically significant. This suggests enhanced/reduced convection mechanisms over subtropical southern Africa, i.e. to the south of the uplands surrounding the Congo basin, depending on the phase of the south Atlantic midlatitude mode.

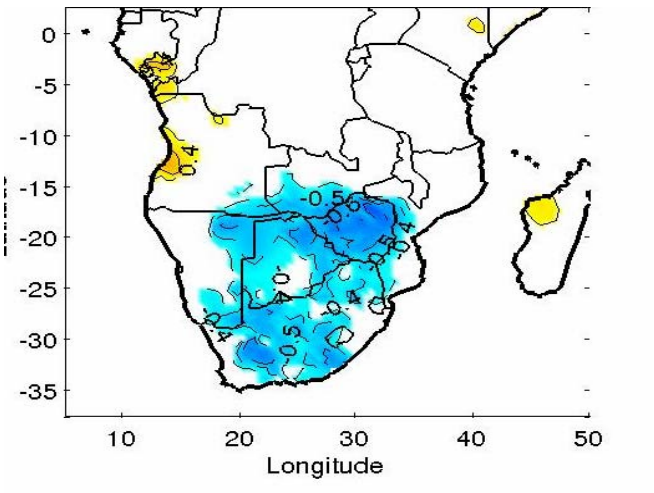

Figure 5: Heterogeneous correlation between HF zonal moisture flux PC1 and CRU TS 2.0 rainfall in January –February over the period [1979-2000].

In conclusion, this mode of zonal moisture linked with the midlatitude westerlies and the south Atlantic anticyclone during mid-summer months (January-February) appears to directly impact rainfall amounts over subtropical areas of southern Africa (south of 15°S).

Using composite analysis for positive and negative events on vertical velocity, zonal moisture fluxes and convergence fields, we investigate deeper the underlying atmospheric mechanisms (not shown). During years when the midlatitude circulation was anomalously to the north (positive events), a decrease in available humidity occurs in the southern subtropics. A concomitant eastward shift of the Walker circulation ascending branch to the southwest Indian ocean and southeastern Africa, reduces convection processes and leads to below normal rainfall to the south of the uplands surrounding the Congo basin. Composites for austral summer months when the midlatitude circulation linked with the south Atlantic anticyclone was shifted southwards (negative events), show an increased moisture input at subtropical latitudes. A strengthened southern subtropical jet is supporting maximum divergence at upper tropospheric levels. This creates a situation where convection processes are enhanced, resulting in above normal rainfall over southern Africa subtropics.

Within the southern tropics, rainfall regimes are largely depending on deep convection processes and water vapour convergence at different tropospheric levels. The second mode of variability extracted from the previous EOF analysis, referred as the Equatorial Westerly mode, contributes the most to moisture input from the Atlantic onto the subcontinent at tropical latitudes. Figure 6 presents the January-February time-series for the corresponding Equatorial Westerly mode expansion coefficient. A threshold at 0.6 of normalized anomalies deviation from the mean defines significant extreme years. We choose respectively (1990, 1995 and 1998) and (1983, 1988, and 1992) as positive/negative events, for which the expression of the Equatorial Westerly mode in zonal fluxes appeared to be significantly enhanced/reduced. Interestingly, all but one year corresponds to the mature phase of ENSO. This could explain the absence of correlation between ENSO and rainfall in central southern Africa (Camberlin et al., 2001).

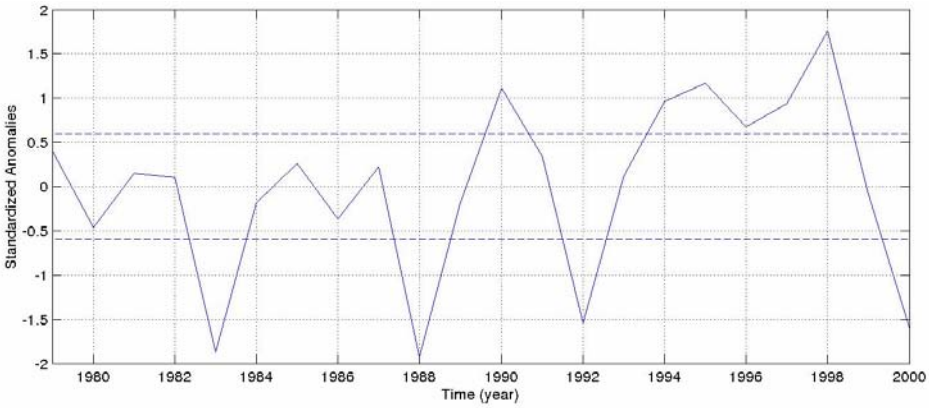

Figure 6: January-February PC2 mode expansion coefficient for high frequency zonal moisture fluxes along the west southern African coast from 1979 to 2000. Dashed lines indicate +/-0.6 levels

Heterogeneous correlations between January-February Equatorial Westerly mode expansion coefficient and CRU TS 2.0 rainfall are presented in Figure 7. High scores for synchronous correlation are found all around the Congo basin, with maximums from east/southeast DRC and northwest Tanzania stretching to the south along the Rift valley and westwards to south Angola. Rainfall composites (not shown) for positive (1990, 1995 and 1998) and negative (1983, 1988, and 1992) years of the January-February moisture flux PC2 time-series confirm the symmetry of the relation with significant anomalies over these areas of maximum correlation scores. Patterns in OLR for similar composites (not shown) exhibit respectively enhanced/reduced convection broadly over the Congo basin with extremes located to the southeast where anomalies are statistically significant. This suggests enhanced or reduced deep convection mechanisms over the east and southeast of the Congo basin depending on the intensity of the Equatorial Westerly mode.

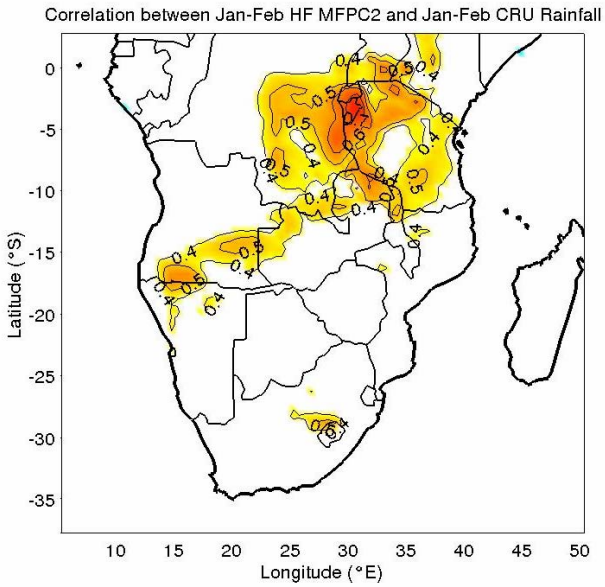

Figure 7: Heterogeneous correlation between HF zonal moisture flux PC2 and CRU TS 2.0 rainfall in January-February over the period [1979-2000].

In conclusion, the modulation in intensity of the monsoon-like westerly flux at tropical latitudes of southern Africa west coast during mid-summer months (January-February) appears to directly impact rainfall amounts all around the eastern/southeastern Congo basin extending as far as 15°S. A similar composite analysis on some atmospheric fields also helped to identify key mechanisms. Composites for austral summer months when this Equatorial Westerly mode had a

particularly strong expression (positive events), show an enhanced moisture input at tropical latitudes that feeds into the deep convection occurring over the Congo basin. Sustained meridional energy fluxes result in above normal rainfall east and south of the Congo belt. During years of reduced equatorial westerly moisture flux (negative events), a deficit of available humidity occurs in the southern tropics. A concomitant eastward shift of the Walker circulation ascending branch to the southwest Indian Ocean and southeastern Africa, reduces convection processes and leads to below normal rainfall over the uplands surrounding the Congo basin.

5.4 Water vapour transport along the east coast of southern Africa

The early summer season has not received so much attention despite its importance for southern African rainfall. Using lead/lag correlations between the expansion coefficients of each mode and rainfall data, it is the period for which the impacts of zonal moisture fluxes variability along the east coast of southern Africa on the local hydrological cycle are found to be the most pronounced. In this respect, November-December vector moisture fluxes maps with contours of mean humidity convergence at 850 mb, 700 mb and 500 mb are presented in Figure 8.

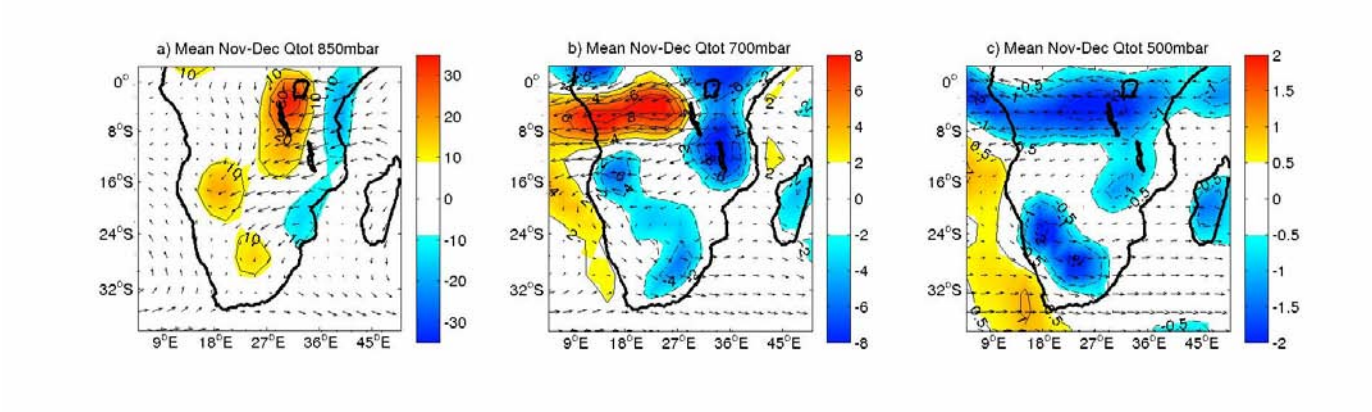

Figure 8: Mean November-December surface moisture fluxes (streamlines in g/kg/m.s^{-1} with arrows scaled at 1 unit/degree of latitude) over the 1979-2000 period, together with contours of moisture convergence (in g/kg/s) at 850 mb (a), 700 mb (b) and 500 mb (c). Positive values contour areas of moisture convergence while negative values refer to moisture divergence at given levels.

The mean November-December climatological structure for zonal moisture fluxes along the east coast of southern Africa is shown in Figure 9.

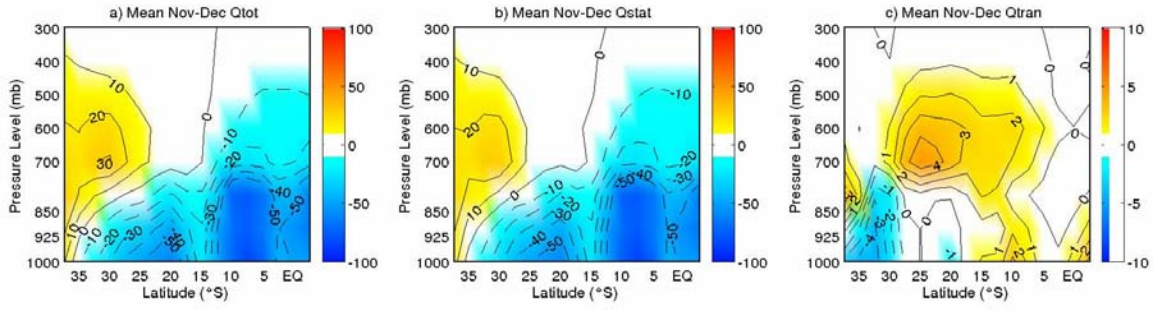

Figure 9: Mean vertical structure (a) of zonal moisture fluxes along the east Southern African coast (in g/kg/m.s^{-1}) for November-December over the 1979-2000 period, together with its stationary (b) and transient (c) components. Positive values correspond to westerly fluxes while negative values refer to easterly fluxes.

During early summer, an easterly moisture flux linked to the northern Indian trades is found between the Equator and 15°S in latitudes and below 500 mb level in altitudes. To the south (between 18°S and 35°S) another easterly flux is driven by the southern Indian trades at surface levels (below 850 mb). South of 35°S, a midtropospheric westerly moisture flux (i.e. between 850 mb to 400 mb) has its main core centred at 700 mb in altitude. Compared to January-February, convective activity seems better developed over the east Congo basin while reduced over the Angola low and the subtropical heat-low locations. North of Madagascar the meridional component of water vapour transport is reduced and no cyclonic circulation is established over the Mozambique channel. Stronger divergence seems to occur along the east coast, extending meridionaly as far as south Mozambique. Along the west coast, the fake monsoon in the tropics is reduced in intensity, thus advecting less moisture over the subcontinent interior.

To overcome stationarity ruptures in NCEP R2 data, the data have been filtered at 8 years and EOF techniques were applied to the high-filtered (HF) zonal moisture fluxes along the east coast of southern Africa using the covariance matrix. The first two leading EOF modes have been retained and the spatial patterns associated are shown in Figure 10.

The first mode is typical of the variations within the northern Indian trades accompanied by changes in the circulation linked with the midlatitude westerlies. It explains about 20.2% of the total variance. Positive loadings are particularly strong from the surface up to 500 mb showing a core maximum at about 15°S around 850 mb levels while loadings of opposite sign are found in the subtropics particularly below 700 mb levels. This mode will be referred to as the tropical Indian easterly mode.

The second mode characterizes the variability linked with the midlatitude westerly circulation and the South Indian anticyclone. It represents 13.7% of the total variance explained. It has simultaneous positive/negative loadings mainly below 700 mb levels, respectively south of 30°S and between 15°S and 10°S. In the following, this mode will be referred to as the midlatitude South Indian mode.t

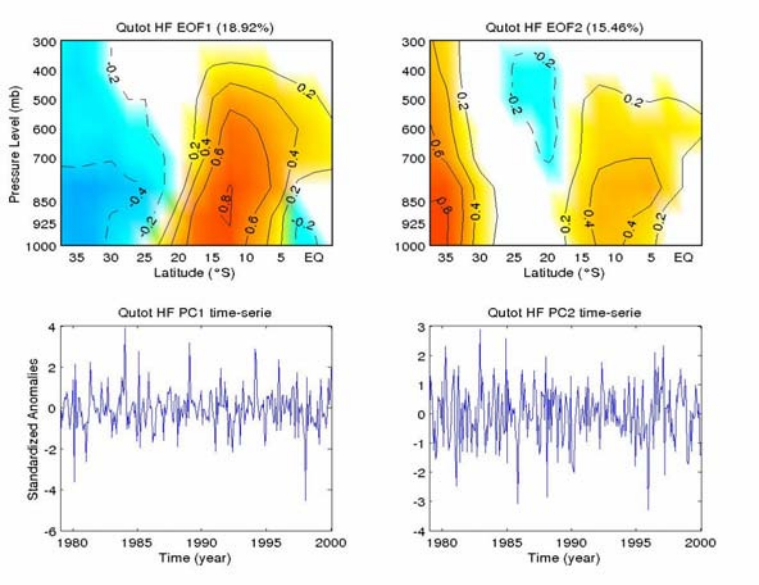

Figure 10: Spatial patterns (top) of the first two EOF leading modes of variability in high frequency (HF) zonal moisture fluxes along the east coast of southern Africa over the 1979-2000 period. Their corresponding expansion coefficients are presented in the bottom panel.

Figure 11 shows the November-December time-series for the first EOF leading mode in high-filtered (HF) zonal moisture fluxes along the east coast of southern Africa.

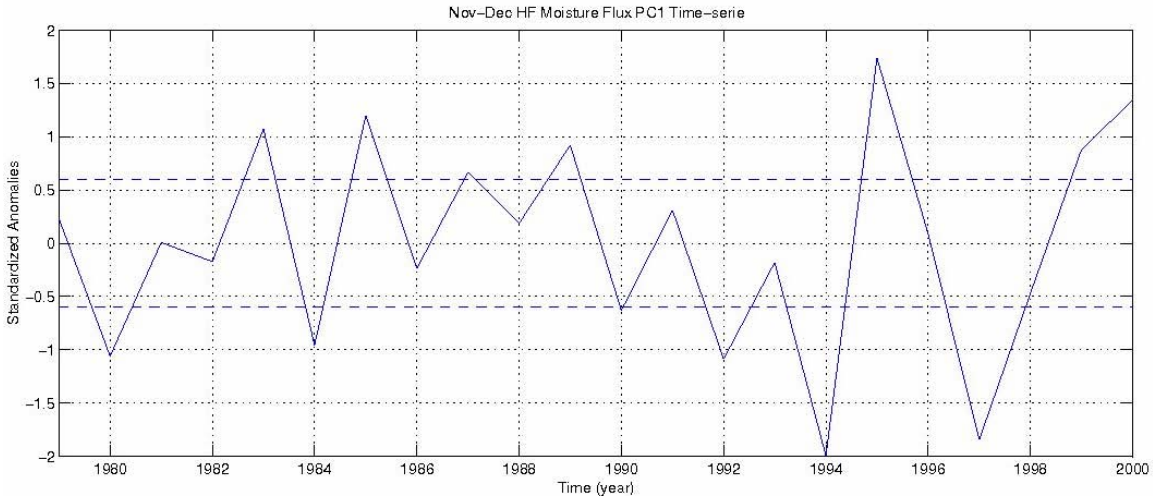

Figure 11: November-December PC1 mode expansion coefficient for high frequency zonal moisture fluxes along the east coast of southern Africa from 1979 to 2000. Dashed lines indicate +/- 0.6 levels.

Heterogeneous correlations between the November-December tropical Indian easterly mode expansion coefficient (ND MFPC1 in the following) and CRU rainfall are presented in Figure 12.

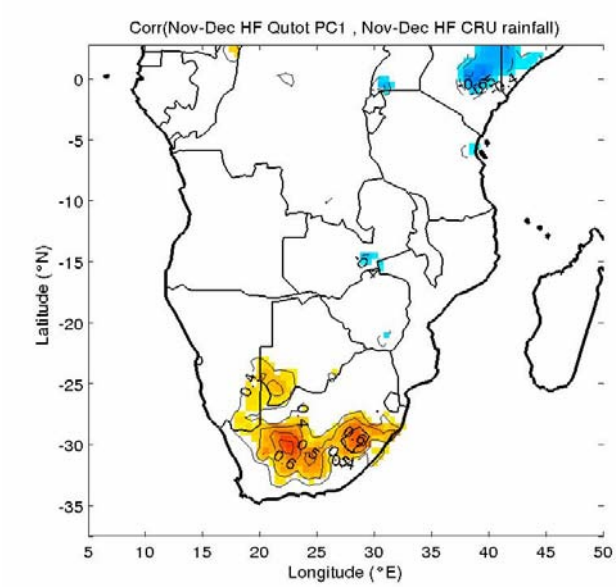

Figure 12: Heterogeneous correlations between HF zonal moisture fluxes PC1 and CRU rainfall in November-December over the 1979-2000 period. The scores presented are significant at 95% level using Monte-Carlo simulations.

High positive scores for synchronous correlation are found over subtropical regions of the subcontinent, with maximums extending from southeast Namibia across to southeast regions of South Africa. Patterns of opposite signs are found simultaneously over northeast southern Africa, mainly over eastern Kenya/southern Somalia. Rainfall composites (not shown) for positive and negative years of the ND MFPC1 time-series confirm the symmetry of the relation with significant anomalies over these areas of maximum correlation scores.

Composite analysis for positive/negative events on vertical velocity, zonal moisture fluxes and convergence fields, we examined deeper the underlying atmospheric mechanisms (not shown). In the positive/negative phases of this mode, less/more humidity is found at tropical latitudes where convection is reduced/favoured (enhanced zonal moisture convergence could play a role during negative events) leading to above/below-normal rainfall east of the Great Rift valley. To the south, a reduced/sustained westerly circulation is found to enhance/reduce convection within the Botswana heat-low. This acts to sustain/weaken the meridional transfer of energy to the south within the SICZ complex, ultimately leading to above/below-normal rainfall over central and southeastern regions of South Africa for positive/negative events respectively.

Figure 13 shows the October-November time-series for the first EOF leading mode in high-filtered (HF) zonal moisture fluxes along the east coast of southern Africa.

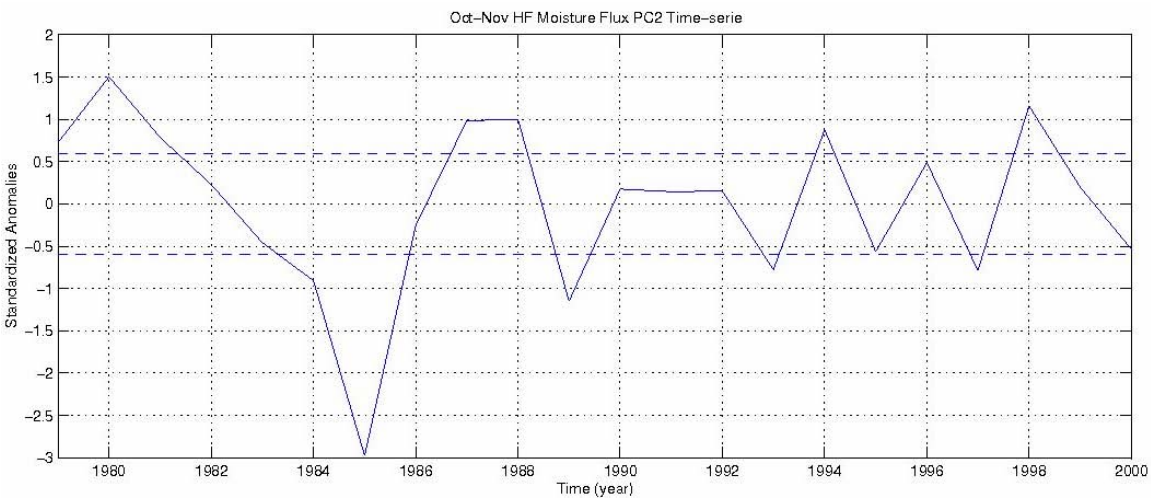

Figure 13: October-November PC2 mode expansion coefficient for high frequency zonal moisture fluxes along the east coast of southern Africa from 1979 to 2000. Dashed lines indicate +/- 0.6 levels.

Heterogeneous correlations between the October-November midlatitude South Indian mode expansion coefficient (ON MFPC2 in the following) and CRU rainfall are presented in Figure 14.

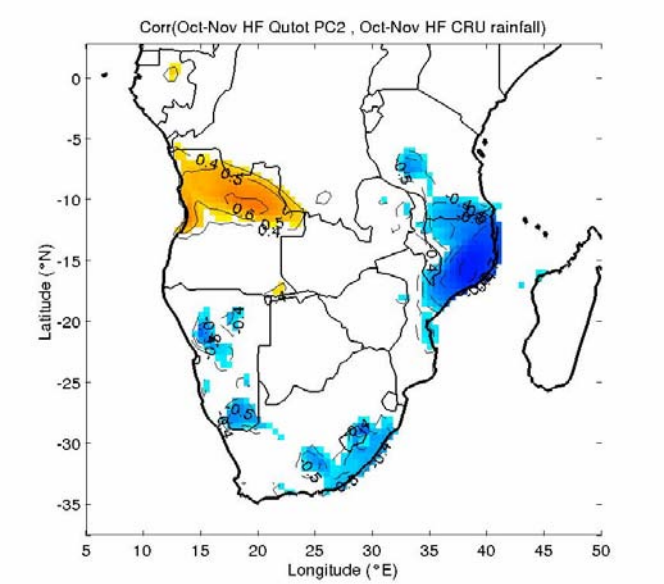

Figure 14: Heterogeneous correlations between HF zonal moisture fluxes PC2 and CRU rainfall in October-November over the 1979-2000 period. The scores presented are significant at 95% level using Monte-Carlo simulations.

High scores for synchronous correlation are found over tropical regions of the subcontinent, showing anticorrelation patterns between western and eastern tropics. Negative maximums are located mainly over northern Mozambique extending to southern/central Tanzania. Significant negative scores are also found over southeast South Africa and the Namibian interior. Positive loadings are located over northern Angola. Rainfall composites (not shown) for positive/negative years of the ON MFPC2 time-series confirm the symmetry of the relation with significant anomalies over these areas of maximum correlation scores.

Similarly, composite analysis for positive/negative events on vertical velocity, zonal moisture fluxes and convergence fields, were used to examine deeper the underlying atmospheric mechanisms (not shown). Enhanced/reduced westerly wind regimes in the midlatitudes are found to decrease/increase moisture availability over southeastern coastal regions of South Africa where convection is inhibited/sustained, leading to below/above-normal rainfall. In particular, during negative events related to this mode of variability, enhanced upper divergence driven by a strengthened subtropical jet helps to favour convective activity over the subtropics. Reduced/sustained advection of moisture inland creates a deficit/excess in rainfall over regions to the north of Mozambique. Along the west coast, sustained/reduced offshore transport results in below/above-average rainfall over Namibia, while reduced/increased eastward advection of moisture leads to an opposite situation over north Angola.

6. Near real time remote sensing in the Tropical Atlantic and the Indian Ocean

6.1 Introduction

The quality of near real time data assimilated by models is a key to the success of any forecasting system. Near real time ocean and atmospheric data can also be used to monitor the ocean state. They can be used to compare present to past conditions. To attain the required time and space resolution is always technically demanding. The closer to real time and the higher the resolution, the higher the cost and the technical and human requirements. However, daily, weekly and monthly near real time intermediate resolution products (4 to 35 km resolution) are freely and readily available with a few days to a weeks delay in many research centres in many parts of the world. Such products include sea surface temperature, wind speed, sea surface height and geostrophic currents. At UCT data are transferred twice a day through ftp transfer; they are automatically processed on a PC that has been converted into a LINUX system. They are displayed on a website in the form of charts of mean and anomalous conditions. Indices and time series of various relevant parameters are also built in real time as well as Hovmoller diagrams, showing propagative features in the upper ocean such as Kelvin and Rossby waves. The scientific objective is to monitor the region of the Tropical Atlantic and Indian Ocean that are known to have an impact on southern African rainfall, with the option of zooming into the Benguela Angola Current system and into the Mozambique Channel. This is the first step towards the development of an early warning system and the production of advisory bulletins similar to those produced for the Pacific Ocean. The web site can be found at http://realtime.sea.uct.ac.za/

6.2 System description

The real-time system is a three-unit system, namely the running unit, the archive unit and the web unit. The running unit makes up the bulk of the system. The running unit consists of a stand alone PC set up with the LINUX operating system and making use of freely available LINUX software. The running unit downloads and processes all data inputs, calculates trends, anomalies, and time series averaged in various domains or performs any relevant statistical operations to check for abnormal conditions. It produces the necessary outputs for the web. All data used and produced by the running unit, that is the raw data fed into the system, the processed data, and the graphical outputs are then archived on the archive unit. The running unit also creates and subsequently updates a database containing descriptions of all the data together with their location on the data server. The most recently updated database is then copied onto the web unit. The archive unit is a data server which acts as a storage facility for all archived data. The web unit consists of a web server and provides the interface between the users and the archive and running units. The latest processed data and the related web outputs are stored on the web unit.

The real-time system aims to be simple and reliable. The web interface is user friendly. The visualization of the information in the real-time system is straightforward and the interpretation of the data is facilitated to the maximum by providing simple colour-coded graphs. The user is able to access data in different regions relevant to southern African rainfall. Since the Pacific is relatively well observed and advisories for that region can be found, we focused on poorly observed region, the Tropical Atlantic and the Indian Ocean with a facility to zoom into the Mozambique Channel and the Angola Benguela Frontal zone, which are data void areas. The real-time system is designed so as to facilitate its future extension.

The real-time system makes use of the following tools:

1 FTP to automatically download input data from designated sites using.
2 NCAR Common Language (NCL) or Octave computer programs to process remote sensing, in-situ or environmental data, produce plots and detect abnormal conditions
3 HTML, PHP and JavaScript programs to design the web pages.

A diagram of the architecture for the real-time system is provided below.

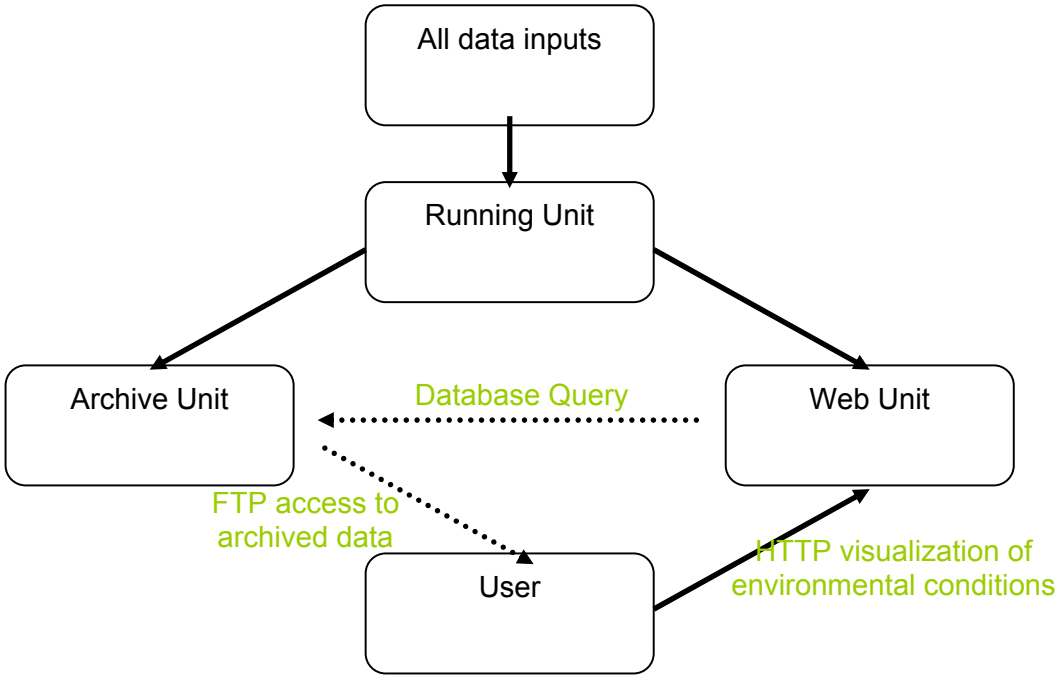

6.3 Data available

Altimetry
Ssalto/Duacs gridded Maps of Absolute Dynamic Topography (MADT), geostrophic currents
Satellite: Jason-1 + Envisat (Topex/Poseidon + ERS)
Data availability: August 2001 to Present
Resolution: 1/3 degree x 1/3 degree on a Mercator grid

Ssalto/Duacs gridded Maps of Sea Level Anomalies (MSLA), computed with respect to a seven-year mean.
Satellite: Jason-1 + Envisat (Topex/Poseidon + ERS)
Data availability:
October 1992 to Present
Resolution: 1/3 degree x 1/3 degree on a Mercator grid

Sea surface temperature

Satellite: TRMM
Sensor: TMI
Data availability: December 1997 to Present
Resolution: 0.25 degree

Wind

Satellite: QuickScat
Sensor: SeaWinds
Data availability:
September 1999 to Present
Resolution: 0.5 degree

Rainfall
A link is provided to the latest global 3-hourly, weekly total, monthly total and monthly anomalies. As those quantities are meaningful to the region we did not calculate it ourselves but used existing web pages.

6.4 Indicators

Central Indian Ocean

This domain is the part of the Indian Ocean most correlated to South Africa rainfall. SST can be modified by abnormal wind speed if sustained for a long period or by modification of the ocean surface layer (about the first 100 to 200 meters above the thermocline). Variation of that layer can be monitored by variation of the sea level from altimetry. The Hovmoller plots allow the propagation of Kelvin and Rossby waves to be followed across the Indian Ocean and differentiate locally related SST variation from remote variation as propagated by Kelvin and Rossby waves.

Indian Ocean Dipole

The Indian Ocean Dipole is a coupled ocean-atmosphere phenomenon in the Indian Ocean. A positive phase of the IOD is normally characterized by anomalous cooling of SST in the south eastern equatorial Indian Ocean and anomalous warming of SST in the western equatorial Indian Ocean. Associated with these changes the normal convection situated over the eastern Indian Ocean warm pool shifts to the west and brings heavy rainfall over east Africa and severe droughts/forest fires over the Indonesian region. The name IOD represents the zonal dipole structure of the various coupled ocean-atmosphere parameters such as SST, rainfall and Sea Surface Height anomalies. Hence the SST index defined on the web site and the Hovmoller graphs of SSH allow Kelvin and Rossby waves to be followed in The Indian Ocean. Kelvin and Rossby waves can modify the structure of the thermocline hence changing the heat content of the surface layer and the associated SST. Wind anomalies also produce SST anomalies.

7. Conclusion

In most respects, this project has fulfilled its objectives. The SPI is already being used by the South African Weather Service on their web site to report on real-time trends in the rainfall climate. Several agencies such as Marine and Coastal Management and the South African Weather Service are making use of near real time information being made available on the project web site (http://realtime.sea.uct.ac.za/) which will continue to operate in terms of a follow-on research contract with the Water Research Commission. The research outcomes also motivated the deployment of an ocean-atmosphere interaction measuring mooring off Angola, being financed by the international community (http://realtime.sea.uct.ac.za/mahyva/html/piratase.html). The discovery of a current in the Indian Ocean, an unexpected outcome of the project, made headlines internationally and locally. For the first time, as a result of this project, it has been possible to link drought in the Western Cape to the vagaries of the Antarctic Oscillation in the Southern Ocean.

The quality and quantity of the publications stemming from this research project testify to the important contribution that has been made in understanding and monitoring climate variability. Despite the great strides that have been made, we are still a long way from understanding all the factors that regulate interannual variability of Southern African climate. Some of the important questions that have emerged are the following:

- Why is there no linear relationship between El Niño Southern Oscillation (ENSO) and SA rainfall variability?
- Why are some El Niño events not linked to drought?
- What is the impact of El Niño and La Niña at the catchment scale?
- What is the role of the Antarctic oscillation (AAO) on summer rainfall?
- What is the interaction of ENSO and AAO and how does this affect Southern African Climate?

Many of these questions will be addressed in the follow-on project that has made continuity of the research possible.

8. Capacity building

Capacity has been developed in the following ways:

Training and supervision of PhD students Nicolas Vigaud, Alberto Mavume and Atanasio Manhique and Master students Mussie Kinedarian and Michael Mehari, Honours students Bjorn Backeberg, Michael Funke and Lionel Delaney.

Atanasio Manhique and Nicolas Fauchereau were sent to France for 3 months to visit our French collaborators.

Mathieu Rouault taught a full module on meteorology in the taught Masters course of the Dept of Oceanography.

Nicolas Vigaud taught Matlab to the Honours students in 2005 and 2006.

Nicolas Fauchereau taught Matlab to the Honours student in 2007 and to the Masters students in 2006.

We also started a special large-scale capacity building exercise in 2004, presented by Mathieu Rouault and Nicolas Vigaud. It was named “Skill for Science” and its main aim has been to empower students with the ability to find and to analyze the data they need for their research projects. It is addressed at PhD and Masters Students. It also aims to provide students with various tips on how to become better scientists. For instance, students are encouraged to join national and international scientific societies and bodies, to subscribe to the newsletter of an international program, use the web to further their knowledge and to do their research online with interactive web-based data analysis. Topics are meteorology, climatology, oceanography and ocean-atmosphere interaction. This class is geared towards the students’ Masters theses, making freshly acquired knowledge readily applicable for these theses. In the second part of the class, students are taught how to further exploit the web by learning how to read the data they need, plot them and apply statistics to these data using the program Matlab. The class has been attended by 15 students.

9. Dissemination of knowledge

9.1 Theses

6 theses:

Vigaud N, (2007) Water vapour transport from the South Atlantic and South Indian Oceans and summer rainfall over Southern Africa. PHD, Dept of Oceanography, June 2007

Mehari M. (2005) Ocean atmosphere interaction and Southern Rainfall in 2002/2003 Master Thesis, Dept of Oceanography

Kinedariam Mussi (2004) Climate variability in Erythree. Master Thesis, Dept of Oceanography

Backeberg B, (2004) A Preliminary Investigation of the Sea Surface Temperature and Surface Wind Covariability in the Southern Ocean south of Africa. Honours Thesis University of Cape Town

Delaney L. (2005) A study of Ocean Atmosphere interaction with Satellite remote sensing Honours Thesis (2005):

Funke M. (2005) Climate and ocean variability at Tristan da Cunha and Gough Island. Honours Thesis

9.2 Chapter in book

Reason C.J.C., P. Florenchie, M. Rouault and J. Veitch, 2006: Influences of large scale climate modes on the BCLME region. Chapter 10 in Forecasting of the Benguela Ecosystem (Eds., V. Shannon, C. Moloney),

9.3 Peer reviewed papers in journals

13 papers in peer rewieved journals:

2007-1 Vigaud N., Richard Y., Rouault M., Fauchereau N: Water vapour transport from the tropical Atlantic and summer rainfall in tropical southern Africa. Climate Dynamics, 28 (2-3) / February, 2007, doi: 10.1007/s00382-006-0186-9 Impact factor 3.4

2007-2 Rouault, M S. Illig, C Bartholomae, C.J.C. Reason and A. Bentamy Propagation and origin of warm anomalies in the Angola Benguela upwelling system in 2001 In Press, Journal of Marine System, Impact factor 1.2

2007-3 Rouault, P. Verley, B. Backeberg Ocean-atmosphere interaction above Agulhas Current eddies, Deep Sea Research, resubmitted, Impact factor 2

2006-1 Reason C. J. C. and M. Rouault Sea surface temperature variability in the tropical southeast Atlantic Ocean and West African rainfall. Geophys. Res. Lett, 33, L21705, doi: 10.1029/2006GL027145, 2006 Impact factor 2.4

2006-2 Siedler, Gerold; Rouault, Mathieu; Lutjeharms, Johann R. E. Structure and origin of the subtropical South Indian Ocean Countercurrent Geophys. Res. Lett., Vol. 33, No. 24, L24609 doi: 10.1029/2006GL027399 Impact factor 2.4

2005-1: Rouault M and Y Richard (2005): Intensity and spatial extent of droughts in Southern Africa. Geophysical Research Letters. Impact factor 2.4. 0 citation.

2005-2: Ansorge I.J., S. Speich., J.R.E. Lutjeharms., G.J. Gõni., C.J. de W. Rautenbach., P.W. Froneman., M. Rouault and S. Garzoli (2005) Monitoring the oceanic flow between Africa and Antarctica: Report of the first Good Hope cruise South African Journal of Science. 101, 29-35. Impact factor ISI 2003: Impact factor 0.93 0 citation

2005-3: Reason C.J.C. and M. Rouault Links between the Antarctic Oscillation and winter rainfall over southwestern South Africa (2005), Geophysical Research Letters. 32, L07705, doi:10.1029/2005GL0022419. Impact factor: 2.4 2 citation

2005-4: Rouault M, JL Melice, C. J.C. Reason and J. R.E. Lutjeharms. (2005) Climate variability at Marion Island, Southern Ocean, since 1960, Journal of Geophysical Research. 110, C05007, doi:10.1029/2004JC002492 . Impact factor: 2.9 0 citation

2004-1: Florenchie, P., CJC Reason, JRE Lutjeharms, M. Rouault, C. Roy and S. Masson, (2004): Evolution of Interannual Warm and Cold events in the South-East Atlantic Ocean, Journal of Climate. Impact factor factor: 3.6 11 citation.

2003-3: Mélice, J.-L., J.R.E. Lutjeharms, M. Rouault and I.J. Ansorge, (2003): Sea Surface temperatures the Subantarctic islands Marion and Gough during the past 50 years, South African Journal of Science, 99, 363-366. Impact factor: 0.93 7 citations.

2003-5: Rouault M. and Y. Richard, (2003) Spatial extension and intensity of droughts since 1922 in South Africa, Water SA 29, 489-500. Impact factor: 0.6, 6 citations.

2003-6: Rouault M and J.R.E. Lutjeharms, (2003) Microwave satellite remote sensing of SST around Southern Africa, South African Journal of Science, 99, 489-494. Impact factor: 0.93, 2 citation.

9.4 Oral presentations

34 oral and poster presentations:

Backeberg B, 2005: A Preliminary Investigation of the Sea Surface Temperature and Surface Wind Covariability in the Southern Ocean south of Africa. 21st South African Society for Atmospheric Science conference

Fauchereau N, Trzaska Y, Richard Y, Roucou P et P. Camberlin, 2003: SST variability in the Southern Indian ocean links to other ocean basins, associated anomalies in the Southern Hemisphere and lead-lags relationships to ENSO. International conference on scale interaction and variability of monsoon. October 6-10, Munnar, Kerala, India.

Fauchereau N. B. Pohl, Richard Y.: 2006: Influence of the Madden-Julian Oscillation on Southern Africa summer rainfall. SANCOR seminar Cape Town June 2006.

Fauchereau N. B. Pohl, Richard Y.: 2006: Influence of the Madden-Julian Oscillation on Southern Africa summer rainfall. 22nd South African Society for Atmospheric Science conference, 4-6 October 2006, Bloemfontein, South Africa.

Funke M, Climate and ocean variability at Tristan da Cunha and Gough Island October 2005 DPT of Oceanography

Manhique A., Reason C., Richard Y., Rydberg L., Rouault M., 2004: Atmospheric and oceanic patterns associated with early summer rainfall in north Mozambique. 20 South African Society for Atmospheric Sciences & African Meteorological Society Conference 2004, Cape Town, South Africa, 24-26 May.

Manhique A., Richard Y., Fauchereau N., Camberlin P., 2004: Interactions tropicales – tempérées et pluviométrie au Mozambique. Actes du XVII^{e} colloque international de climatologie, Climat "Mémoire du temps", Caen , France, 8-10 septembre.

Rouault, M., P. Florenchie, N. Fauchereau, C. J. C. Reason, 2003: South East Atlantic Warm Events And Southern African Rainfall. PIRATA 9 and South Atlantic CLIVAR workshops, 3/8 February 2003, Agra, Brazil.

Rouault, M.: Scientific rational for the South East extension of the Pilot Research Moored Array in the Tropical Atlantic. LODYC seminar, Paris, France, 1 April 2003.

Rouault, M.: Scientific rational for the South East extension of the Pilot Research Moored Array in the Tropical Atlantic. EGS Conference, Nice, France, 7/11 April 2003.

Rouault M and Y Richard, Spatial extension and intensity of droughts in Southern Africa since 1901, SASAS Conference Cape Town, September 2004

Rouault M, Status of the PIRATA SEE extension project, PIRATA workshop, Fortaleza, Brazil December 2004

Rouault M, Propagation and origin of warm anomalies in the Benguela Angola Benguela upwelling system in 2001., PIRATA workshop, Fortaleza, Brazil December 2004

Rouault M and Y Richard, Spatial extension and intensity of droughts in Southern Africa since 1901, Biennial Groundwater Conference Pretoria. March 2005.

Rouault M and M Rouault: Near-realtime remote sensing in the Tropical Atlantic, PIRATA workshop, Toulouse, France 2005

Rouault M and Y. Richard, Impact of El Nino on Southern Africa. First International Conference on El Nino phenomenon. Guayaquil, Equator, May 2005.

Rouault M and M Rouault: Near-realtime remote sensing in the Tropical Atlantic, SAMS, Durban, July 2005

Rouault M, JL Melice, C. J.C. Reason and J. R.E. Lutjeharms. Climate variability at Marion Island, Southern Ocean, since 1960, SAMS, Durban, July 2005

Rouault M, Ocean Atmosphere Interaction: application to South African climate seminar LOCEAN, Paris, October 2005.

Rouault M, Ocean Atmosphere Interaction: application to South African climate HDR presentation UBO Brest, October 2005

Rouault M and Y. Richard, Impact of El Nino on Southern Africa. Africa Monsoon Multidisciplinary Analysis workshop, Dakar, November 2005.

Rouault M, (2006) First results from the PIRATA South East extension 'Kizomba' Mooring, 26 September 2006, SANCOR seminar, Cape Town, South Africa

Rouault M, (2006) First results from the PIRATA South East extension 'Kizomba' Mooring, SASAS Conference, 5/6 October, Bloemfontein, South Africa

Rouault M, (2006) Warming of the Ocean: implication for South African Climate, SASAS Conference, 5/6 October, Bloemfontein, South Africa

Rouault M, (2006) Status of the PIRATA South East extension 'Kizomba' Mooring, PIRATA workshop, 3-5 November 2006, Miami, USA.

Rouault M, (2006) First results from the PIRATA South East extension 'Kizomba' Mooring, PIRATA workshop, 3-5 November 2006, Miami, USA.

Rouault M, (2007) Warming of the Ocean: implication for South African Climate, SASAS Conference, 5/6 October, Bloemfontein, South Africa

Vigaud N., Richard Y: 2006: On the Role of Water Vapor Transport from the Tropical Atlantic and Summer Rainfall in Tropical Southern Africa. 20-24 February, Ocean Sciences Meeting, Honolulu, Hawaii, USA.

Vigaud N., Rouault M., Richard Y., Fauchereau N., 2006: On the Role of Water Vapour Transport from the Tropical Atlantic and Summer Rainfall in Tropical Southern Africa. 8th International Conference on Southern Hemisphere Meteorology and Oceanography, 24–28 April, Foz do Iguaçu, Paraná State, Brazil.

10. Bibliography

Adler, R.F., Huffman, G. J., Chang, A., Ferraro, R., Xie, P., Janowiak, J., Rudolf, B., Schneider, U., Curtis, S., Bolvin, D., Gruber, A., Susskind, J., Arkin, P., Nelkin, E. 2003: The Version-2 Global Precipitation Climatology Project (GPCP) Monthly Precipitation Analysis (1979–Present), Journal of Hydrometeorology, 4, 147-1167.

Anctil F, Larouche W and AA Viau (2002) Exploration of the standardized precipitation index with regional analysis. Can. J. Soil Sci. 82 (1) 115-125

Anthes, R.A., Tropical cyclones, their evolution, structure and effects, Meteorol. Mon., 19, 1-208, 1982

Belkin, I. M., and A. L. Gordon, Southern Ocean fronts from the Greenwich meridian to Tasmania. J. Geophysis. Res., 101(C2), 3675-3696, 1996.

Bentamy, Abderrahim, Katsaros, Kristina B., Mestas-Nuñez, Alberto M., Drennan, William M., Forde, B. Evan. and H. Roquet, 2003: Satellite estimates of wind speed and latent heat flux over the global oceans. J. Climate, 16(4) , 637–656.

Boyd, A. J., J. Salat and Maso M., 1987: The seasonal intrusion of relatively saline water on the shelf off northern and central Namibia: The Benguela and comparable ecosystems. South Afr. J. Mar. Sci., 5, 107–120.

Birol, F., and R. Morrow (2001), Source of the baroclinic waves in the southeast Indian Ocean. J. Geophys. Res., 106(C9), 145 - 160.

Birol, F., and R. Morrow (2003), Separation of quasi-semiannual Rossby waves from the eastern boundary of the Indian Ocean, J. Marine Res., 61, 707-723.

Boebel, O., Lutjeharms, J., Schmid, C., Zenk, W., Rossby, T., Barron, C., 2003. The Cape Cauldron: a regime of turbulent inter-ocean exchange. Deep-Sea Research II 50, 57-86.

Bourras, D., Reverdin, G., Giordani, H., Caniaux, G.,2004. Response of the atmospheric boundary layer to a mesoscale oceanic eddy in the northeast Atlantic. Journal of Geophysical Research 109, D18114, doi:10.1029/2004JD004799.

Bubnov, V.A., Egorikhin, V.D., 1980: Study of water circulation in the Tropical Atlantic. Deep-Sea Research Part A 26 (Suppl. II), 125–136.

Burnett, A.W. and A.R. McNicoll, Interannual Variations in the Southern Hemisphere Winter Circumpolar Vortex: Relationships with the Semiannual Oscillation J. Clim. 13, 991-999, 2000.

Byrne, D.A., Gordon, A.L., Haxby, W.F., 1995. Agulhas Eddies: a synoptic view using Geosat ERM data. Journal of Physical Oceanography 25, 902-917.

Carton, J. A., and B. Huang, 1994: Warm events in the Tropical Atlantic. J. Phys. Oceanogr., 24, 888–903.
Carton, J.A, X. Cao, B. S. Giese, and A. M. da Silva, 1996: Decadal and interannual SST variability in the Tropical Atlantic. J. Phys. Oceanogr., 26, 1165–1175.

Carton J.A., and Z.X. Zhou, 1997: Annual cycle of sea surface temperature in the Tropical Atlantic ocean, J. Geophys. Res., 102, 27813-27824

Casey, K. S., and P. Cornillon, 2001: Global and regional SST trends. J. Climate, 14, 3801–3818.

Chambers, D.P., B.D. Tapley, and R.H. Stewart, Measuring heat storage changes in the equatorial Pacific: A comparison between TOPEX altimetry and Tropical Atmosphere-Ocean buoys, J. Geophys. Res., 103, 18591-18597, 1998.

Chelton, D.B., Wentz, F.J., Gentemann, C.L., de Szoeke, R.A., Schlax, M.G., 2000. Satellite microwave SST observations of transequatorial tropical instability waves. Geophysical Research Letters 27, 1239-1242.

Chelton, D.B., Schlax, M.G., Freilich, M.H., Milliff, R.F., 2004. Satellite measurements reveal persistent small-scale features in ocean winds. Science 303, 978-983.

Chelton, D.B., Wentz, F.J., 2005. Global high-resolution satellite observations of sea-surface temperature for numerical weather prediction and climate research. Bulletin of the American Meteorological Society 86, 1097-1115.

Chown, S. L., and V. R. Smith, 1993: Climate-change and the short-term impact of feral house mice at the Sub-Antarctic Prince-Edward-Islands. Oecologia, 96(4), 508-516.

Colberg, F., C.J.C. Reason, and K. Rodgers, 2004: South Atlantic response to ENSO induced climate variability in an OGCM. J. Geophys. Res., 109, C12015, 10.1029/2004JC002301.

Davidson, K.L., Boyle, P.J., Gautier, C., Hanson, H.P., and Khalsa, S.J.S., 1991. Medium- to large-scale atmospheric variability during the Frontal Air-Sea Interaction Experiment. Journal of Geophysical Research 96, 8531-8551.

Compagnucci RH, EA Agosta and WM Vargas (2002) Climatic change and quasi-oscillations in central-west Argentina summer precipitation: main features and coherent behaviour with southern African region. Climate Dyn., 18(5) 421-435.

Dai A and KE Trenberth, (1998) Global variation in droughts and wet spells: 1900-1995. Geophys. Res. Let. 25 3367-3370.

Domonkos P (2003) Recent precipitation trends in Hungary in the context of larger scale climatic changes Nat Hazards 29 (2) 255-271

Donahue, K.A., and J.M. Toole (2003), A near-synoptic survey of the Southwest Indian Ocean, Deep-Sea Res. II, 50, 1893-1931

Ducet, N., P.-Y. Le Traon, and G. Reverdin, 2000: Global high resolution mapping of ocean circulation from TOPEX/Poseidon and ERS-1/2. J. Geophys. Res., 105, 19477-19498.

Friehe, C.A., Shaw, W.J., Rogers, D.P., Davidson, K.L., Large, W.G., Stage, S.A., Crescenti, G.H., Khalsa, S.J.S., Greenhut, G.K., Li, F., 1991. Air-sea fluxes and surface layer turbulence around a SST front. Journal of Geophysical Research 96, 8593-8609.

Goddard, L. and N. E. Graham, 1999. The importance of the Indian Ocean for simulating precipitation anomalies over eastern and southern Africa. J. Geophys. Res., 104: 19099-19116.

Gordon, A.L., Weiss, R.F., Smethie, W.M., Warner, M.J., 1992. Thermocline and Intermediate Water communication between the South Atlantic and Indian Oceans, Journal of Geophysical Research 97, 7223–7240.

Greatbatch, R.J., On the role played by upwelling of water in lowering sea surface temperatures during the passage of a storm, J. Geophys. Res., 90, 11751-11755, 1985.
Price, J. F., Upper ocean response to a hurricane, J. Phys Oceanogr., 11, 153-175, 1981.

Fairall, C.W., E.F. Bradley, D.P. Rogers, J.B. Edson, G.S. Young, 1996b: Bulk parameterization of air-sea fluxes for TOGA COARE., J. Geophys. Res. 101, 3747-3764.

Florenchie, P., JRE Lutjeharms, C.J.C. Reason, S. Masson and M. Rouault, 2003: Source of the Benguela Niños in the South Atlantic Ocean, Geophys. Res. Lett., 30, doi:10.1029/2003GL017172.

Florenchie, P., CJC Reason, JRE Lutjeharms, M. Rouault, C. Roy and S. Masson, 2004: Evolution of Interannual Warm and Cold events in the South-East Atlantic Ocean, J. Climate, 17, 2318-2334

Fyfe, J. C. (2003) Extratropical Southern Hemisphere Cyclones: Harbingers of Climate Change? J. Climate 16: 2802-2805

Gammelsrød, T., C. H. Bartholomae, D. C. Boyer, V. L. L. Filipe, and M. J. O'Toole, 1998: Intrusion of warm surface water along the Angolan–Namibian coast in February–March 1995: The 1995 Benguela Niño. South Afr. J. Mar. Sci., 19, 41–56.

Gordon, A.L., Bosley, K.T., 1991: Cyclonic gyre in the Tropical South Atlantic. Deep-Sea Research 38 (Suppl.), S323–S343.

Genthon, C, G. Krinner, M. Sacchettini (2003) Interannual Antarctic tropospheric circulation and precipitation variability, Clim. Dyn., 21 (4) 289-307 DOI: 10.1007/s00382-003-0329-1

Gillet N.P and D W. J. Thompson (2003) Simulation of recent Southern Climate Change, Science, 302, 273-275.

Gong, D., and S. Wang, 1999: Definition of Antarctic oscillation index. Geophys. Res. Lett., 26, 459–462

Hall, Alex, Visbeck, Martin, 2002 Synchronous Variability in the Southern Hemisphere atmosphere, Sea Ice, and Ocean Resulting from the Annular Mode J. Clim. 15: 3043-3057.

Hardman-Mountford, N.J., Richardson, A.J., Agenbag, J.J., Hagen, E., Nykjaer, L., Shillington, F.A. and Villacastin, C. 2003. Ocean climate of the southeast Atlantic observed from satellite data and wind models. Progress in Oceanography, 59: 181-221.

Hanawa, K., and L.D. Talley, (2001), Mode Waters, in Ocean Circulation and Climate, G. Siedler, J. Curch, J.Gould, Eds. (Academic Press, San Diego, CA, 2001), pp.373 – 386.

Hardman-Mountford, N.J., Richardson, A.J., Agenbag, J.J., Hagen, E., Nykjaer, L., Shillington, F.A. and Villacastin, C. 2003. Ocean climate of the southeast Atlantic observed from satellite data and wind models. Progress in Oceanography, 59: 181-221.
Hayes MJ, Svoboda MD, Wilhite DA and OV Vanyarkho (1999) Monitoring the 1996 drought using the Standardized Precipitation Index. BAMS 80 429-438.

Hines, K. M., D. H. Bromwich, and G. J. Marshall, 2000: Artificial surface pressure trends in the NCEP–NCAR reanalysis over the Southern Ocean and Antarctica. J. Clim., 13, 3940–3952

Hines, Keith M., Bromwich, David H., Marshall, Gareth J.Artificial 200 Surface Pressure Trends in the NCEP–NCAR Reanalysis over the Southern Ocean and Antarctica, Journal of Climate 13: 3940-3952

Hirst, C., and S. Hastenrath, 1983: Atmosphere-ocean mechanisms of climate anomalies in the Angola-Tropical Atlantic sector, J. Phys. Oceanogr., 13, 1146–1157.

llig S., B. Dewitte, N. Ayoub, Y. du Penhoat, G. Reverdin, P. De Mey, F. Bonjean and G.S. E. Lagerloef, 2004: Interannual Long Equatorial Waves in the Tropical Atlantic from a High Resolution OGCM Experiment in 1981-2000. J. Geophys. Research., 109, No. C2, C02022, doi:10.1029/2003JC001771.

Hurrell, J. W., and H. van Loon, 1994: A modulation of the atmospheric annual cycle in the Southern Hemisphere. Tellus, 46A, 325–338.

IRI (2002) Climate Digest, March 2002

IRI (2003) Climate Digest, March 2003

IRI (2004) Climate Digest, March 2004

Jones, J. M., Widmann, Martin Instrument- and Tree-Ring-Based (2003) Estimates of the Antarctic Oscillation Journal of Climate 16: 3511-3524

Jones, J. M., Widmann, Martin Instrument- and Tree-Ring-Based (2003) Estimates of the Antarctic Oscillation Journal of Climate 16: 3511-3524

Jones, P. D., Moberg, A., 2003: Hemispheric and Large-Scale Surface Air Temperature Variations: An Extensive Revision and an Update to 2001 J. Climate, 16, 206-223.
Josey, S.A., Kent, E.C., Taylor, P.K.,1999. New insights into the ocean heat budget closure problem from analysis of the SOC air-sea flux climatology. Journal of Climate 12, 2856-2880.

Jury,M.R; Levey KM; Makarau A (1996) Mechanisms of short-term rainfall variability over Southern Africa. WRC Report Number: 436/1/96

Jury,M R; Mulenga HM; Mason SJ; Brandao A(1998) Development of an objective statistical system to forecast summer rainfall over South Africa Report Number: 672/1/98.

Lloyd-Hughes B and MA Saunders (2002) A drought climatology for Europe. Int. J. Clim.
22 (13): 1571-1592.

Kantha, L.H., and C.A. Clayson (2000), Numerical Models of Oceans and Oceanic Processes, Academic Press, San Diego, CA, 940 pp

Kalnay, E. et. al., 1996: The NCEP/NCAR, 40-Year Reanalysis Project. Bull. Amer. Meteor. Soc., 77, 437–471.

Karstensen, J., and D. Quadfasel (2002), Water subducted into the Indian Ocean subtropical gyre, Deep-Sea Res.II 49, 1441-1457.

Katz, E. J., 1997: Waves along the equator in the Atlantic. J. Phys.Oceanogr., 27, 2536–2544.

Keyantash J and JA Dracup (2002) The Quantification of Drought: An Evaluation of Drought Indices. BAMS 83 1167-1180.

Kidson, John W. 1999: Principal Modes of Southern Hemisphere Low-Frequency Variability Obtained from NCEP–NCAR Reanalyses. Journal of Climate: Vol. 12, No. 9, pp. 2808–2830

Kiladis, G. N., and K. C. Mo, 1998: Interannual and intraseasonal variability in the Southern Hemisphere. Meteorology of the Southern Hemisphere, D. J. Karoly and D. G. Vincent, Eds., Amer. Meteor. Soc., 307–336.

Killworth, P.D., D.B. Chelton, and R.A de Szoeke (1997), The speed of observed and theoretical long extra-tropical planetary waves. J.Phys.Oceanogr., 27, 1946 -1966
Komuscu AU (1999) Using the SPI to analyze spatial and temporal pattern of drought in Turkey. Drought Network News 11 7-13.

Kostianoy, A. G., and J. R. E. Lutjeharms, 1999: Atmospheric effects in the Angola-Benguela Frontal Zone, J. Geophys. Res., 104, 20,963– 20,970,.

Kwok, R., and J. C. Comiso 2002: Southern Ocean Climate and Sea Ice Anomalies Associated with the Southern Oscillation. Journal of Climate, 15, 487-501.

Lana X, Serra C, Burgueno A (2002) Patterns of monthly rainfall shortage and excess in terms of the standardized precipitation index for Catalonia (NE Spain). Int. J. Clim. 21 (13) 1669-1691.
Lass, H. U., M. Schmidt, V. Mohrholz, and G. Nausch, 2000: Hydrographic and current measurements in the area of the Angola–Benguela front. J. Phys. Oceanogr., 30, 2589–2609.

Levitus, S., J. I. Antonov, T. P. Boyer, and C. Stephens (2001), World Ocean Database 1998, Natl. Oceanic and Atmos. Admin., Silver Spring. Md.

Lindesay JA and CH Vogel (1990) Historical evidence for Southern Oscillation-southern African rainfall relationships. Int. J. Clim. 10 679-689.

Louw W.J. (1982) Oscillations in Orange free State Rainfall. Technical paper (South Africa Weather Bureau) no. 11, Weather Bureau, Dept. of Transport. 52 p

Lutjeharms, J. R. E. and H. R. Valentine, 1984: Southern Ocean thermal fronts south of Africa. Deep-Sea Research, 31(12), 1461 - 1476.

Lutjeharms, J.R.E., Valentine, H.R., 1988a. Eddies at the Sub-Tropical Convergence south of Africa. Journal of Physical Oceanography 18, 761-774.

Lutjeharms, J.R.E., Valentine, H.R., 1988b. On mesoscale ocean eddies at the Agulhas Plateau. South African Journal of Science 84, 194-200.

Lutjeharms, J.R.E., van Ballegooyen, R.C., 1988. The retroflection of the Agulhas Current. Journal of Physical Oceanography 18, 1570-1583.

Marshall, G. J. ,2003: Trends in the Southern Annular Mode from Observations and Reanalyses. Journal of Climate 16, 4134-4143.

Marshall, G. J., P. A. Stott, J. Turner, W. M. Connolley, J. C. King, and T. A. Lachlan-Cope (2004), Causes of exceptional atmospheric circulation changes in the Southern Hemisphere, Geophys. Res. Lett., 31, L14205, doi:10.1029/2004GL019952.

McCarthy, M.C., and L.D Talley (1999), Three-dimensional isoneutral potential vorticity structure in the Indian Ocean, J. Geophys. Res. 104(C6), 13251-13267

McKee TB, NJ Doesken and J Kleist (1993) The relationship of drought frequency and duration to time scales. Pre-prints, 8th Conf. on Appl. Climat., 17-22 January, Anaheim, CA, 179-184.

McKee TB, NJ Doesken and J Kleist (1995) Drought monitoring with multiple time scales. Pre-prints, 9th Conf. on Appl. Clim., Dallas, TX, 233–236.

Mey, R.D., Walker, N.D, Jury, M.R., 1990. Surface heat fluxes and marine boundary layer modification in the Agulhas Retroflection Region, Journal of Geophysical Research 95, 15997-16015.

Min SK, Kwon WT, Park EH, et al. (2003) Spatial and temporal comparisons of droughts over Korea with East Asia Int. J. Clim. 23 (2) 223-233.

Meehl G.A., J. W. Hurrell, and H. van Loon, 1998: A modulation of the mechanism of the semiannual oscillation in the Southern Hemisphere. Tellus, 50A, 442–450
Mercier H., M. Arhan and J.R.E. Lutjeharms, 2003: Upper-layer circulation in the eastern Equatorial and South Atlantic Ocean in January–March 1995, Deep-Sea Research I 50, 863–887

Mo, Kingtse C. 2000: Relationships between Low-Frequency Variability in the Southern Hemisphere and Sea Surface Temperature Anomalies. Journal of Climate: Vol. 13, No. 20, pp. 3599–3610

Mohrholz, V., M. Schmidt, and J. R. E. Lutjeharms, 2001: The hydrography and dynamics of the Angola–Benguela frontal zone and environment in April 1999. South Afr. J. Sci., 97, 199–208.

Monteiro, P. M. S., A. van der Plas, V. Mohrholz, E. Mabille, A. Pascal, and W. Joubert (2006), Variability of natural hypoxia and methane in a coastal upwelling system: Oceanic physics or shelf biology?, Geophys. Res. Lett., 33, L16614, doi:10.1029/2006GL026234.

Moore, D.W., P. Hisard, J. McCreary, J. Merle, J. O'Brien, J. Picaut, J.M Verstraete, and C. Wunsch, 1978: Equatorial adjustment in the Eastern Atlantic, Geophys. Res. Lett., 5, 637-640.

Moroshkin, K.V., Bubnov, V.A., Bulatov, R.P., 1970. Water circulation in the eastern South Atlantic. Oceanology 10, 27–34.

Mulenga, H.M., M. Rouault and C.J.C. Reason, 2003: Dry summers over NE South Africa and associated circulation anomalies, Climate Research, 25, 29-41.

Nauw, H. M. van Aken, J. R. E. Lutjeharms, and W. P. M. de Ruijter (2006), Intrathermocline eddies in the Southern Indian Ocean, J. Geophys. Res, 111, C03006, doi:10.1029/2005JC002917, 2006.

New, M., Hulme, M., and P.D. Jones. 2000: Representing Twentieth-Century Space–Time Climate Variability. Part II: Development of 1901–96 Monthly Grids of Terrestrial Surface Climate. J. Climate, 13, 2217–2238.

Nicholson, S.E. and D. Entekhabi, 1987: The nature of rainfall variability in equatorial and southern Africa: Relationships with SST along the southwestern coast of Africa. J. Clim. and Applied Meteorology 26, 561–578.

O'Connor, B.M., R.A Fine, and D.B. Olson (2005), A global comparison of subtropical underwater formation rates, Deep-Sea Res. I 52, 1569-1590.

O'Neill, L.W., Chelton, D.B., Esbensen, S.K., Wentz, F.J., 2005. High-resolution satellite observations of SST modification of the marine atmospheric boundary layer over the Agulhas Return Current. Journal of Climate 18, 2706-2723.

Pakhomov, E.A., McClelland, J.W., Bernard, K., Kaehler, S. and Montoya J.P. (2004) Spatial and temporal shifts in stable isotope values of bottom-dwelling shrimp Nauticaris marionis at the sub-Antarctic archipelago. Mar. Biol., 144: 317-325.

Philander, S.G.H., 1986: Unusual condition in the Tropical Atlantic in 1984, Nature, 322, 236-238.

Philander, S.G.H. and R.C. Pacanowski, 1986: A model of the seasonal cycle of the Tropical Atlantic, J. Geophys. Research, 91, 14 192-14 206.

Philander, S.G.H., 1990: El Niño, La Nina and the Southern Oscillation, Academic Press, 293 pp.

Price, J. F., Upper ocean response to a hurricane, J. Phys Oceanogr., 11, 153-175, 1981.

Quartly, G.D., J.J.H. Buck, M.A. Srokosz, and A.C. Coward (2006), Eddies around Madagascar — The retroflection re-considered, J.Mar. Systems, doi:10.1016/j.jmarsys.2006.06.001

Rayner N. A., D. E. Parker, E. B. Horton, C. K. Folland, L. V. Alexander, D. P. Rowell, E. C. Kent, and A. Kaplan, Global analyses of sea surface temperature, sea ice, and night marine air temperature since the late nineteenth century, J. Geophys. Res., 108 (D14), 4407, doi:10.1029/2002JD002670, 2003.

Reason, C.J.C., 1999: Interannual warm and cool events in the subtropical / mid-latitude South Indian Ocean region. Geophys. Res. Lett., 26, 215-218.

Reason, C.J.C. and H.M. Mulenga, 1999: Relationships between South African rainfall and SST anomalies in the South West Indian Ocean. Int. J. Climatol., 19, 1651-1673.

Reason, C.J.C., 2000: Multidecadal climate variability in the subtropics / midlatitudes of the Southern Hemisphere oceans. Tellus, 52A, 203-223.

Reason, C.J.C., R.J. Allan, J.A. Lindesay and T.J. Ansell, 2000: ENSO and climatic signals across the Indian Ocean basin in the global context: Part I, interannual composite patterns. Int. J. Climatol., 20, 1285-1327.

Reason, C.J.C. and M. Rouault, 2002: ENSO-like decadal patterns and South African rainfall. Geophys. Res. Lett., 29 (13), doi:10.1029/2002GL014663.

Reason, C.J.C., M. Rouault, J.-L. Melice and D. Jagadeesha, 2002: Interannual winter rainfall variability in SW South Africa and large scale ocean-atmosphere interactions. Met. Atmos. Phys., Special Issue on Atmosphere- surface interactions, 80 (1-4), 19-29.
Reason, C.J.C., D. Jagadheesha and M. Tadross, 2003: A model investigation of interannual winter rainfall variability over southwestern South Africa and associated ocean-atmosphere interaction. S. Afr. J. Sci., 99, 75-80.

Reason CJC; Hermes J; Singleton A; Lutjeharms JRE(2003) Modelling variability in the South West Indian Ocean and its influence on South Africa's climate WRC Report Number: 868/1/03

Reason, C.J.C. and A. Keibel, Tropical cyclone Eline and its unusual penetration and impacts over the southern African mainland, Weath. Forecast., 19, 789-805, 2004
Renwick, J. A. (2004), Trends in the Southern Hemisphere polar vortex in NCEP and ECMWF reanalyses, Geophys. Res. Lett., 31, L07209, doi:10.1029/2003GL019302

Reynolds, R. W., and T. M. Smith, 1994: Improved global sea surface temperature analyses using optimum interpolation. J. Climate, 7, 929–948.

Richard Y and I Poccard (1998) A statistical study of NDVI sensitivity to seasonal and interannual rainfall variations in Southern Africa. Int. J. Remote Sensing 19 2907-2920.

Richard Y, S Trzaska, P Roucou and M Rouault (2000) Modification of the Southern African rainfall variability /El Niño Southern Oscillation relationship. Climate Dyn. 16 886-895.

Richard Y, N Fauchereau, I Poccard, M Rouault and S. Trzaska (2001) XXth Century Droughts in Southern Africa Spatial and temporal variability, teleconnections with oceanic and atmospheric conditions. Int. J. Clim, 21 873-885.

Ridderinkhof, H., and W.P.M. de Ruijter, Moored current observations in the Mozambique Channel, Deep-Sea Res. II, 50, 1933-1955, 2003.

Rio, M.-H., and F. Hernandez (2004), A mean dynamic topography computed over the world ocean from altimetry, in situ measurements, and a geoid model, J. Geophys. Res., 109, C12032, doi:10.1029/2003JC002226.

Rouault, M., A.M. Lee-Thorp (1997) Fine-Time resolution measurements of atmospheric boundary layer properties between Cape Town and Marion Island. South African Journal of Marine Sciences, 17, 281-296. Impact factor: 0.93 2 citations.

Rouault M; Lutjeharms JRE; Lee-Thorp AM; Jury,M.R.,Maiodina M (1999) Air-sea interaction over the Agulhas current and implications for South African weather WRC Report Number: 374/1/99

Rouault, M., A.M. Lee-Thorp and J.R.E. Lutjeharms (2000) Observations of the atmospheric boundary layer above the Agulhas Current during along current winds. Journal of Physical Oceanography, 30, 70-85 Impact factor: 2.2 6 citations

Rouault, M., I. Jobard, S. A. White and J. R. E. Lutjeharms (2001). Studying rainfall events over South Africa and adjacent oceans using the TRMM satellite. South African Journal of Science, 97, 455-460. Impact factor: 0.93 1 citation

Rouault, M. and J.R.E. Lutjeharms (2000) Air-sea exchange over an Agulhas eddy at the Subtropical Convergence. The Global Atmosphere and Ocean System. 7, 125-150. Impact factor none yet but paper cited in Science

Rouault, M., S. A. White, C. J. C. Reason J. R. E. Lutjeharms and I. Jobard (2002) Ocean-Atmosphere Interaction in the Agulhas Current and a South African extreme weather event. Weather and Forecasting, Vol 17, 4, 655-669, Impact factor: 1.07, 4 citations.

Rouault M; Reason CJ; Lutjeharms JRE; Mulenga H; Richard Y; Fauchereau N; Trzaksa S. (2003) Role of the oceans in South Africa's rainfall WRC Report Number: 953/1/03
Rouault M. and Y. Richard, (2003) Spatial extension and intensity of droughts since 1922 in South Africa, Water SA 29, 489-500. Impact factor: 0.6, 2 citations.

Rouault M and J.R.E. Lutjeharms, (2003) Microwave satellite remote sensing of SST around Southern Africa, South African Journal of Science, 99, 489-494. Impact factor: 0.93, 1 citation.

Rouault M, C. J. C. Reason, J.R.E. Lutjeharms and A. Beljaars (2003) NCEP Reanalysis and ECMWF operational model underestimation of latent and sensible heat fluxes above the Agulhas Current, Journal of. Climate, 16, 776-782. Impact factor: 3.6 2 citations

Rouault, M, P. Florenchie, N. Fauchereau, C. J. C. Reason (2003) South East Atlantic Warm Events And Southern African Rainfall. Geophysical Research Letter, 29, 13, 10.1029/2002GL014663 Impact factor: 2.4 2 citations

Rouault M and Y Richard (2005): Intensity and spatial extent of droughts in Southern Africa. Geophysical Research Letters. Impact factor 2.4. 0 citation.

Rouault M, JL Melice, C. J.C. Reason and J. R.E. Lutjeharms. (2005) Climate variability at Marion Island, Southern Ocean, since 1960, Journal of Geophysical Research. 110, C05007, doi:10.1029/2004JC002492 . Impact factor ISI 2003: 2.9 0 citation

Saffir, H.S., Saffir-Simpson Scale for Hurricanes, Herbert S. Saffir Consulting Engineers, Coral Gables, Florida, 21-23, 1974.

Samelson, R. M., E. D. Skyllingstad, D. B. Chelton, S. K. Esbensen, L. W. O'Neill, and N. Thum, 2006. A note on the coupling of wind stress and sea surface temperature. Journal of Climate, 19, 1557-1566

Schott, F.A., M. Dengler, and R. Schoenefeldt (2002), The shallow overturning circulation of the Indian Ocean, Progr.Oceanogr. 53, 57-103.

Schouten, M.W., de Ruijter, W.P.M., van Leeuwen, P.J., Lutjeharms, J.R.E., 2000. Translation, decay and splitting of Agulhas rings in the southeastern Atlantic Ocean, Journal of Geophysical Research 105, 21913-21926, 10.1029/1999JC00046.

Seiler RA, M. Hayes and L Bressan (2002) Using the standardized precipitation index for flood risk monitoring. Int. J. Clim.22 1365-1376.

Servain , J. Busalacchi, M. J. McPhaden, A. D. Moura, G. Reverdin, M. Vianna, and S. E. Zebiak, 1998: A Pilot Research Moored Array in the Tropical Atlantic (PIRATA). Bull. Amer. Meteor. Soc., 79, 2019–2031.

Shannon, L. V., A. J. Boyd, G. B. Brundrit, and J. Taunton-Clark, 1986: On the existence of an El Niño-type phenomenon in the Benguela system, J. Mar. Res., 44, 495– 520.

Shannon, L.V., Nelson, G., 1996. The Benguela: large scale features and processes and system variability. In: Wefer, G., Berger, W.H., Siedler, G., Webb, D.J. (Eds.), The South Atlantic: Present and Past Circulation. Springer, Berlin, pp. 644.

Shay, L.K., G.J. Goni, and P.G. Black, Effects of a warm oceanic feature on Hurricane Opal, Mon. Weath. Rev., 128, 1366-1383, 2000.

Shindell, D. T., and G. A. Schmidt (2004), Southern Hemisphere climate response to ozone changes and greenhouse gas increases, Geophys. Res. Lett., 31, L18209, doi:10.1029/2004GL020724

Silvestri, G.E. and C.S. Vera, 2003: Antarctic Oscillation signal on precipitation anomalies over southeastern South America. Geophys. Res. Lett., 30, 2115, doi:10.1029/2003GL018277.

Simmonds, I., and K. Keay, 2000: Variability of Southern Hemisphere extratropical cyclone behavior, 1958–97. J. Climate., 13, 550–561

Smith, V. R., 2002: Climatic change in the Sub-Antarctic: an illustration from Marion Island. Climate Change, 52, 345-357.

Smith, V. R., and M. Steenkamp, 1990: Climatic change and its ecological implications at a sub-Antarctic island. Oecologia, 85(1), 14-24.

South African Weather Bureau (1972) District rainfall for South Africa and the annual march of rainfall over southern Africa. South African Weather Bureau, WB35, Pretoria.

Stammer, D., F.J. Wentz, and C.L. Gentemann, Validation of microwave sea surface temperature measurements for climate purposes. J.Climate, 16, 73-87,2002.

Stramma, L. and F. Schott, 1999. The mean flow field of the Tropical Atlantic ocean. Deep-Sea Res., 46, 279- 303.

Stramma, L., and J.R.E. Lutjeharms (1997), The flow field of the subtropical gyre in the South Indian Ocean, J. Geophys. Res., 102, 5513-5530.

Svoboda, M, D LeComte, M Hayes, R Heim, K Gleason, J Angel, B Rippey, R Tinker, M Palecki, D Stooksbury, D Miskus, S Stephens (2002) The Drought Monitor BAMS 83 1181-1190.

Sweet, W., Fett, R., Kerling, J., LaViolette, P. 1981. Air-sea interaction effects in the lower troposphere across the north wall of the Gulf Stream, Monthly Weather Review 109, 1042-1052.

Tennant, W. (2004), Considerations when using pre-1979 NCEP/NCAR reanalyses in the southern hemisphere, Geophys. Res. Lett., 31, L11112, doi:10.1029/2004GL019751

Tennant, W.J., 1999. Numerical forecasting of monthly climate over South Africa, Int. J. Climatol., 19, 1319-1336.

Tennant WJ and BC Hewitson, 2002: Intra-seasonal rainfall characteristics and their importance to the seasonal prediction problem. Int. J. Climatol., 22, 1033-1048

Tennant WJ and Reason CJC, 2005: Associations between the global energy cycle and regional rainfall in South Africa and Southwest Australia. J. Climate
Thompson, D. W. J., and J. M. Wallace, 2000: Annular modes in the extratropical circulation. Part I: Month-to-month variability. J. Climate, 13, 1000–1016

Thompson, David W. J., Wallace, John M., Hegerl, Gabriele C. Annular Modes in the Extratropical Circulation (2000). Part II: Trends Journal of Climate 13: 1018-1036

Thompson, D. W. J., and S. Solomon, 2002: Interpretation of recent Southern Hemisphere climate change. Science. 296, 895–899

Toole, J.M., and B.A Warren (1993), A hydrographic section across the subtropical South Indian Ocean, Deep-Sea Res. 40, 1973-2019.

Trenberth, KE. (1997) The Definition of El Niño. BAMS 78 2771-2777.

Trenberth, KE and DP Stepaniak (2002) Indices of El Niño Evolution. J Clim. 14 1697-1701.

Tyson PD, Dyer TGJ and MN Mametse (1975) Secular changes in South African rainfall: 1880 to 1972. Quarterly Journal of the Royal Meteorological Society, 101 817–833.

Tyson, PD, GRJ Cooper and TS McCarthy (2002) Millenial to multi-decadal variability in the Climate of Southern Africa. Int. J. Clim., 22 1105-117. DOI:10.1002/joc.787.

Van Aken, H.M., van Veldhoven, A.K., Veth, C., de Ruijter, W.P.M., van Leeuwen, P.J., Drijfhout, S.S., Whittle, C.P., Rouault, M., 2003. Observations of a young Agulhas ring, Astrid, during MARE in March 2000. Deep-Sea ResearchII 50, 167-195.

Van Heerden J, DE Terblanche and GC Schulze (1988) The Southern Oscillation and South African summer rainfall. J. Climatol. 8 577-597.

Van Loon, Harry. 1967: The Half-Yearly Oscillations in Middle and High Southern Latitudes and the Coreless Winter. Journal of the Atmospheric Sciences: Vol. 24, No. 5, pp. 472–486

Van Loon, Harry, Kidson, John W., Mullan, A. Brett Decadal Variation of the Annual Cycle in the Australian Dataset Journal of Climate 1993 6: 1227-1231

Van Loon, H.and K Tourpali 1995 Antarctic ozone trends in the troposphere of Southern Hemisphere, Meteorologica 20 101-108.

Vauclair, F, and Y. du Penhoat, 2001: Interannual variability of the upper layer of the Tropical Atlantic Ocean from in situ data between 1979 and 1999, Climate Dynamics, 17, 527 – 546.

Wyrtki K., (1975), Fluctuations of the dynamic topography in the Pavcific Ocean, J. Phys. Oceanogr. 5, 450-459.

Wyrtki, K., (1971): Oceanographic Atlas of the International Indian Ocean Expedition, National Science Foundation Publication, OCE/NSF 86-00-001Washington, DC, 531 pp.

Wu H, MJ Hayes , A Weiss and H Q (2001) An evaluation of the Standardized Precipitation Index, the China-Z Index and the statistical Z-Score. Int. J. Clim. 21(6) 745-758.

Xie, S., 2004. Satellite observations of cool ocean–atmosphere interaction. Bulletin of the American Meteorological Society 85, 195-208.

Xie, S.-P., H. Annamalai, F. A. Schott, and J. P. McCreary, 2002: Structure and mechanisms of south Indian Ocean climate variability. J. Climate., 15, 867–878.

Xie, S.-P., and J.A. Carton, 2004: Tropical Atlantic variability: patterns, mechanisms, and impacts, in “Ocean-Atmosphere Interaction and Climate Variability”, edited by C. Wang, C., S.-P. Xie, and J. A. Carton, ed.s 2004

Yamagata, T. and S. Iizuka, 1995. Simulation of the tropical thermal domes in the Atlantic: a seasonal cycle. J. Phys. Oceanog., 25, 2,129- 2,140.